2004

Inorganic and biological applications of inductively coupled plasma mass spectrometry and electrospray mass spectrometry

Fumin Li
Iowa State University

Inorganic and biological applications of inductively coupled plasma mass spectrometry and electrospray mass spectrometry

by

Fumin Li

A dissertation submitted to the graduate faculty

in partial fulfillment of the requirements for the degree of

DOCTOR OF PHILOSOPHY

Major: Analytical Chemistry

Program of Study Committee:
R. S. Houk (Major Professor)
Daniel W. Armstrong
Marc Porter
Victor Lin
Walt Trahanovsky

Iowa State University

Ames, Iowa

2004

Graduate College
Iowa State University

This is to certify that the doctoral dissertation of

Fumin Li

has met the dissertation requirements of Iowa State University

Signature was redacted for privacy.

Major Professor

Signature was redacted for privacy.

For the Major Program

This dissertation is dedicated to my parents, Hongji Li and Xiucong Xin.

TABLE OF CONTENTS

CHAPTER 1

GENERAL INTRODUCTION

PART I: Historical Perspective of ICP-MS

The inductively coupled plasma (ICP) is an atmospheric pressure ion source, created by an electrical discharge, which is maintained by radio frequency power coupled to it through load coils. The concept of plasma produced by radio frequency was pioneered by Reed[1] as early as 1960s. The inductively coupled plasma (ICP) was used as the excitation source in atomic emission spectroscopy (AES) for multi-element analysis at trace levels independently by Greenfield et al.[2] and Fassel et al.[3-4] at late 1960s. This technique became a powerful tool in trace elemental analysis[5-6] with the enormous effort from Fassel and coworkers.

However, the analysis of trace metals by ICP-AES was hindered by spectral interferences. Thus, an alternative multi-element analysis method was desired, which ideally could circumvent the aforementioned problem yet still has the merits provided by ICP-AES, i.e. speed and ease of use. Mass spectrometry was an ideal candidate, which offered low detection limit, essential for trace level, simple spectra and adequate resolution. Gray[7] demonstrated mass spectrometry was a sensitive tool for elemental analysis by introducing solution into a DC plasma at atmospheric pressure. This ion source, unfortunately, was not a practical one for elemental analysis mainly due to its low plasma temperature (~ 4000 K) and the concomitant low ionization efficiency for a range of elements. In contrast, the inductively coupled plasma (ICP) could be maintained at much higher temperature, ~ 7000

K, and was, therefore, a better source for all elements. Houk et al.[8] in 1980 reported the first analytical ICP-MS mass spectra. ICP-MS has since been rapidly developed into a standard and mature technique and becomes the method of choice for elemental and isotopic analysis.[9] In addition to multi-element[10] (up to 70) analysis ability, ICP-MS has excellent sensitivity as high as 10^9 cps/ppm, detection limit as low as part per quadrillion, and large dynamic range, up to 8 orders of magnitude.[11-13] It has environmental,[14-16] clinical,[17-19] biological,[20-22] geological,[23-24] semiconductor industries[25-26] and nuclear[27] applications.

ICP-MS Instrumentation

Like in any mass spectrometer, ICP-MS also has four main components: ion source (the ICP), vacuum system, mass analyzer and detector. Each section will be detailed in the following discussion. Note that ion extraction will be treated separately although it is not listed as a main component.

Inductively Coupled Plasma (ICP). Shown in Figure 1 is a schematic diagram of the ICP torch. It consists of three concentric quartz tubes, through which inert gas or gases, usually Ar, is introduced to the ICP. The outer gas, or coolant gas, flows through the outer tube at 15-18 L/min; This gas serves to sustain the plasma and protect the tube walls. The intermediate tube provides the auxiliary gas, about 1 L/min, to keep the hot plasma out the tip of inner tube. A third gas, called sample gas or aerosol gas, introduces the nebulized sample aerosol into the plasma and is usually 1 L/min.

The torch is coupled by a water-cooled load coil, usually copper or silver, a few millimeters below the top end. The RF generator, operated at either 27 or 40 MHz, provides a power of 600-1500 watts[28] to the load coil. The plasma is initiated by free electrons

supplied by a spark from Tesla coil. Electrons, moving in circular orbits, are accelerated by the induced magnetic field within the torch and collide with the argon atoms, which are ionized as a result. In this process, the electrical energy from the RF generator is converted to electrons' kinetic energy, which is the energy origin for ionization.

The plasma is ignited and heated as a result of numerous collisions between free electrons and argon atoms. Most of the RF energy is coupled to the outer or induction region of the plasma, where the temperature can be up to 10,000 K. Gas in the center channel is heated mainly by conduction and radiation from the induction region, where the temperature is between 5,000 and 7,000 K. As the sample aerosol goes through the central channel, it undergoes desolvation, vaporization, atomization, ionization and finally excitation in sequence. Ions are subsequently extracted into the mass spectrometer from the normal analytical zone (NAZ) of the plasma.

Vacuum System. Note that the ICP is operated at atmospheric pressure and ions produced are at ambient atmosphere as well. Mass spectrometry, in comparison, requires a high vacuum condition (less than 10^{-5} torr) so that ions can reach the detector without substantial loss by collision with background gas. Therefore, the ICP-MS instrument requires a differential pumping system. Most ICP-MS instruments have three stages of pumping, separated by three orifices, namely sampler, skimmer and differential pumping orifice. A mechanical pump is used in the first stage, which is between the sampler and skimmer. The pressure is approximately 1 torr at this stage. The second stage houses the ion lenses, which are located right behind the skimmer. The pressure is maintained at about 10^{-4} torr through either a turbo or diffusion pump. The third stage begins after the ion lens, where

mass analyzer is held. If necessary, additional ion lenses are set in the third stage to help better focus and transmit ions to detector. The pressure is typically 10^{-5} torr or less.

Ion Extraction. Ion extraction process from plasma into the vacuum is critical for ICP-MS measurement because it affects ion transmission efficiency and eventually the overall sensitivity. Ions generated by the ICP, a quasi-neutral mixture of neutrals, electrons and ions, flow through a sampler to the first vacuum stage. The sampler hole is approximately 1 mm in diameter and cooled by water. The gas sampled by the sampling orifice expands to form a supersonic jet due to the substantial pressure difference between atmosphere (1 atm) and the vacuum in the first stage chamber (1 torr). Collisions occur in the first few orifice diameters after the sampled gas passes the sampling orifice. The zone of silence, free of collision, is located downstream of the supersonic jet, where the entrained ions obtain the same supersonic velocity as neutral gas molecules. The skimmer, with an orifice diameter of 0.8 mm (slightly smaller than sampler), is positioned at roughly two-thirds of the distance to the onset of Mach disc to further extract ions. This sampling happens in such a short period of time, ~3 μs, that ions change little in nature or relative percentage, and recombination between ions and electrons is minimal.

After ions leave the skimmer, they are escorted to the mass analyzer by a series of ion lenses. The quasi-neutral condition breaks down because only positively charged ions are focused while electrons are expelled and most of the neutrals are pumped. The extracted ion beam is subsequently guided to the mass analyzer, where the mass-to-charge separation is realized.

Ion Detection. The discrete dynode electron multiplier (EM) can be used for direct current measurements (analog detection mode) or for pulse counting measurement (counting

detection mode). Analog mode is more suitable for high ion signal to extend the dynamic range, which otherwise will be saturated by the gain of the detector. As in counting mode, the electron pulse is sensed and pre-amplified, which then goes to a digital discriminator set at a certain threshold to reduce the random and unspecified noise. In contrast, this mode works better for low ion signal intensities.

Mass Spectrometers. Almost every major type of commercially available mass spectrometer has been coupled with the ICP source. The first mass analyzer used with the ICP was quadrupole mass filter,[8, 29] which remains the most common used mass spectrometer in ICP-MS mainly due to its ease of use and affordability. However, these devices only provide unit resolution, about 400 ($m/\Delta m$) in the first stability region for ICP-MS purposes. This resolving power is not enough to separate different ions with the same nominal mass. It is known the most severe drawback in ICP-MS is the spectral interference posed by polyatomic ions associated with plasma gas, i.e. Ar. It requires, for example, about 2500 resolving power in order to separate $^{56}Fe^{+}$ (53.9349) from $^{40}Ar^{16}O^{+}$ (53.9573), which is not attainable with quadrupole analyzer. More details about quadrupole will be addressed in the second part. Other mass analyzers include magnetic sector,[30] time-of-flight (TOF),[31-33] ion trap[34-35] and ion cyclotron resonance (ICR).[36]

Work on the ICP-MS part of this dissertation is done with a magnetic sector mass analyzer. This instrument provides a mass resolution up to 12,000.[30, 37-38] This allows the elimination of almost all spectral interference caused by polyatomic ions, which makes accurate elemental analysis for some problematic elements possible. The device is a double focusing sector mass spectrometer with reverse Nier-Johnson geometry. The magnetic sector separates ions according to their mass-to-charge ratios and provides the directional focusing

at the same time. The second focusing is achieved by an electrostatic analyzer (ESA), proceeded by the sector. Only ions with the same energy range have the same moving radius in ESA, which thereby reduces velocity broadening.

Sample Introduction. Sample introduction is one of the most important factors in ICP-MS measurements to obtain accurate and precise results.[10] For instance, a change in plasma temperature would alter the ionization efficiency of different elements. An ideal sample introduction system would generate aerosol that represents the sample solution, has constant density and small droplet distribution.

There are a variety of sample introduction systems for ICP-MS. Solution nebulization is most widely used to deliver liquid sample as an aerosol of fine droplets to the ICP, where they undergo desolvation, vaporization, atomization and ionization. A pneumatic nebulizer is a typical sample introduction system, in which the liquid sample is delivered to a thin tube, nested inside a large one. Gas, usually Ar, is supplied to the outer tube and shatters the liquid into droplets and then fine aerosol at the nebulizer tip. The aerosol produced often has a wide range of particle size distribution. A chamber, usually located right after the nebulizer, is used to remove large particles, while allowing small ones to proceed to the plasma directly. Low nebulization efficiency, less than 2%, is the disadvantage of conventional pneumatic nebulizer. Several other nebulizers have been designed to improve sample introduction efficiency. These categories include ultrasonic nebulizer,[39-40] direct injection nubulizer[41-43] and microconcentric nebulizer (MCN). Of particular note is the microconcentric nebulizer, which gains increasing popularity for its high efficiency ($\geq$50%) and reduced sample uptake ($<$ 0.2 L/min from 1 L/min). Shown in Figure 2 is a schematic diagram of solution sample introduction system to ICP-MS. It consists of a microconcentric

nebulizer and a spray chamber. Solution sample introduction offers certain advantages, such as ease of calibration solution standards and possibility of LC-ICP-MS experiments.

Solution method, nevertheless, is not suitable for the direct analysis of solid sample, which is often dissolved by acid. The process might be labor extensive, time consuming and risky of contamination. Therefore, several techniques have been used for direct solid sample introduction to the ICP, which includes arc ablation,[44] glow discharge,[45] electrothermal evaporation[46] and laser ablation.[47-48]

Surface Analysis by ICP-MS

There is a growing demand for analytical methods that can determine the elemental composition of surface layers of solids. Mass spectrometric methods for the surface analysis of inorganic elements, at trace or ultratrace level, providing sensitive and multi-elemental analysis capabilities, have been established. Of the methods suitable for surface analysis, secondary ion mass spectrometry (SIMS) is most widely used to analyze trace elements on different solid surfaces or thin layers.[49] The profiled depth is in the range of 1-10 nm, which depends on various factors such as energy and mass of incoming ions, nature of the sample materials. Laser ablation ICP-MS[50] can also be used in surface analysis although the crater depth produced by LA is deeper than in SIMS. Advantages of direct surface analysis include less time and cost for sample preparation and minimal contamination. Quantification for solid sample, however, is usually difficult if no matrix-matched standard reference material is available.

ICP-MS, a well-established method for solution analysis, gains increasing popularity for the analysis of solid sample after dissolution.[49] Compared to the direct solid analysis,

acid dissolution[51] has long been used in the preparation of solid samples. Vapor phase decomposition (VPD) was applied to determine atomic impurities in silicon oxide layers in semiconductor production.[52] Douglas et al.[53] used rapid sample dissolution by electroerosion with concentrated HCl or HNO_3 as sample introduction to ICP-MS. Dissolution with concentrated mineral acid, i.e. HNO_3, was used to determine tungsten in drugs.[54] Microwave coupled acid decomposition[55-56] is the other widely used method because it is relatively easy to control microwave power to dissolve refractory materials. The potential drawbacks of solid analysis by acid dissolution are possible sample contaminations and time and cost involved in the sample preparation.

LC-ICP-MS and its Applications to Bacteria

It is known that many elements are essential to human health, whereas others are considered to be toxic. It is the specific elemental forms that strongly affect its uptake, accumulation, transport and interaction with metalloids. Therefore, complete characterization, i.e. oxidation state, chemical ligand association and complex form, is crucial to assess elemental essentiality vs toxicity. Elemental speciation typically consists of separation technique, which is followed by a sensitive and element-specific detector. Of various combinations of separation and detection methods, high performance liquid chromatography (HPLC) with inductively coupled plasma mass spectrometry (ICP-MS) has emerged as one of the most popular techniques due to its sensitivity, multi-elemental capability, versatility and robustness. A wide range of separation mechanisms have been

coupled with ICP-MS, including three most widely used separations, i.e. reverse phase (RP),[57] size exchange chromatography (SEC)[58] and ion-exchange chromatography (IEC).[59]

Houk and Thompson[40] in 1986 first demonstrated ICP-MS as an on-line multi-elemental detector for HPLC. The publication of that hyphenate HPLC with ICP-MS has increased dramatically since then.[60] This work focuses significantly on environmental,[15-16, 24] clinical,[17, 19, 61-62] and biological applications.[16, 21, 63-64]

Size exclusion chromatography coupled with ICP-MS has been used for the analysis of biological molecules.[65] Perfusion chromatography, a special version of SEC, was applied to separate microbes from large and small molecules.[66] Various groups have demonstrated the unique utility of LC-ICP-MS in the determination of trace elements in bacteria.[67-70]

PART II: Historical Perspective of Electrospray Mass Spectrometry

The electrospray process was studied experimentally as early as 1917 by Zeleny,[71] long before its application to mass spectrometry. Then it was Dole et al.[72-73] who took the first step to combine electrospray technique with mass spectrometry, in which they tried to determine the molecular weight distribution of synthetic polystyrene. Although with some success in Dole's situation, the idea of using electrospray as an ionization technique for mass spectrometry was almost abandoned. It was not until 1984 when Yamashita and Fenn[74-75] successfully demonstrated electrospray as an ionization method for mass spectrometry. Even since then, combination of electrospray, a soft-ionization process which preserves the structural information of analytes as in the solution, and mass spectrometry has revolutionized the study of biomolecules.[76-79] At approximately the same time, Aleksandrov et al.[80] investigated inorganic ions by ESI-MS. The application of ESMS as a tool to probe the inorganic chemistry[81-82] has witnessed the exponential growth in publications in the past ten years.

Electrospray Ionization Process

Electrospray is a technique that transfers ions from solution to gas phase. There are three major steps responsible for the production of gas-phase ions as illustrated sequentially in Figure 3: (1) the production of charged droplets; 2) solvent evaporation and repeated droplet fission, and (3) final generation of gas phase ions.

Production of Charged Droplets. Shown in stage I of Figure 3 is a scheme of the production of charged droplets (only positive mode is exampled for simplicity). Analyte

solution is pumped (~1-10 μL/min) through an open-ended metal capillary, often held at 2-4 kV, which is located about 0.5-3 cm from the counter-electrode, usually grounded. The electric field at the capillary tip is extremely high, ~10^6 V/m for instance,[83] because of the small capillary tip, ~100 μm. In the pure ES mode, electrostatic interaction is the only force for droplet formation. The high electric field E_c penetrates the solution at the tip and separation of positive and negative ions takes places. In positive ES mode, positive ions drift downstream to the counter electrode, while negative ones move in the opposite direction. When the mutual repulsion of positively charged species at the surface exceeds the surface tension, the surface begins to expand and the so-called Taylor cone[84] is formed. Under strong electric field, the cone is not stable and fine filament is emitted, from which the charged droplets are formed downstream. In a more common pneumatically assisted ES, a nebulization gas, usually air or N_2, is applied to facilitate droplet formation. This results in a more stable spray current because of the more consistent production of aerosol, which otherwise will be affected by high solution flow rate or sample matrix. Another common source is known as "nanoelectrospray" or "nanospray"[85] and uses extremely small inner diameter tip, 1-2 μm. Advantages include better ion production efficiency due to high charge-to-mass ratio and significant low sample consumption rate, 20-40 nL /min,[86] which is particularly important for precious biological samples.

Solvent Evaporation and Repeated Droplet Fission. As the charged droplets travel toward the MS entrance, the solvent is evaporated mainly by the high temperature (250 °C) within the heated capillary and partially by thermal energy of the ambient air. The organic solvent is usually added to increase evaporation rate. The charge on the droplets remains constant during this process because the emission of ions at this stage is highly endoergic.

The droplets shrink as a result. With the decrease of droplet radius, the surface charge density increases to the Rayleigh stability limit, when droplets undergo "uneven fission". This means two or more particles with unequal mass and charge are generated. Gomez and Tang[87] estimated that these small offspring droplets contain only 2% mass of parent droplets while retaining 15% of the charge, a 7-fold increase on the charge-to-mass ratio. This cycle of solvent evaporation and Rayleigh fission occurs repeatedly, leading to even smaller charged droplets.

Generation of Gas Phase Ions. There are two mechanisms proposed for the formation of gas phase ions from small, highly charged droplets, although neither model receives unanimous acceptance.[88-90] The first one is Dole's Charged Residue Model (CRM).[91] It reasons that a droplet that contains only one ion will be formed eventually after cycles of solvent evaporation and Rayleigh fission, as supported by some recent work.[92] The ion may be a single ion or solvated one. The second mechanism is ion evaporation model (IEM), proposed by Iribarne and Thomson.[93-94] The charged droplets undergo the same physical changes as in CRM. However, the solvated gas-phase ions are emitted directly from the droplet surface when the electrostatic repulsion is sufficient to overcome the surface tension. This intermediate stage of droplet evolution depends mainly on the number of charges on the droplet and the radius of the droplet.

Triple Quadrupole Mass Spectrometer

Quadrupole Mass Analyzer. A quadrupole consists of four hyperbolic, equidistant metal rods, which are mounted to very high dimensional accuracy (<10 μm). RF and DC voltages are applied to the opposite pairs, which are connected together. The DC voltage is positive for one pair and negative for the other while RF voltages are the same in magnitude but 180° out of phase. The ions are injected along the axis and only ions of interest will have a stable trajectory through the rods whereas others are deflected if DC and RF voltages are chosen properly.[95-96] Quadrupole mass analyzer[97] has been widely used, especially for applications where accurate mass measurement and high resolution are not required. There are advantages of quadrupole mass analyzer, i.e.1) it can be operated at relatively high pressure, ~10^{-5} torr, 2) it is a mechanically simple device and thus easy to use.

Triple Quadrupole Mass Analyzer. The core of a triple-stage quadrupole mass spectrometer, as shown in Figure 4, is the quadrupole. The configuration follows the sequence as Q1, first mass analyzer, Q2, a collision cell and Q3, the second mass analyzer. Obviously, this instrument has two mass analyzers Q1 and Q3, which enable the capability of tandem in space mass spectrometry function in addition to the full scan performance.

ESI-MS of Inorganic Ions and Threshold Study

Unlike most atomic-based ionization techniques, such as the ICP, electrospray does not really create ions. Rather, it transfers ions in solution to the gas phase. Thus, the softness of the ionization process preserves important solution information, such as the oxidation state and form of an ion, which is crucial for inorganic ions in toxicology. For instance, the biological role of chromium varies greatly depending on its chemical form. Cr^{III} is an

essential nutrient for living organisms, believed to help activate insulin,[98] whereas Cr^{VI} can cause various forms of cancer.[99] Electrospray, which preserves structural information, is helpful to study chromium speciation. ES-MS has been applied in the determination of most elements across the periodic table, including alkali,[100-101] alkaline earth,[102-103] transition metals,[104-107] the lanthanides[108-109] and some non-metals, such as halides.[110] Most of these studies focus on metal-ligand complexes, which range from counter-ion to solvent, from multi-dendate ligands to biological molecules.

Mass spectrometry is more than a structural tool and has useful capabilities in thermochemistry. Armentrout[111] shows the ability to measure thermochemical properties by tandem mass spectrometry, using a specially designed guided ion beam mass spectrometry. Thermochemistry studies by collisionally induced dissociation (CID)[112-115] have been extensively carried out for both main group elements[116-117] and transition metal ions.[118-119] However, there is no report of using a commercially available triple quadrupole instrument to estimate the thermochemistry.

Dissertation Objective and Organization

This dissertation concentrates on novel applications of both ICP-MS and ESI-MS on inorganic and biological materials, i.e. bacteria. Chapter 2 is a manuscript accepted by *Applied Spectroscopy* that describes a new surface analysis method of steel by controlled dissolution with ICP-MS. Chapter 3 is a manuscript, ready to submit to *Analytical Chemistry* for publication, which investigates the behavior of bacteria in the ICP and its influence in the quantification of U in bacteria calibrated by inorganic U standard. This is a continuation of the previous project "Coupling Perfusion Chromatography with ICP-MS to Monitor

Microbial Removal of Uranium", published in *Analytical Chemistry* (see APPENDIX). Our results lay out the possible platform for the direct quantification of trace elements within bacteria by using inorganic standards instead of microorganisms with known amount of metal, and show firstly that bacteria behave similarly as large wet droplets in the ICP.

In Chapter 4, the formation of metal nitrate complexes in negative ES mode and their collision-induced dissociation patterns are investigated. The commercial-grade triple quadrupole instrument is applied to estimate the dissociation threshold of $Fe(NO_3)_4^-$. The study has been published in *Journal of the American Society for Mass Spectrometry*. A general conclusion with some suggestions for future work can be found in Chapter 5.

References:

1. Reed, T. B. *J. Appl. Phys.* **1961**, 32, 821.
2. Greenfield, S.; Jones, I. L.; Berry, C. T. *Analyst* **1964**, 89, 713.
3. Wendt, R. H.; Fassel, V. A. *Anal. Chem.* **1965**, 37, 920.
4. Fassel, V. A. *Science* **1978**, 4364, 183.
5. Dickinson, G. W.; Fassel, V. A. *Anal. Chem.* **1969**, 41, 1021.
6. Fassel, V. A.; Kniseley, R. N. *Anal. Chem.* **1974**, 46, 1110A.
7. Gary, A. L. *Analyst* **1975**, 100, 289.
8. Houk, R. S.; Fassel, V. A.; Flesch, G. D.; Svec, H. J.; Gray, A. L.; Taylor, C. E. *Anal. Chem.* **1980**, 52, 2283.
9. Houk, R. S. *Acc. Chem. Res.* **1994**, 27, 333.
10. Jarvis, K. E.; Gray, A. L.; Houk, R. S. **Handbook of Inductively Coupled Plasma Mass Spectrometry**, Blackie & Son, Glagow, 1992.
11. Houk, R. S. *Anal. Chem.* **1986**, 58, 97A.
12. Montaser, A. **Inductively Coupled Plasma Mass Spectrometry**, Wiley-VCH, New York, 1998.
13. Houk, R. S. in **Handbook of Elemental Speciation: Techniques and Methodology**, John Wiley & Sons, New York, 2003.
14. Huang, C. W.; Jiang, S. J. *J. Anal. At. Spectrom.* **1993**, 8, 681.
15. Rodushkin, I.; Ruth, T. *J. Anal. At. Spectrom.* **1997**, 12, 1181.
16. Bird, S. M.; Uden, P. C.; Tyson, J. F.; Block E.; Denoyer, E. *J. Anal. At. Spectrom.* **1997**, 12, 785.
17. Shum, S. C. K.; Pang, H. M.; Houk, R. S. *Anal. Chem.* **1992**, 64, 2444.

18. Probst, T. U.; Berryman, N. G.; Lemmen, P.; Weissfloch, L.; Auberger, T.; Gabel, D.; Carlsson, J.; Larsson, B. *J. Anal. At. Spectrom.* **1997**, 12, 1115.

19. Lafuente, J. M. G.; Dlaska, M.; Sanchez, M. L. F.; Sanz-medel, A. *J. Anal. At. Spectrom.* **1998**, 13, 423.

20. Crews, H. M.; Clarke, P. A.; Lewis, D. J.; Owen, L. M.; Strutt, P. R.; Izquierdo, A. *J. Anal. At. Spectrom.* **1996**, 11, 1177.

21. VandenBroeck, K.; Vandecasteele, C.; Geuns, J. M. C. *J. Anal. At. Spectrom.* **1997**, 12, 987.

22. Kotrebai, M.; Birringer, M.; Tyson, J. F.; Block, E.; Uden, P. C. *Analyst* **2000**, 125, 71.

23. Hall, G. E. M.; Pelchat, J. –C. *J. Anal. At. Spectrom.* **1997**, 12, 103.

24. Carignan, J.; Hild, P.; Mevelle, G.; Morel, J.; Yeghicheyan, D. *Geostand. Newslett.* **2001**, 25, 187.

25. Morin, M.; Kimura, T.; Koyanagi, M.; Hirose, M.; Friedt, J. M. *Solid State Tech.* **1993**, 36(4), 45.

26. Ajluni, C. *Electronic Design* **1995**, 43(14), 38.

27. Heres, A. P.; Noe, M. C. *Nuclear Technology* **1996**, 115, 146.

28. Greenfield, S.; Montaser, A. **Inductively Couple Plasmas in Analytical Atomic Spectroscopy** Montaser, A.; Golightly, D. W. eds.; 2nd edition, VCH, London, 1992.

29. Date, A. R.; Gray, A. L. *Analyst* **1981**, 106, 1255.

30. Bradshaw, N.; Hall, E. F. H.; Sanderson, N. E. *J. Anal. At. Spectrom.* **1989**, 4, 801.

31. Myers, D. P.; Li, G.; Mahoney, P. P.; Hieftje, G. M. *J. Am. Soc. Mass Spectrom.* **1995**, 6, 400.

32. Mahoney, P. P.; Ray, S. J.; Myers, D. P.; Li, G.; Yang, P.; Hieftje, G. M. *Abstr. Pap. Amer. Chem. Soc.* **1996**, 211, 7.

33. Mahoney, P. P.; Ray, S. J.; Hieftje, G. M. *Appl. Spectrosc.* **1997**, 51, A16.

34. Koppenaal, D. W.; Barinaga, C. J.; Smith, M. R. *J. Anal. Atom. Spectrom.* **1994**, 9, 1053.

35. Barinaga, C. J.; Koppenaal, D. W. *Rapid commun. Mass Spectrom.* **1994**, 8, 71.

36. Milgram, K. E.; White, F. M.; Goodner, K. L.; Watson, C. H.; Koppenaal, D. W.; Barinaga, C. J.; Smith, B. H.; Winefordner, J. D.; Marshall, A. G.; Houk, R. S.; Eyler, J. R. *Anal.Chem.* **1997**, 69, 3714.

37. Jakubowski, N.; Moens, L.; Vanhaecke, F. *Spectrochim. Acta Part B* **1998**, 53, 1739.

38. Latkoczy, C.; Prohaska, T.; Stingeder, G.; Wenzel, W. W. *Fresenius' J. Anal. Chem.* **2000**, 368, 256.

39. Mermet, J. M.; Pobin, J. P. *Anal. Chem.* **1968**, 40, 1918.

40. Thompson, J. J.; Houk, R. S. *Anal. Chem.* **1986**, 58, 2541.

41. LaFreniere, K. E.; Fassel, V. A.; Eckels, D. E. *Anal. Chem.* **1987**, 59, 879.

42. Wiederin, D. R.; Smith, F. G.; Houk, R. S. *Anal. Chem.* **1991**, 63, 219.

43. Acon, B. W.; McLean, J. A.; Montaser, A. *J. Anal. At. Spectrom.* **2001**, 16, 852.

44. Jiang, S. J.; Houk, R. S. *Anal. Chem.* **1986**, 58, 1739.

45. Hang, W.; Walden, W. O.; Harrison, H. W. *Anal. Chem.* **1996**, 68, 1148.

46. Park, C. J.; Hall, G. E. M. *J. Anal. At. Spectrom.* **1987**, 2, 473.

47. Gray, A. L. *Analyst* **1985**, 110, 551.

48. Aeschilman, D. B.; Bajic, S. J.; Baldwin, D. B.; Houk, R. S. *J. Anal. At. Spectrom.* **2003**, 18, 1008.

49. Becker, J. S.; Dietze, H. –J. *Spectrochim. Acta Part B* **1998**, 53, 1475.

50. Horn, I.; Guillong, M.; Günther, D. *Appl. Surface Sci.* **2001**, 182, 91.

51. Bock, R. **A Handbook of Decomposition Methods in Analytical Chemistry**, Wiley & Sons, 1979.

52. Krushevska, A.; Tan, S.; Passer, M.; Liu, X. R. *J. Anal. At. Spectrom.* **2000**, 15, 1211.

53. Douglas G.; Michael B.; Gundars R. *Spectrochim. Acta Part B* **2003**, 58, 1325.

54. Wang, T. B.; Ge, Z. H.; Wu, J.; Li, B.; Liang, A. -S. *J. Pharm. Biomed. Analysis* **1999**, 19, 937.

55. Kingston, H. M.; Jassie, L. B. *Materials Research Society Symposium Proceedings* **1998**, 124(Microwave Process. Mater.), 121.

56. Kingston, H. M.; Jassie, L. B. *J. Res. Natl. Bur. Stand. (U. S.)* **1998**, 93, 269.

57. Montes-Bayon, M.; B'Hymer, C.; Leon, C. P.; Caruso, J. A. *J. Anal. At. Spectrom.* **2001**, 16, 945.

58. Szpunar, J. *Analyst* **2000**, 125, 963.

59. Larsen, E. H.; Hansen, M.; Fan, T.; Vahl, M. *J. Anal. At. Spectrom.* **2001**, 16, 1403.

60. Montes-Bayon, M.; DeNicola, K.; Caruso, J. A. *J. Chromatogr. A* **2003**, 1000, 457.

61. Nagaoka, M. H.; Maitani, T. *Analyst* **2000**, 125, 1962.

62. Evans, E. H.; Caruso, J. A. *J. Anal. Atom. Spectrom.* **1993**, 8, 427.

63. Vela, N. P.; Heitkemper, D. T.; Stewart, K. R. *Analyst* **2001**, 126, 1011.

64. Francesconi, K.; Visoottiviseth, P.; Sridokchan, W.; Goessler, W. *Sci. Total Environ.* **2002**, 284, 27.

65. Wang, J.; Dreessen, D.; Wiederin, D. R.; Houk, R. S. *J. Amer. Chem. Soc.* **1998**, 120, 5793.

66. Berthod, A.; Zhang, B.; Armstrong, D. W. *J. Sep. Sci.* **2003**, 26, 20.

67. Allardyce, C. S.; Dyson, P. J.; Abou-Shakra, F. R.; Birtwistle, H.; Coffey, J. *Chem. Commu.* **2001**, 24, 2708.

68. Kuroda, K.; Yoshida, K.; Yasukawa, A.; Wanibuchi, H.; Fukushima, S.; Endo, G. *Applied Organometallic Chemistry* **2001**, 15, 548.

69. Michalke, B.; Witte, H.; Schramel, P. *J. Anal. At. Spectrom.* **2001**, 16, 593.

70. Leopold, I.; Fricke, B. *Analytical Biochemistry* **1997**, 252, 277.

71. Zeleny, J. *Phys. Rev.* **1917**, 9, 562.

72. Dole, M.; Mack, L. L.; Hines, R. L.; Mobley, R. C.; Ferguson, L. D.; Alice, M. B. *J. Chem. Phys.* **1968**, 49, 2240.

73. Mack, L. L.; Kralik, P.; Rheude, A.; Dole, M. *J. Chem. Phys.* **1970**, 52, 4977.

74. Yamashita, M.; Fenn, J. B. *J. Phys. Chem.* **1984**, 88, 4451.

75. Yamashita, M.; Fenn, J. B. *J. Phys. Chem.* **1984**, 88, 4671.

76. Chait, B. T.; Kent, S. B. *Science* **1992**, 257, 1885.

77. Gatlin, C. L.; Turecek, F. in *Electrospray Ionization Mass Spectrometry-Fundamentals, Instrumentation, and Applications*, Cole, R. B. Wiley: New York, **1997**, p527.

78. Burlingame, A. L.; Boyd, R. K.; Gaskell, S. J. *Anal. Chem.* **1996**, 68, 599R.

79. Colton, R.; D'Agostino, A.; Traeger, J. C. *Mass Spectrom. Rev.* **1995**, 14, 79.

80. Aleksandrov, M. L.; Gall, L. N.; Krasnov, N. V.; Nikolaev, V. I.; Shkurov, V. A. *Zh. Anal. Khim.* **1985**, 40, 1570.

81. Stewart, I. I.; Horlick, G. *Trends Anal. Chem.* **1996**, 15, 80.

82. Stewart, I. I. *Spectrochim. Acta Part B* **1999**, 54, 1649.

83. Kebarle, P.; Ho, Y. H. in *Electrospray Ionization Mass Spectrometry-Fundamentals, Instrumentation, and Applications*, Cole, R. B. Wiley: New York, **1997**, p8.

84. Taylor, G. I. *Proc. Roy. Soc. A.* **1964**, 280, 383.

85. Wilm, M.; Mann, M. *Int. J. Mass Spectrom. Ion Processes* **1994**, 136, 167.

86. Wilm, M.; Mann, M. *Anal. Chem.* **1996**, 68, 1.

87. Kebarle, P.; Tang, L. *Anal. Chem.* **1993**, 65, 972A.

88. Fenn, J. B. *J. Am. Soc. Mass Spectrom.* **1993**, 4, 524.

89. Tang, L. ; Kebarle, P. *Anal. Chem.* **1993**, 65, 3654.

90. Winger, B. E.; Light-Wahl, K. J.; Ogorzalek-Loo, R. R.; Udseth, H. R.; Smith, R. D. *J. Am. Soc. Mass Spectrom.* **1993**, 4, 536.

91. Striegel, A. M.; Timpa, J. D.; Piotrowiak, P.; Cole, R. B. *Int. J. Mass Spectrom. Ion Processes* **1997**, 162, 45.

92. Wang, G. D.;Cole, R. B. *Anal. Chem.* **1998**, 70, 873.

93. Iribarne, J. V.; Thomson, B. A. *J. Chem. Phys.* **1976**, 64, 2287.

94. Thomson, B. A.; Iribarne, J. V. *J. Chem. Phys.* **1979**, 71, 4451.

95. Miller, P. E.; Denton, M. B. *J. Chem. Educ.* **1986**, 63, 617.

96. Dawson, P. H. *Mass spectrom. Rev.* **1986**, 5, 1.

97. McEwen, P. E.; Larsen, B. S. in *Electrospray Ionization Mass Spectrometry-Fundamentals, Instrumentation, and Applications*, Cole, R. B. Wiley: New York, **1997**, p177.

98. Da Silva, J.; Williams, R. *The Biological Chemistry of the Elements, the Inorganic Chemistry of Life*, Clarendon Press, Oxford, NY, **1991**, p541.

99. Ottaway, J. M.; Fell, G. S. *Pure Appl. Chem.* **1986**, 58, 1707.

100. Fish, K. J.; Henderson, W.; Dance, I. G.; Willett, G. D. *J. Chem. Soc. Dalton Trans.* 1996, 21, 4109.

101. Young, D. -S.; Hung, H. -Y.; Liu, L. K. *Rapid Commun. Mass Spectrom.* 1997, 11, 769.

102. Fery-Forgues, S.; Lavabre, D.; Rochal, A. D. *N. J. Chem.* **1998**, 22, 1531.

103. Wang, K. S.; Gokel, G. W. *Pure Appl. Chem.* 1996, 68, 1267.

104. Bortolini, O.; Conte, V.; DiFuria, F.; Moro, S. *Eru. J. Inorg. Chem.* **1998**, 8, 1193.

105. Bond, A. M.; Colton, R.; Gable, R. W.; Mackay, M. F.; Walter, J. N. *Inorg. Chem.* **1997**, 36, 1181.

106. Bates, G. B.; Cole, E.; Parker, D.; Kataky, R. *J. Chem. Soc. Dalton Trans.* **1996**, 13, 2693.

107. Romero, F. M.; Ziessel, R.; Dupont-Gervais, A.; Van-Dorsselaer, A. *Chem. Commun.* ***1996***, 4, 551.

108. Lau, R. L. C.; Jiang, J. Z.; Ng, D. K. P.; Chan, T. W. D. *J. Am. Soc. Mass Spectrom.* **1997**, 8, 161.

109. Renaud, F.; Piguet, C.; Bernardinelli, G.; Bunzli, J. C. G.; Hopfgartner, G. *Chem. Eur. J.* **1997**, 3, 1646.

110. Blades, A. T.; Klassen, J. S.; Kebarle, P. *J. Am. Chem. Soc.* **1995**, 117, 10563.

111. Armentrout, P. B. *J. Am. Soc. Mass Spectrom.* **2002**, *13*, 419.

112. Muntean, F.; Armentrout, P. B. *J. Chem. Phys.* **2001,** 115, 1213.

113. Armentrout, P. B. *Int. J. Mass Spectrom.* **2000**, 200, 219.

114. Ariston, N.; Armentrout, P. B. *J. Cluster Science* **1990,** 1, 127-142.

115. Rodgers, M. T.; Ervin, K. M.; Armentrout, P. B. *J. Chem. Phys.* **1997,** 106, 4499.

116. Rodgers, M. T.; Armentrout, P. B. *J. Phys. Chem. A* **1997,** 101, 1238.

117. Andersen, A.; Muntean, F.; Walter, D.; Rue, C.; Armentrout, P. B. *J. Phys. Chem. A* **2000,** 104, 692.

118. Rodgers, M. T.; Armentrout, P. B. *Mass Spectrom. Rev.* **2000,** 19, 215.

119. Aristov, N.; Armentrout, P. B. *J. Phys.Chem.* **1986,** 90, 5135.

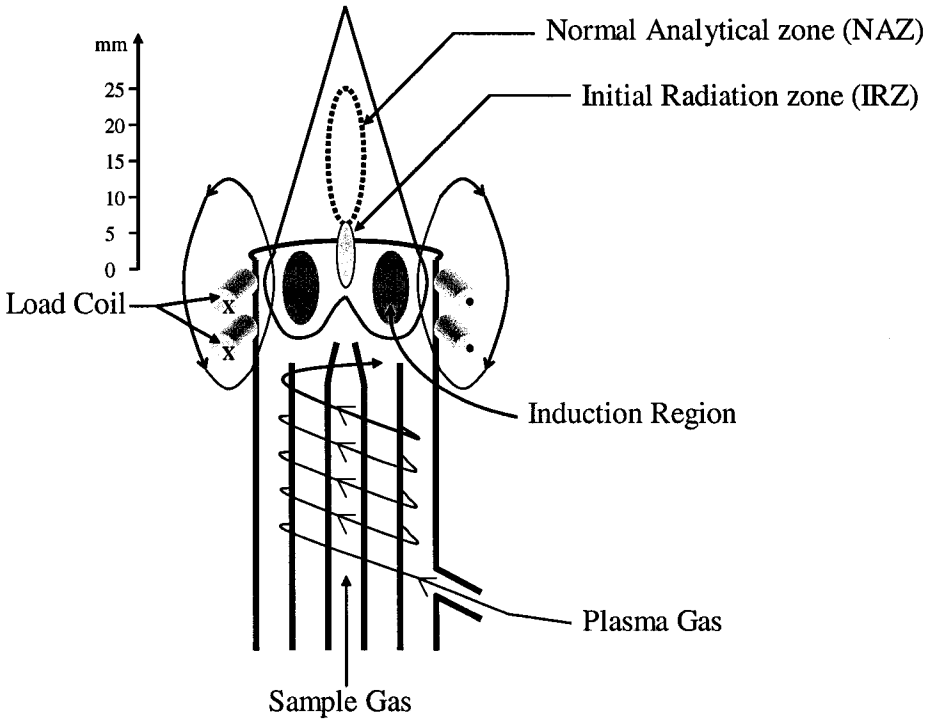

Figure 1: Schematic diagram of the ICP torch

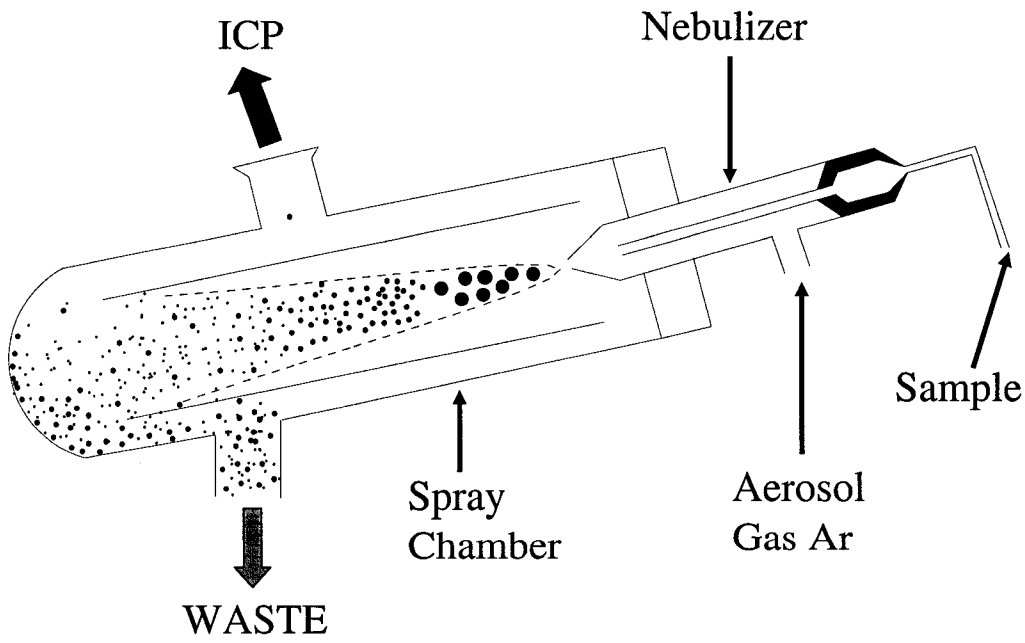

Figure 2: Nebulizer and spray chamber

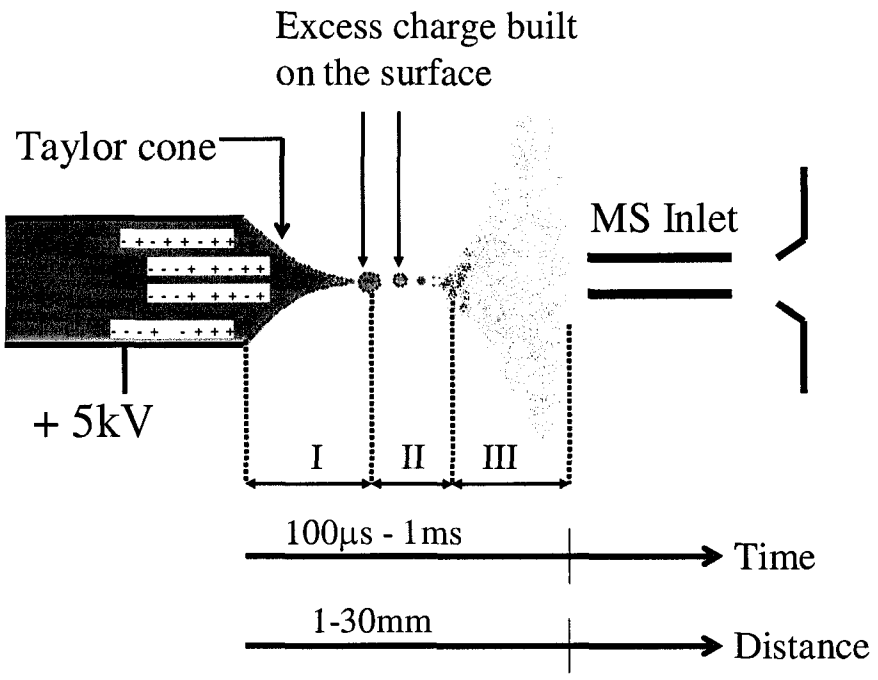

Figure 3: Schematic diagram of electrospray

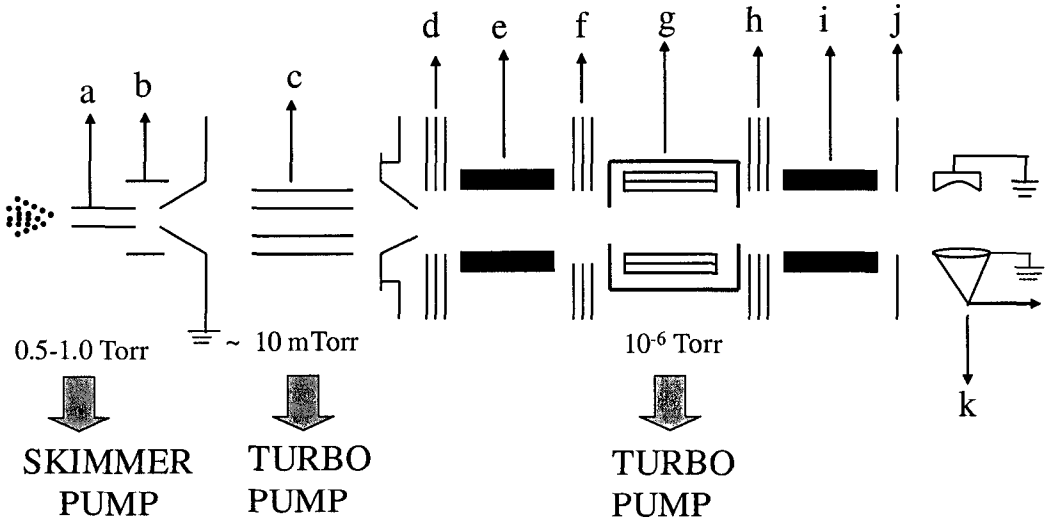

Figure 4: Schematic diagram of TSQ 7000 ESI-MS. a)capillary tube, b) tube lens, c)octopole, d)lens set 1(LS1), e) Q1, f)lens set 2(LS2), g) Q2, collision cell, h) lens set 3(LS3), i) Q3, j)L41, k) detector

CHAPTER 2

CONTROLLED DISSOLUTION FOR ELEMENTAL ANALYSIS OF SAMPLE LAYERS BY INDUCTIVELY COUPLED PLASMA – MASS SPECTROMETRY: A FEASIBILITY STUDY

A paper accepted by *Applied Spectroscopy*

Fumin Li and R. S. Houk

ABSTRACT

Aqueous acid mixtures at room temperature are used to partially dissolve steel samples. The dissolved elements are washed off the surface, diluted, and then determined by inductively coupled plasma – mass spectrometry (ICP-MS) using a magnetic sector mass analyzer. The amount of material removed is measured from the amount of Fe dissolved and increases linearly with HNO_3 concentration in the etch acid. Analyte concentrations in the solid are determined from the signal ratio of "(analyte ion)/Fe^+". The shape of a plot of mass of element removed vs. nitric acid concentration yields information about the efficiency of the removal process and the likely chemical form of the element in the sample. For elements like Mn, Al and W in steel, these plots have the same linear shape as that for the major element (Fe), and the measured concentrations agree well with the certified values. For problem elements like Nb and Ta, the plots have two linear regions with different slopes, and

measured concentrations are lower than the certified values. Laser ablation ICP-MS and scanning electron microscopy (SEM) measurements show these elements to be associated together in the solid in refractory grains that are not dissolved to the same extent as the Fe matrix. For steel, the amount of Fe dissolved corresponds to an average depth of at least 4 μm or 20,000 atomic layers.

INTRODUCTION

There is a growing demand for analytical methods that can determine the elemental composition of thin solid layers. New applications include semiconductors, layered materials, and nanomaterials. Secondary ion mass spectrometry (SIMS) and Auger electron spectroscopy are two established methods for this task. In particular, SIMS provides depth resolution of the order of a monolayer as well as lateral resolution. Within the purview of atomic spectroscopy, certain variations of X-ray fluorescence,[1-3] and glow discharge emission spectrometry[4-6] and MS[7-10] have potential value for layer analysis with depth resolution in the sub-micrometer range. These latter three methods do not provide lateral resolution; laser ablation ICP-MS[11-12] can do so.

One general weakness of some of these methods is a variation of analyte signal with the matrix composition. Thus, quantitative analysis often requires matrix-matched standards. It is not easy to make such materials for solid samples. Rutherford backscattering spectrometry (RBS)[6, 13-14] is an exception in that solid calibration standards are usually not required. RBS also provides some depth resolution, usually ~ 10 nm but sometimes as good as a few Å. It is usually nondestructive, unless additional sputtering is employed to provide access to buried layers, and some facilities can make RBS measurements with samples

outside the vacuum system. RBS has some difficulties measuring light elements in a matrix of heavy atoms; other ion scattering or nuclear methods can be employed in these cases.[13] Sample heterogeneity and sampling concerns are also issues for methods where the signal arises only from discrete spatial locations.

In standard dissolution procedures for elemental analysis of solids, the sample is usually dissolved completely. The total amount of sample is determined simply from the sample mass. The objective of the present study is to evaluate ICP-MS for quantitative elemental analysis of dissolved layers from solids, rather than the entire material. The amount of sample dissolved is determined from the amount of major element(s) present in the solution.

Like most analytical innovations, such a capability would have potential advantages and disadvantages relative to other methods. The ability to calibrate response using standard solutions is the main potential advantage. Modern ICP-MS instruments have very high dynamic range, so it should be possible to measure the signal ratio of analyte element to matrix element for quantification. Comparison of trace element signals to those for major elements is often done for quantification in laser ablation ICP-MS.[15] If necessary, it should be straightforward to determine the trace elements first in a concentrated sample, then dilute the sample to quantify the major elements. Spectral resolution of peaks from elements adjacent to the main components, e.g., Mn in steel, should not be a problem. Matrix effects will occur if enough solid is removed, but the calculation of ion ratios (either with internal standards or the major elements) should correct for them.

There is an extensive literature on acid decomposition,[16-17] etching of metals,[18] and other related topics. The need to handle the sample cleanly without contamination and to remove the various constituents uniformly are also obvious issues to be addressed.

One type of controlled dissolution followed by ICP-MS is already used widely in a key application: vapor phase decomposition (VPD) for determination of atomic impurities in silicon oxide layers in semiconductor production.[19-22] The solid is etched in an HF atmosphere. Contaminants are collected by "rolling" a small drop of water or aqueous acid (~ 200 to 500 μL) around the surface of the solid. The new low flow micronebulizers are well suited to analysis of the resulting single drop. The sampled depth can be as small as a few hundred atomic layers.

These VPD measurements are facilitated by two fortunate characteristics. First, the solid surface is hydrophobic. The single droplet remains as one bead as it is rolled around, so contaminants can be collected in a very small drop with little dilution. Second, most of the etched silicon is often removed as gaseous SiF_4 during a subsequent evaporation step. The resulting droplet does not have an exorbitant concentration of silicon matrix.

One hypothesis of the present work is that similar measurements can be done on other solids where the matrix remains in solution. This paper is meant to be an initial evaluation of this concept. It is more of a description of an experimental protocol to evaluate the feasibility of this concept rather than a final, definitive demonstration. It should be noted that these types of measurements with dissolved layers will not provide lateral resolution; LA-ICP-MS, SIMS and RBS remain the methods of choice for elemental analysis with both lateral and depth resolution.

Becker and co-workers[23] describe experiments that are also related to the present work. They dissolve thin layers of perovskite for elemental analysis by ICP-MS. One key difference from our experiment is that they dissolve the layers fully, whereas we seek ways to regulate the amount dissolved. We both exploit the high sensitivity and selectivity provided by magnetic sector mass spectrometers for these measurements. Other established sample preparation methods related to the present work include microwave extraction for "soft" dissolution of intact elemental species[24] and selective leaching procedures in geochemistry.[25]

EXPERIMENTAL

Dissolution Procedure for Steel Disks. The device used for partial dissolution is shown in Figure 1. The sample is a steel standard reference material (1167, low alloy steel, NIST). The goal is to compare measured and certified concentrations, and the same sample is etched and analyzed repeatedly. Therefore, a fresh sample surface is prepared by polishing the steel with various grades of emery paper (100 to 600 grit) and a Kimwipe, washing with deionized water, and drying. A Teflon O-ring (16 mm ID) is held tightly to the flat surface of the steel sample with two clamps. The etching acid (100 μL) is added evenly inside the Teflon O-ring. The system is covered in an empty dessicator and allowed to stand for 10 minutes at room temperature. The surface is then washed with one of three solvents (described below), and the wash is collected and diluted to 50 mL with the same solvent. The resulting solution was often diluted further by a factor of 100 before analysis.

All sample handling procedures were carried out in a clean room (Class 100, Microvoid Air Control), which greatly reduced the incidence of contaminated specimens.

Sample bottles were cleaned by acid washing in a solution of 7% HNO_3, 5% H_2O_2 and 6% HF for at least 24 hours prior to use.

Reagents. Fuming nitric acid (~ 70%) and concentrated hydrofluoric acid (~ 49%) were purchased from J. T. Baker and used without further purification. For the initial etching step, the fuming nitric acid was diluted with deionized water (18 MΩ, Barnstead Nanopure II, Newton MA) to concentrations of 5% to 50%. In some experiments, HF at 5% was also added to the nitric acid solutions. For dilution of the resulting mixture of etch acid + dissolved elements, three solvents were evaluated: deionized water, 1% nitric acid in deionized water, and 1% nitric acid + 0.5% hydrofluoric acid in deionized water. These acid mixtures were made fresh daily.

ICP-MS Measurements. A Finnigan Element 1 magnetic sector instrument[26-28] was used in medium resolution ($m/\Delta m = 4000$) for all elements. A platinum torch injector and platinum sampler and skimmer cones were used because of the HF in the samples. ICP operating conditions and sampling position were selected to maximize analyte ion signals for Li^+, In^+ and U^+ at a forward power of 1.2 kW.

Most measurements were done by solution nebulization using a Teflon microconcentric nebulizer (ES-20100, Elemental Scientific, Inc.) with natural uptake at ~100 μL/min. The nebulizer was operated in a small, Teflon, Scott-type double pass spray chamber at room temperature. It was rinsed briefly between samples with a small dose of 2% HF followed by the blank solution. In our experience, the HF rinse helps prevent loss of uptake by the nebulizer. Prompt removal of the sample uptake line and insertion into the new sample bottle also helps prevent inclusion of several air bubbles in the sample tube, which can also stop natural uptake.

The most abundant isotope of each element, including $^{56}Fe^{+}$, was monitored. The mass spectrometer was operated under electrostatic scanning conditions (mass window 175%, 40 samples per peak, 50 runs per sample, sample time 0.03 s, settling time 0.001 s). During these "E scans" the magnetic field was varied to values appropriate for each isotope monitored. Sensitivity was calibrated with external standard solutions that were prepared volumetrically. These calibrations included measurement of the major element Fe. The mass of sample removed was determined from the amount of Fe in the solutions. Blank count rates were subtracted from the gross signals from the sample.

Laser ablation measurements were done by line scans across the sample using a commercial system (LSX-100, CETAC Technologies, 266 nm, 1.5 mJ/pulse, spot diam. ~75 μm, repetition rate 10 Hz). SEM measurements (JSM-5910, JEOL Electron Optics, Tokyo, accelerating voltage 15 kV, specimen current ~ 0.08 nA) were also done on one of the etched samples.

RESULTS AND DISCUSSION

Effect of Composition of Etching Acid and Solvent on Dissolution of Steel. The first acid added inside the O-ring (Figure 1) attacks the sample surface and is called the etch acid. One set of experiments involves determining whether the removal rate could be manipulated by varying the composition of the etch acid. For the results presented below, this etch acid was 5% aqueous HF with various concentrations of aqueous HNO_3 between 5 and 50%.

Figures 2 and 3 show the dissolved amounts of the major element Fe and other elements for the various etch acids when three different aqueous solvents were used to

remove the dissolved elements and dilute the samples. These solvents were deionized water, 1% HNO_3 and 1% HNO_3 + 0.5% HF. Note that the etch acids were diluted greatly by the solvents, so the concentration of etch acid should not affect the sensitivity of the ICP-MS device for analyte ions.

For sake of discussion we call these plots dissolution curves. First we describe dissolution curves for Fe, Mn and Al (Figure 2). For these elements, the plots of mass dissolved vs. nitric acid concentration in etch solution are roughly linear. Addition of HF to the solvent displaces the lines upward. We believe the HF in the solvent promotes better retention in solution of material that was dissolved in the prior etching step. The HF additive to the solvent does not greatly affect the slopes of the lines.

For Ti and W (Figure 3a and b) the mass dissolved increases nonlinearly with nitric acid concentration unless HF is present in the solvent. For the refractory elements Nb and Ta (Figure 3c and d) the curves have two distinct regions of different slope. Without HF, little Nb or Ta is removed unless the HNO_3 concentration exceeds 25%. Use of HF in the solvent mitigates the problem for Nb and Ta but does not eliminate it.

It is our hypothesis that the shapes of these curves provide information about the removal rate of the analytes. Elements like Mn, whose dissolution curve has the same shape as that of the matrix (Fe in this case), are probably removed along with the matrix. The concentration ratio of trace element to major element in the resulting solution should resemble that in the solid sample. Addition of HF to the solvent causes the same, twofold signal increase for Fe, Mn and Al. Elements like Ta whose dissolution curve has a different shape than that of the major element may be removed to a different (probably lower) extent. This hypothesis is evaluated in the next sections.

Comparison of Measured and Certified Concentrations. These results are measured using the most effective solvent, 1% HNO_3 + 0.5% HF. For the well-behaved elements Mn, Al and W (Figure 4) the plots of measured elemental concentration vs. etch acid concentration are flat lines close to the certified concentrations. There are several high results in these curves that are attributed to occasional contamination of a particular sample. An example to be remembered for future discussion is the measurement for Al at 10% HNO_3, labeled with an asterisk in Figure 4b. Without HF in the solvent the measured concentrations for W were well below those expected (data not shown). Retention of W in solution commonly requires HF to form WF_n complexes.[10]

Measured concentrations for Ti, Nb, and Ta (Figure 5) are generally below the expected values. These elements are normally considered difficult to dissolve and to keep in solution. For Nb and Ta these low concentration values are consistent with the dissolution curves (Figure 3b and c), which are decidedly nonlinear. The dissolution curve for Ti is moderately so.

Note that the Ti result at 10% HNO_3 is too high in Figure 5a. This was the same solution as that which yielded the high result for Al (Figure 4b). Both Ti and Al are common constituents of dust, so it appears that this sample was contaminated in this fashion, even though these samples were handled in a clean room. Early dissolution experiments that were not done in clean room were plagued by such problems.

Estimate of Depth of Sample Removed. The depth of the layer removed from the steel sample is estimated as follows. The minimum amount of Fe removed for the lowest acid concentration in Figure 2a is approximately 5.8 mg. Using the density of the steel sample, the volume of solid removed is 0.74 mm^3. The cross sectional area inside the Teflon

O-ring (Figure 1) is 200 mm^3, so the average depth removed is ~ 4 μm. This value corresponds to approximately 20,000 layers of Fe atoms. From the intercept in Figure 2a, use of HF with 5% HNO_3 removes about 60,000 atomic layers, and the more concentrated acids remove still more Fe.

Laser Ablation ICP-MS and SEM Measurements. Discussions with metallurgists indicated that the problem elements like Ti, Nb and Ta are probably not distributed homogeneously throughout the steel samples. Instead, these elements are expected to be localized together in refractory grains such as carbides. To evaluate this explanation, laser ablation ICP-MS was used to examine the spatial homogeneity of the sample. Simple line scans show that a well-behaved element like Mn is distributed uniformly (Figure 6a), whereas the problem elements Ti, Nb and Ta are not (Figure 6b). Many of the signal spikes for these latter three elements are observed at the same time, which indicates they occur together in the sample. Even though the laser spot size (75 μm) is much larger than the probable size of the grains, the basic observations that these elements are distributed heterogeneously and that they tend to occur together in discrete spatial locations is still valid.

SEM was also used to examine the morphology of the etched samples. Figure 7 shows an image from a sample that was etched with 30% HNO_3 + 5% HF. The unetched surface is on the left with the etched surface to the right. The etching process has eroded the Fe and left discrete grains behind. X-ray spectra were measured from many such grains and the nearby, underlying dark areas. Typical spectra are shown for the four locations in Figure 8. Grains 1 and 2 appear light in Figure 7 because they are insulators. These grains contain Nb, Zr, Ti and possibly Ta, although Ta lines were difficult to distinguish from those for Si and Cu. In general, we did not see high levels of C in these grains. Sites 3 and 4 contain

little of these "difficult" elements and correspond mainly to Fe metal and iron oxide, respectively.

From this information, the low results for Ti, Nb and Ta can be explained. The etch acid attacks the Fe layers faster than the grains. Residues of the grains remain behind as the etch acid proceeds down into the sample. Elements that are present as atoms located mainly in the Fe are removed to the same extent as the Fe, so the signal ratio of that element to the Fe^+ signal reflects the overall composition of the solid. Elements located mainly in the grains dissolve more slowly than the Fe layers, so their measured concentrations are too low. Even if the total amount dissolved is larger than the recommended sample size, elements in the grains are underrepresented in the solution if the grains don't go into solution at the same rate as the surrounding iron atoms. In conventional dissolution, where the entire solid is brought into solution, such grains often persist until the final stages of the procedure and do not go into solution until the temperature is maximum.

CONCLUSIONS

For a complex matrix like steel, the low results for the problem elements in Figure 5 do indicate a problem for the original objective of this work, quantitative multielemental analysis of layers of solids. However, it is interesting to note that this partial dissolution procedure also provides information about the speciation of the elements in the solid, which may have other practical applications. It would also be valuable to evaluate whether heating the solid sample or some of the new microwave extraction procedures, like those used for "soft" extraction of intact compounds from solids,[16] would make the dissolution rate more uniform yet still slow enough for depth resolution for the problem elements found in this study.

ACKNOWLEDGMENT

Murray Kaplan, Anna Carmo and Jeanne Stewart in the Department of Food Science and Human Nutrition, Iowa State University, provided access to the clean room. CETAC Technologies provided the laser ablation system, and Spex Certiprep donated the solution standards. Paul Berge gave advice on the probable chemical forms of the elements in the steel sample. Fran Laabs provided the SEM results.

This manuscript has been authored by Iowa State University of Science and Technology under Contract No. W-7405-Eng-82 with the U. S. Department of Energy. This research was supported by the Chemical and Biological Sciences Program, Office of Basic Energy Sciences. The U. S. Government retains, and the publisher, by accepting the article for publication, acknowledges that the United States Government retains a non-exclusive,

paid-up, irrevocable, worldwide license to publish or reproduce the published form of this manuscript, or allow others to do so, for U. S. Government purposes.

SAFETY NOTE

The acids used in these procedures are potentially dangerous. Hydrofluoric acid especially must not be used without proper training and protection, including an HF-specific spill kit and salve.

REFERENCES:

1. Y. C. Sasaki, K.Hirokawa, Appl. Surface Sci. **47**, 371 (1991).
2. R. Klockenkamper and A von Bohlen, Spectrochim. Acta Part B **44B**, 461 (1989).
3. J. Knoth, H. Schwenke and U. Weisbrod, Spectrochim. Acta Part B **44B**, 477 (1989).
4. A. Bengston, "Depth Profile Analysis," in *Glow Discharge Plasmas in Analytical Spectroscopy*, R. K. Marcus and J. A. C. Broekaert, Eds. (Wiley, Chichester UK, 2003), Ch. 5.
5. R. Payling P. Chapon, K. Shimizu, R. Passetemps, A. Jadin, Y. Bourgeois, K. Crener, M. Aeberhard and J. Michler, "Surfaces, Thin Films and Coatings," in *Glow Discharge Plasmas in Analytical Spectroscopy*, R. K. Marcus and J. A. C. Broekaert, Eds. (Wiley, Chichester UK, 2003), Ch. 8.
6. K. Wagatsuma, "Comparison of Glow Discharge Atomic Spectrometry with Other Surface Analytical Methods," in *Glow Discharge Plasmas in Analytical Spectroscopy*, R. K. Marcus and J. A. C. Broekaert, Eds. (Wiley, Chichester UK, 2003), Ch. 9.

7. A. Raith, R. C. Hutton and J. C Hueneke, J. Anal. Atomic Spectrom. **8**, 867 (1993).

8. L. M. He, K. Putyera, J. D. Meyer, L. R. Walker and W. Y. Lee, Metallurgical Matls. Trans. A: Phys. Metallurgy Matls. Sci. **33A**, 3578 (2002).

9. L. A. De las Heras, O. L. Actis-Dato, M. Betti, E. H. Toscano, U. Tocci, R. Fuocco and S. Giannarelli, Microchem. J. **67**, 333 (2000).

10. I. T. Spitsberg and K. Putyera, Surface Coatings Technol. **139**, 35 (2001).

11. I. Horn, M. Guillong and D. Günther, Appl. Surface Sci. **182**, 91 (2001).

12. M. Guillong and D. Günther, Spectrochim. Acta Part B **56B**, 1219 (2001).

13. K.-P. Lieb, Contemp. Phys. **40**, 385 (1999).

14. E. J. Knystautas, "New Trends in Rutherford Backscattering Spectrometry," in *Ion Beam Analysis of Surfaces and Interfaces of Condensed Matter Systems*, P. Chakraborty, Ed. (Nova Science, New York, 2003), p. 59.

15. B. Hattendorf, C. Latkoczy and D. Gunther, Anal. Chem. 75, 341A (2003).

16. R. Bock, *A Handbook of Decomposition Methods in Analytical Chemistry*, Wiley, 1979, p. 197 and 199.

17. I. Jarvis, "Sample Preparation for ICP-MS," in *Handbook of ICP-MS*, K. E. Jarvis, A. L. Gray and R. S. Houk, Blackie: London, 1992, Chap. 7.

18. G. Petzow and G. Elssner, Etching, and A. O. Benscoter, "Carbon and Alloy Steels," in *ASM Handbook: Metallography and Microstructures*, Vol. 9, ASM International, 1985, pp. 60-63 and 169-173.

19. A. Krushevzka, S. Tan, M. Passer and X. R. Liu, J. Anal. Atomic Spectrom. **15**, 1211 (2000).

20. E. Jones Ferrero and D. Posey, J. Anal. Atomic Spectrom. **17**, 1194 (2002).

21. A. Danel, T. Lardin, C. Giroud and F. Tardif, Matls. Sci. Eng. B102, 213 (2003).

22. M. B. Shabani, Y. Shiina, F. G. Kirsicht and Y. Shimanuki, Matls. Sci. Eng. B102, 238 (2003).

23. S. F. Boulyga, H.-J. Dietze, and J. S. Becker, J. Anal. Atomic Spectrom. **16**, 598 (2001).

24. V. O. Schmitt, J. Szupunar, O. F. X. Donard and R. Lobinski, Canad. J. Anal. Sci. Spectrosc. **42**, 41 (1997).

25. G. E. M. Hall, J. Geochem. Exploration **61**, 1 (1998).

26. I. Feldmann, W. Tittes, N. Jakubowski, D. Stuewer and U. Giessman, J. Anal. Atomic Spectrom. 9, 1007 (1994).

27. L. Moens and N. Jakubowski, Anal. Chem. **70**, 251A (1998).

28. R. S. Houk, "Elemental Speciation by ICP-MS with High Resolution Instruments," in *Handbook of Elemental Speciation, Techniques and Methodology*, R. Cornelis, J. A. Caruso, H. M. Crews and K. Heumann, Eds., (Wiley, Chichester UK, 2003), Ch. 5.7.

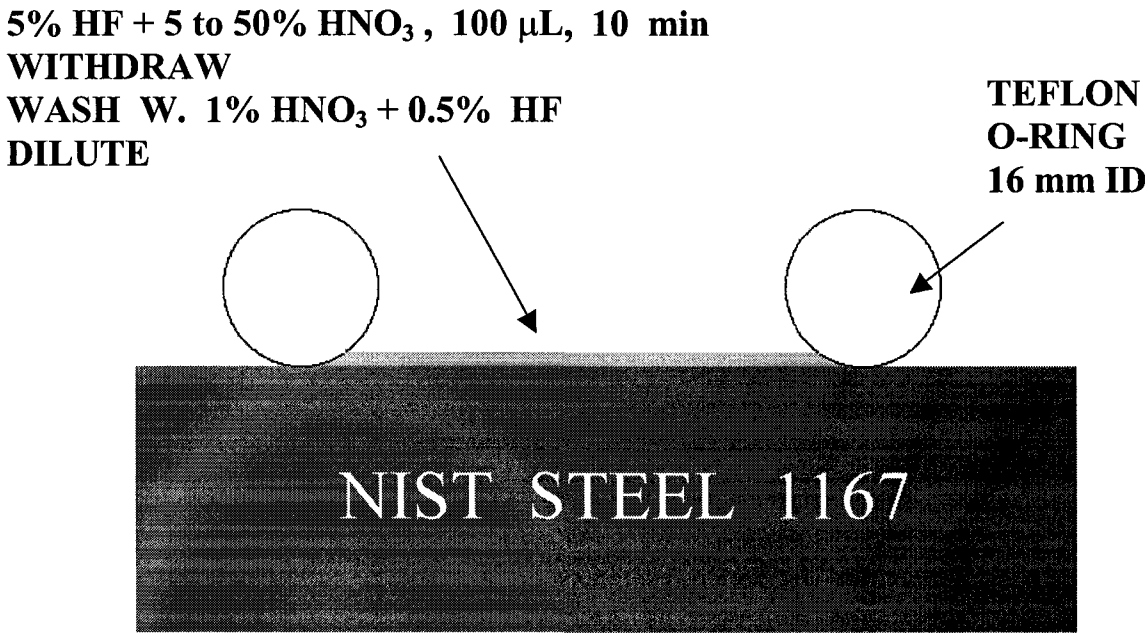

Figure 1. Side view of controlled dissolution apparatus for the steel disk sample.

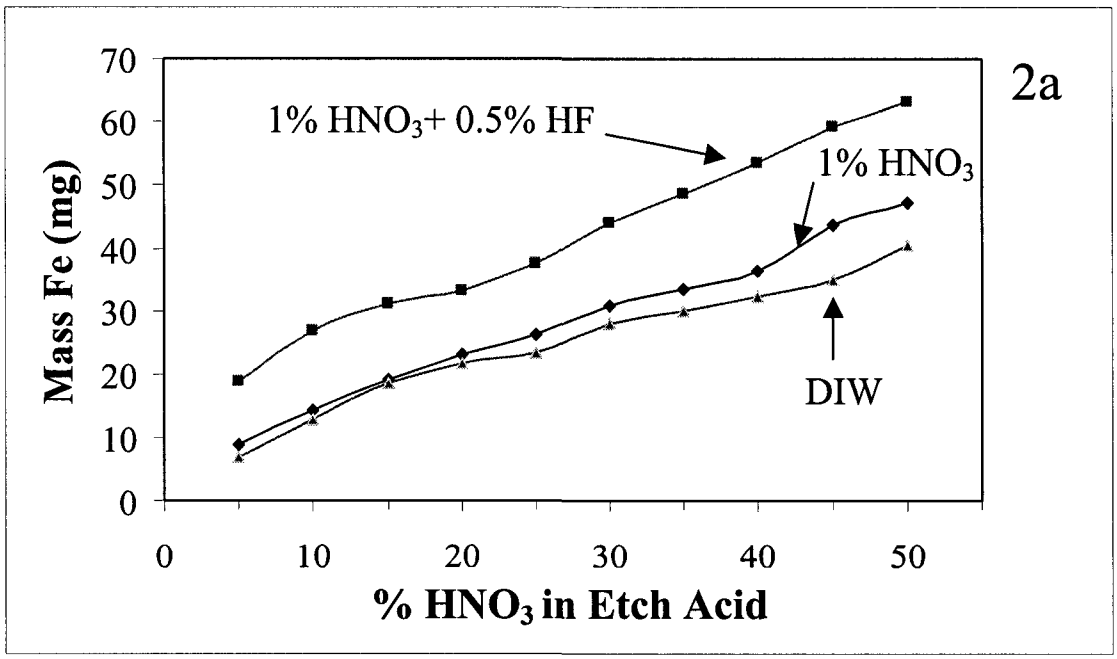

Figure 2a, b and c. Dissolution curves for Fe, Mn, and Al in steel using etch acids of various HNO_3 concentrations with three solvents. Each etch acid also contained 5% HF.

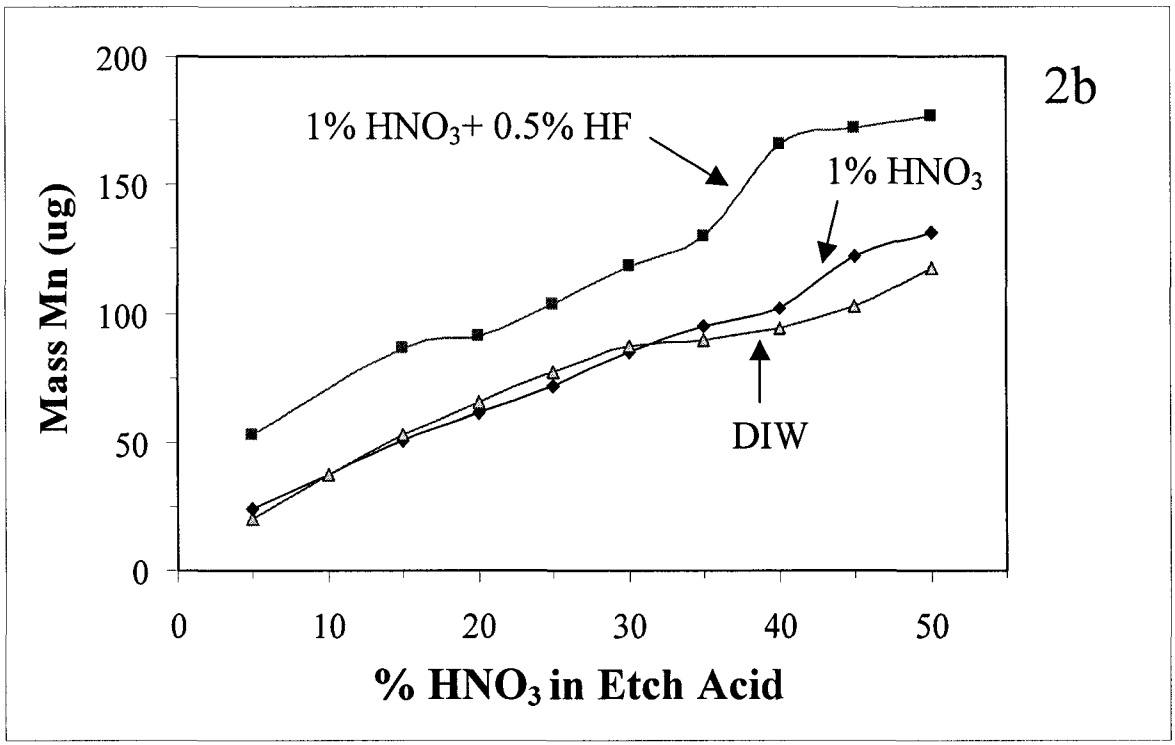
200
150
100
50
0
Mass Mn (ug)
1% HNO3+ 0.5% HF
1% HNO3
DIW
0
10
20
30
40
50
% HNO3 in Etch Acid

2b

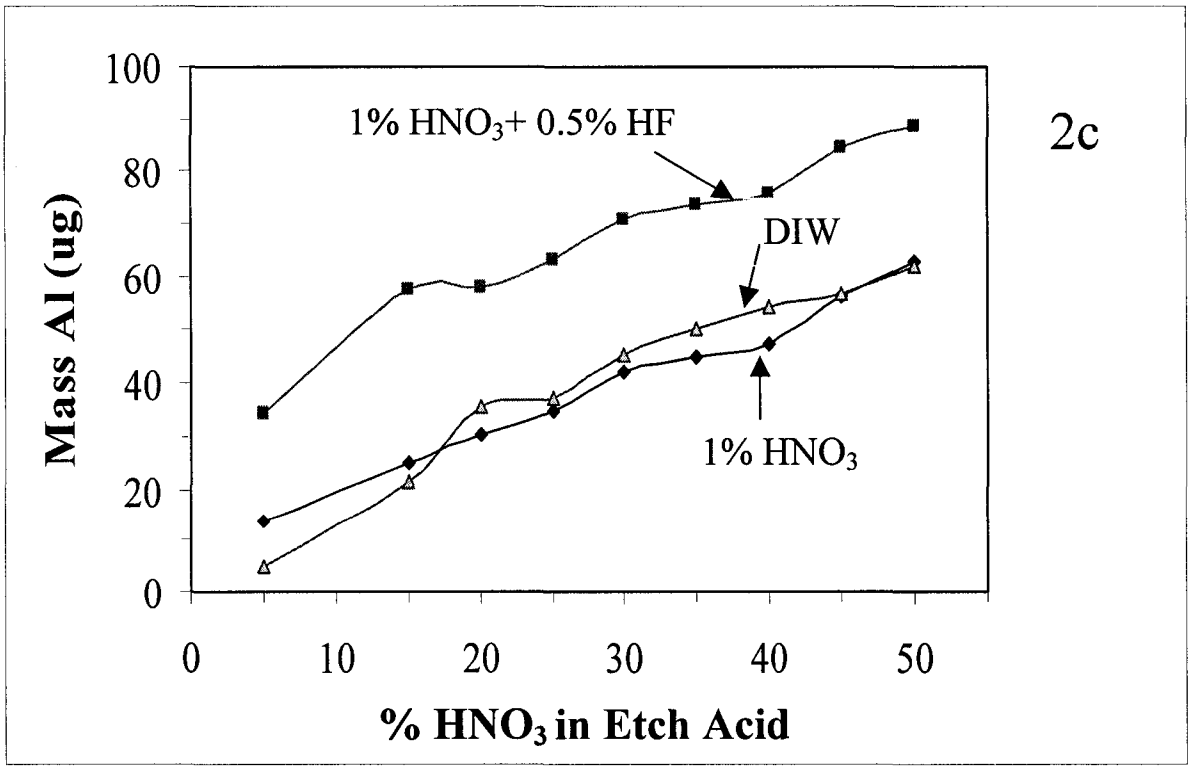
100
80
60
40
20
0
Mass Al (ug)
1% HNO3+ 0.5% HF
DIW
1% HNO3
0
10
20
30
40
50
% HNO3 in Etch Acid

2c

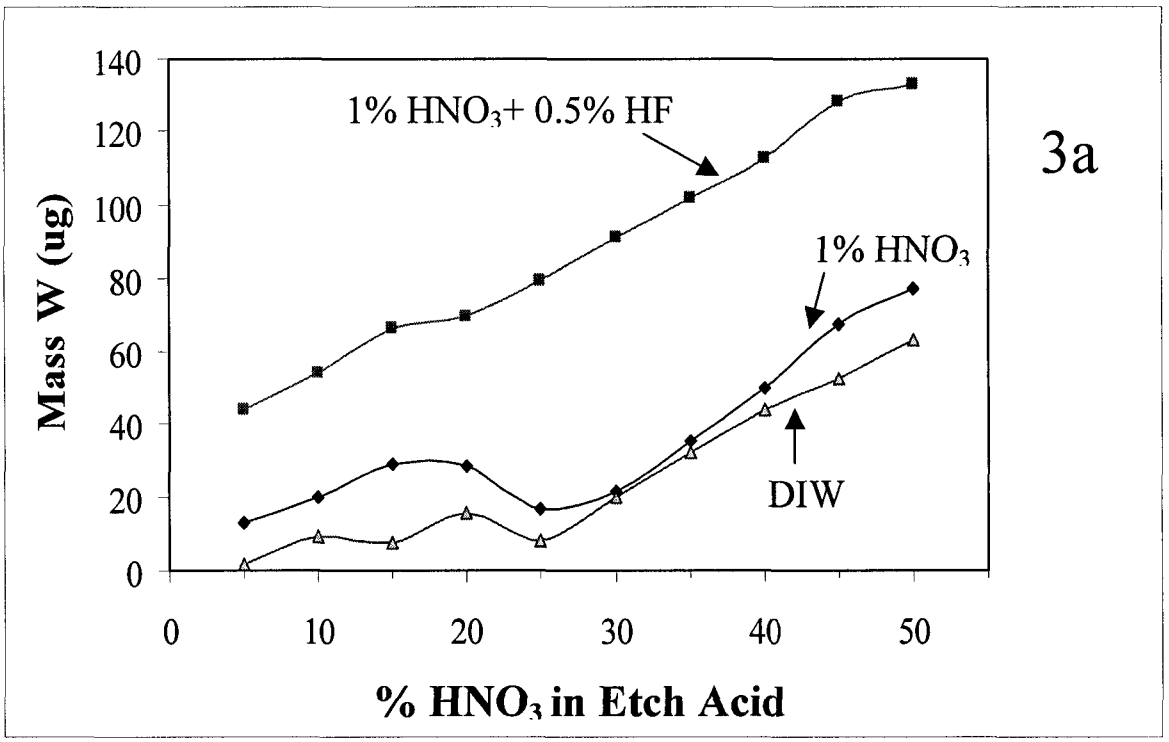

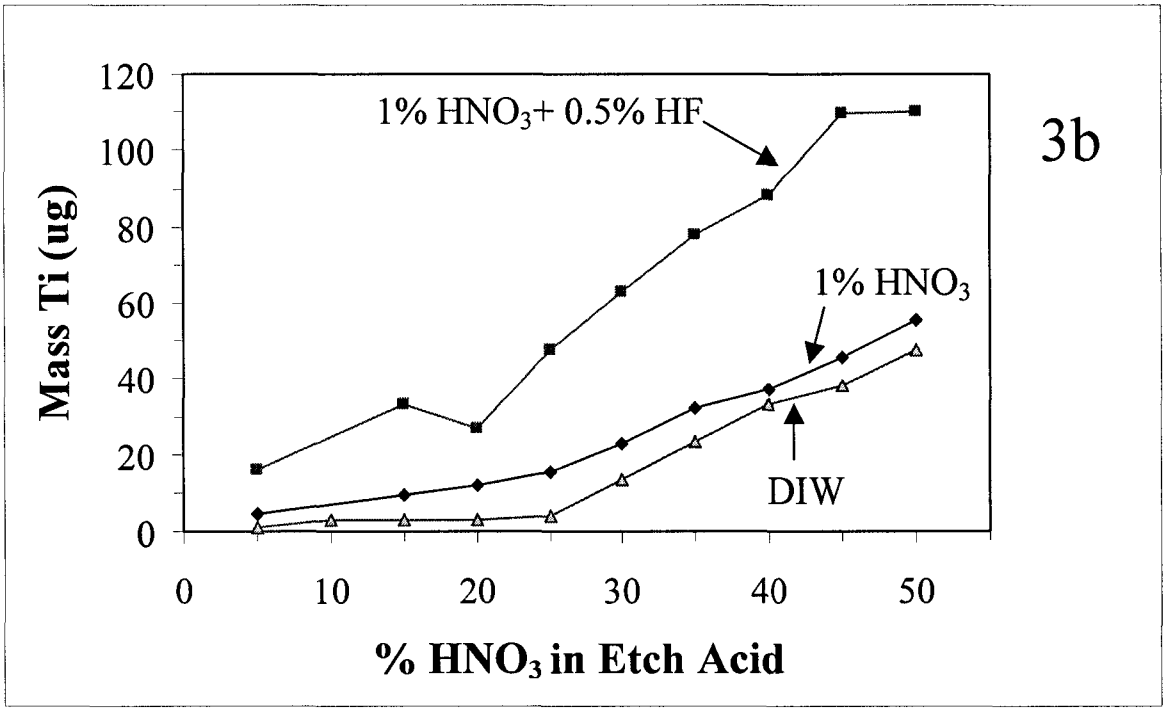

Figure 3a, b, c and d. Dissolution curves for W, Ti, Nb and Ta in steel using various etch acids and solvents. Note the two separate regions with different slopes, especially for Ta. HF in the solvent makes the curve for W linear and puts more Nb and Ta into solution at low HNO_3 concentrations.

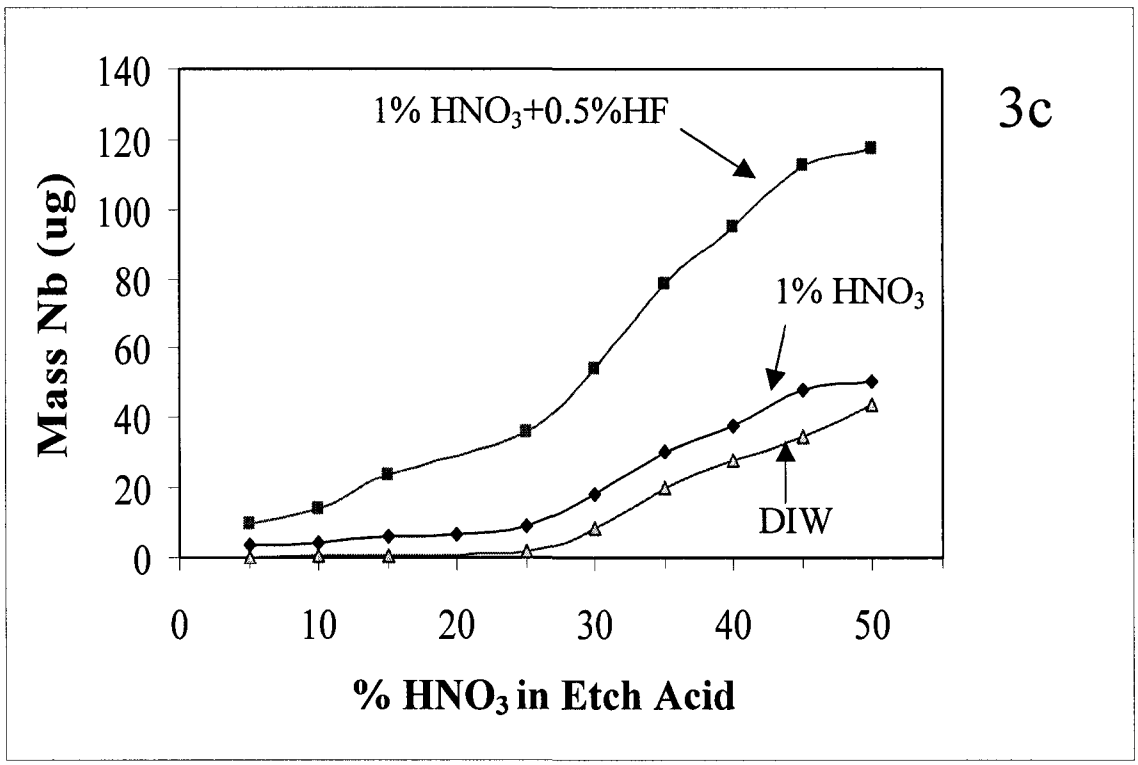
140
120
100
80
60
40
20
0
Mass Nb (ug)
1% HNO3+0.5%HF
1% HNO3
DIW
0
10
20
30
40
50
% HNO3 in Etch Acid

3c

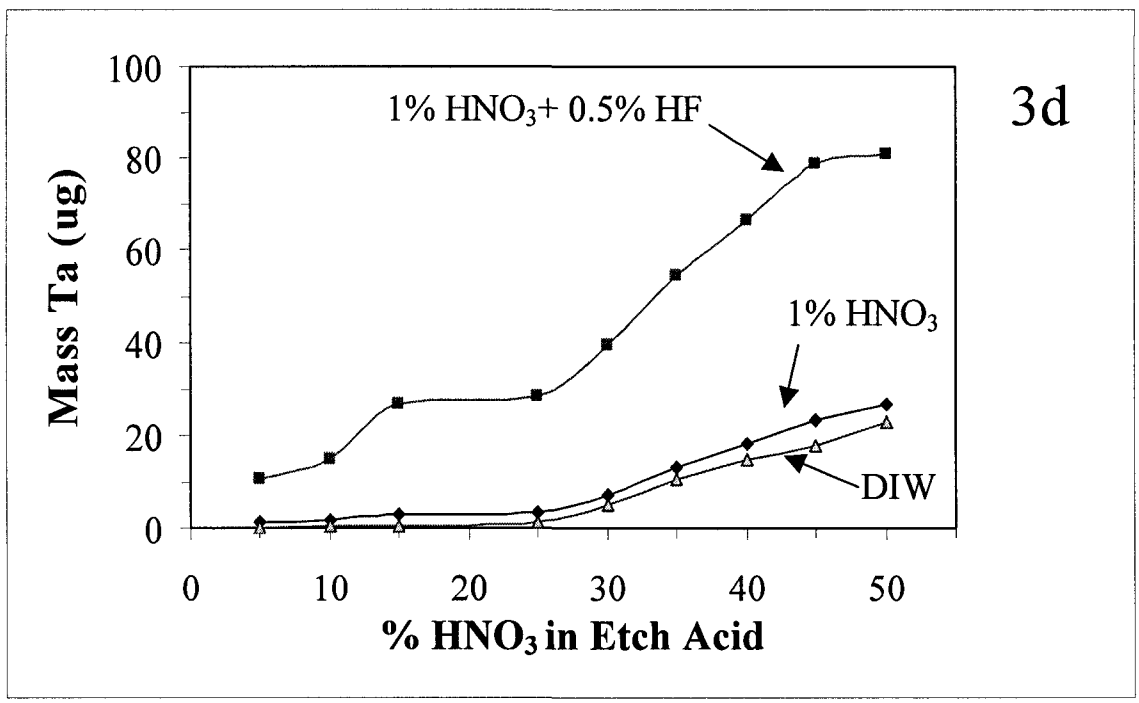
100
80
60
40
20
0
Mass Ta (ug)
1% HNO3+ 0.5% HF
1% HNO3
DIW
0
10
20
30
40
50
% HNO3 in Etch Acid

3d

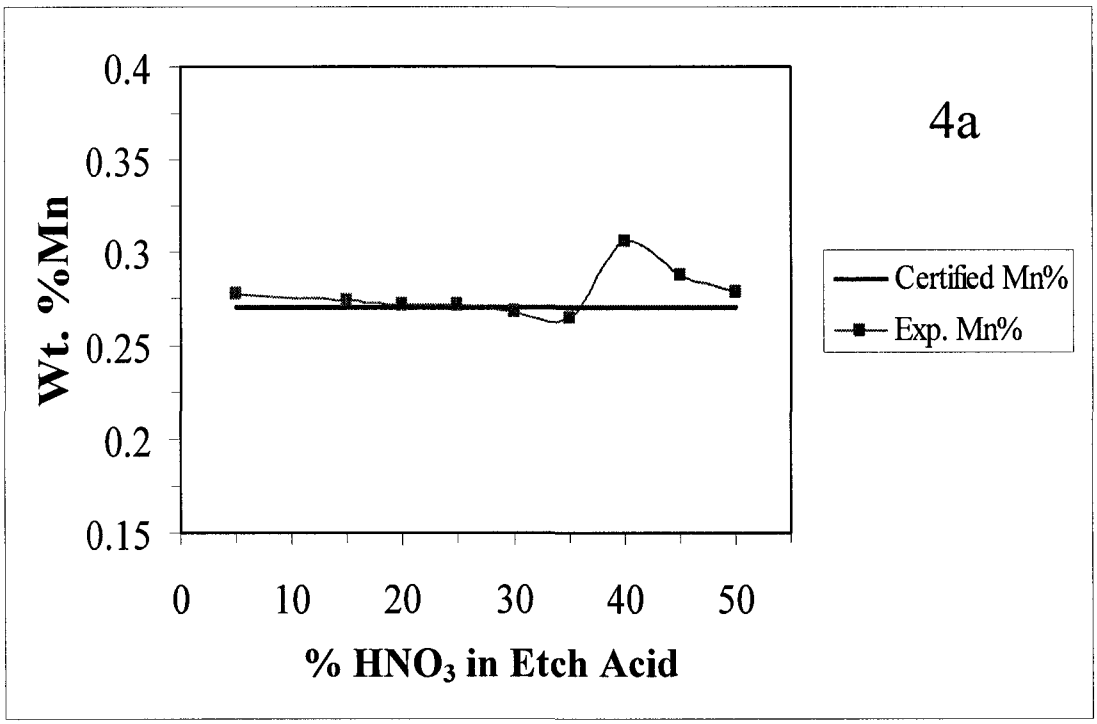

Figure 4a, b and c. Comparison of measured and certified concentrations for "well-behaved" elements Mn, Al and W in steel at various concentrations of HNO_3 etch acid. The solvent is 1% HNO_3 + 0.5% HF.

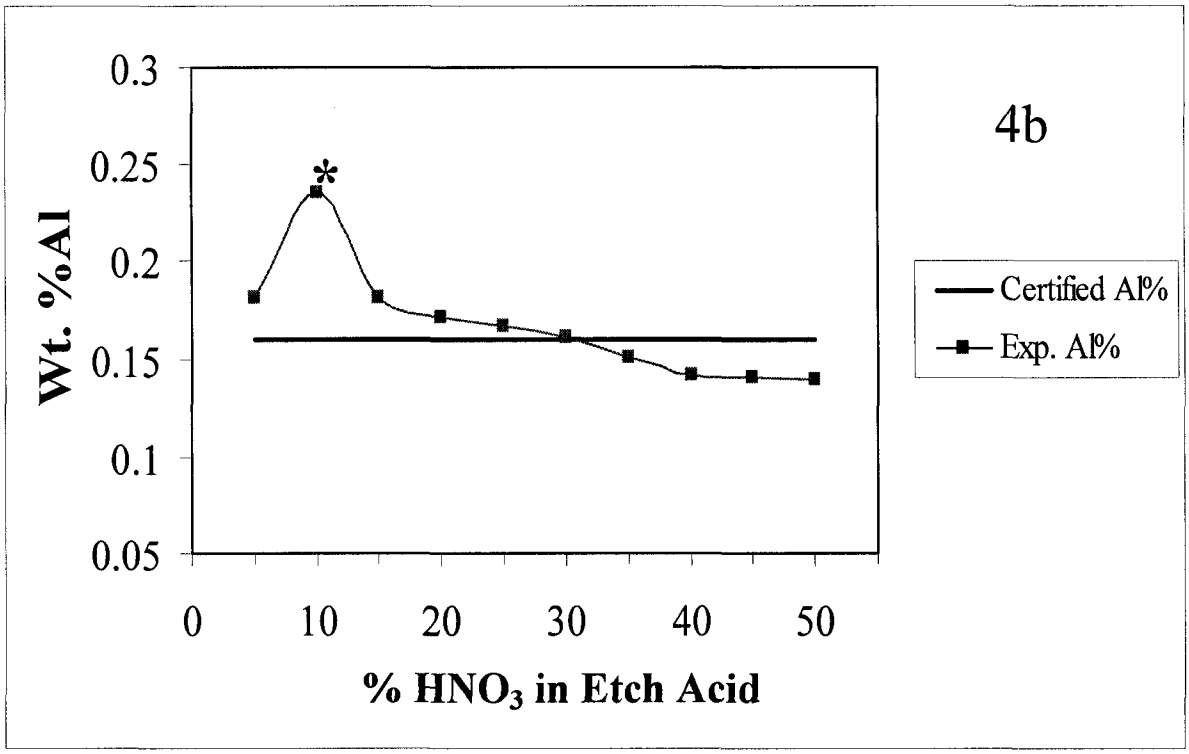
0.3
0.25
0.2
0.15
0.1
0.05
Wt. %Al
*
0
10
20
30
40
50
% HNO3 in Etch Acid
Certified Al%
Exp. Al%
4b

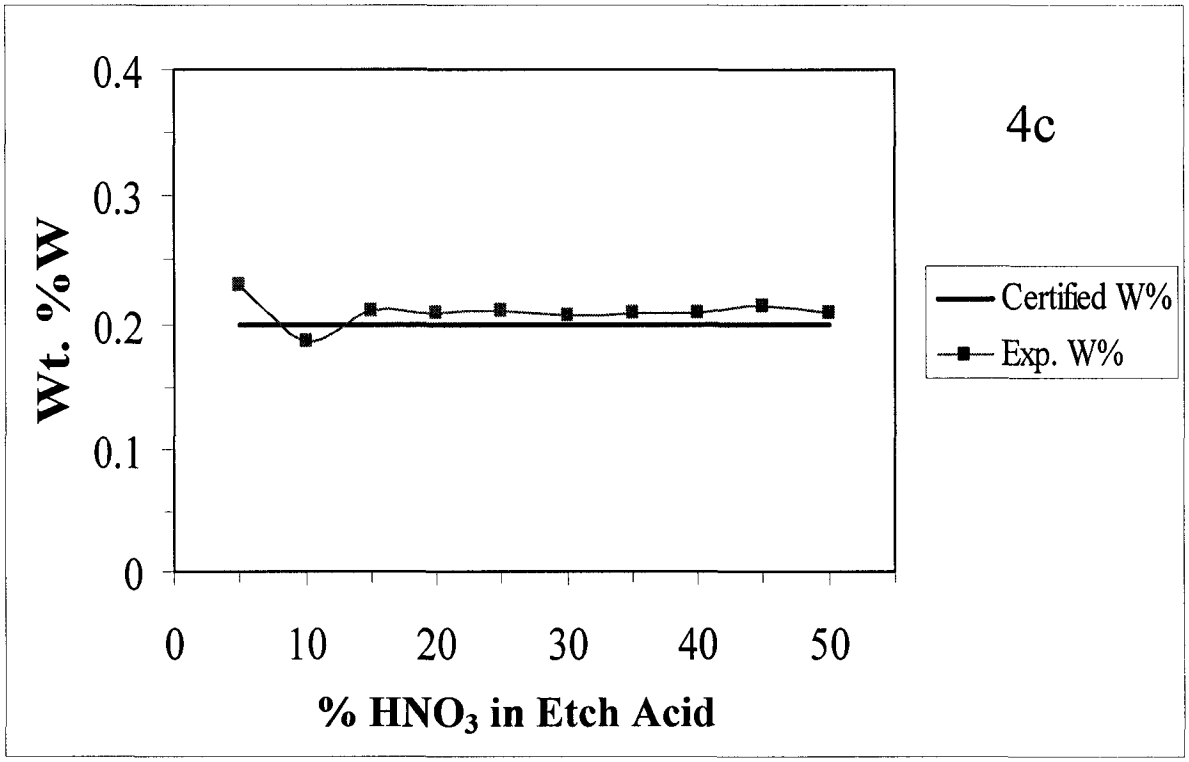
0.4
0.3
0.2
0.1
0
Wt. %W
0
10
20
30
40
50
% HNO3 in Etch Acid
Certified W%
Exp. W%
4c

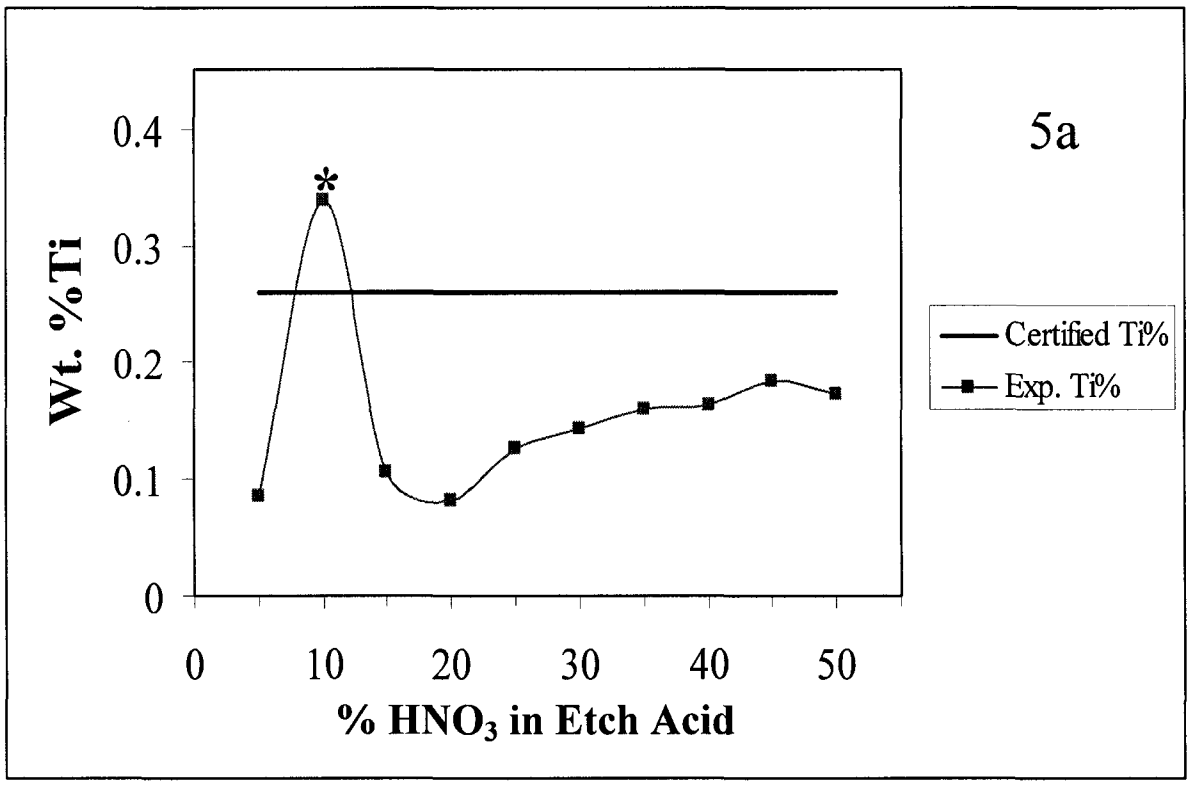

Figure 5a, b and c. Comparison of measured and certified concentrations for "problem" elements Ti, Nb and Ta in steel at various concentrations of HNO_3 etch acid. The solvent is 1% HNO_3 + 0.5% HF.

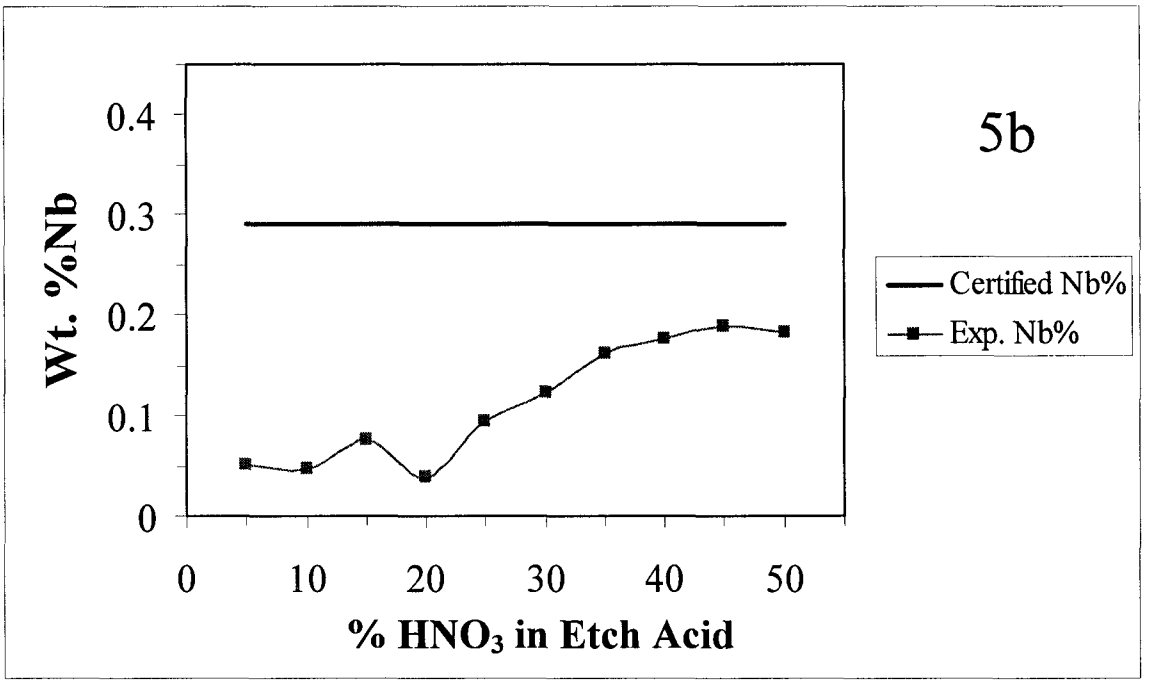
5b
Wt. %Nb
0.4
0.3
0.2
0.1
0
0
10
20
30
40
50
% HNO3 in Etch Acid
Certified Nb%
Exp. Nb%

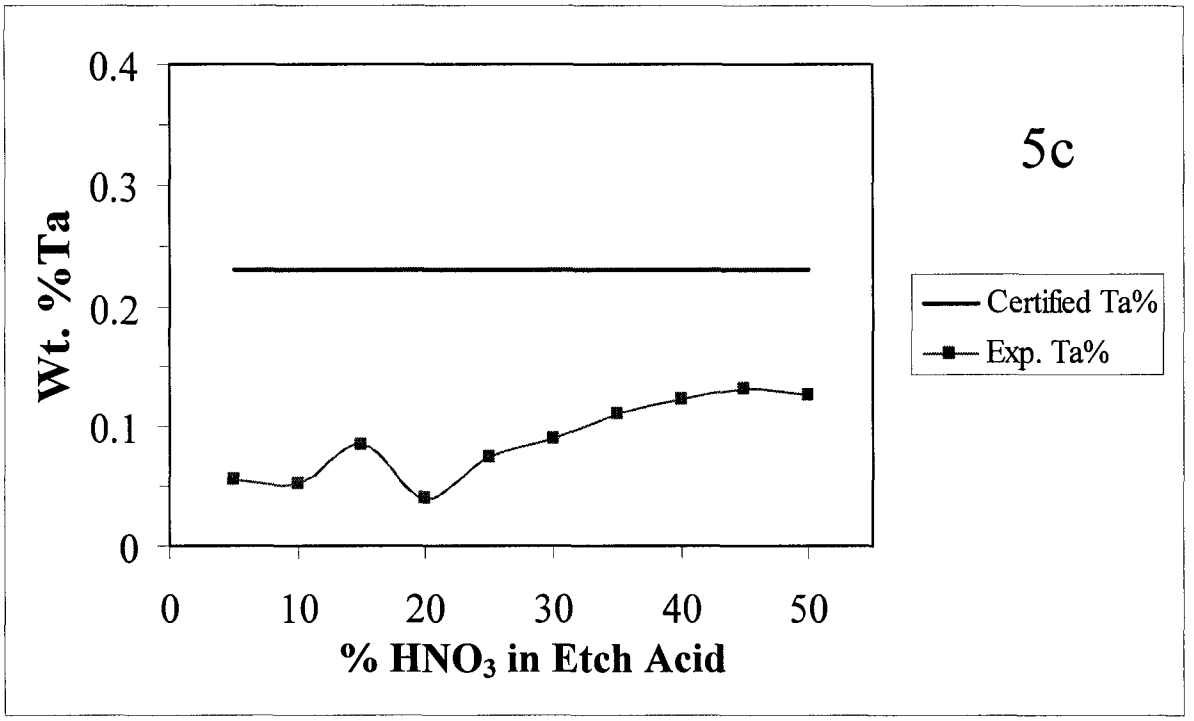
5c
Wt. %Ta
0.4
0.3
0.2
0.1
0
0
10
20
30
40
50
% HNO3 in Etch Acid
Certified Ta%
Exp. Ta%

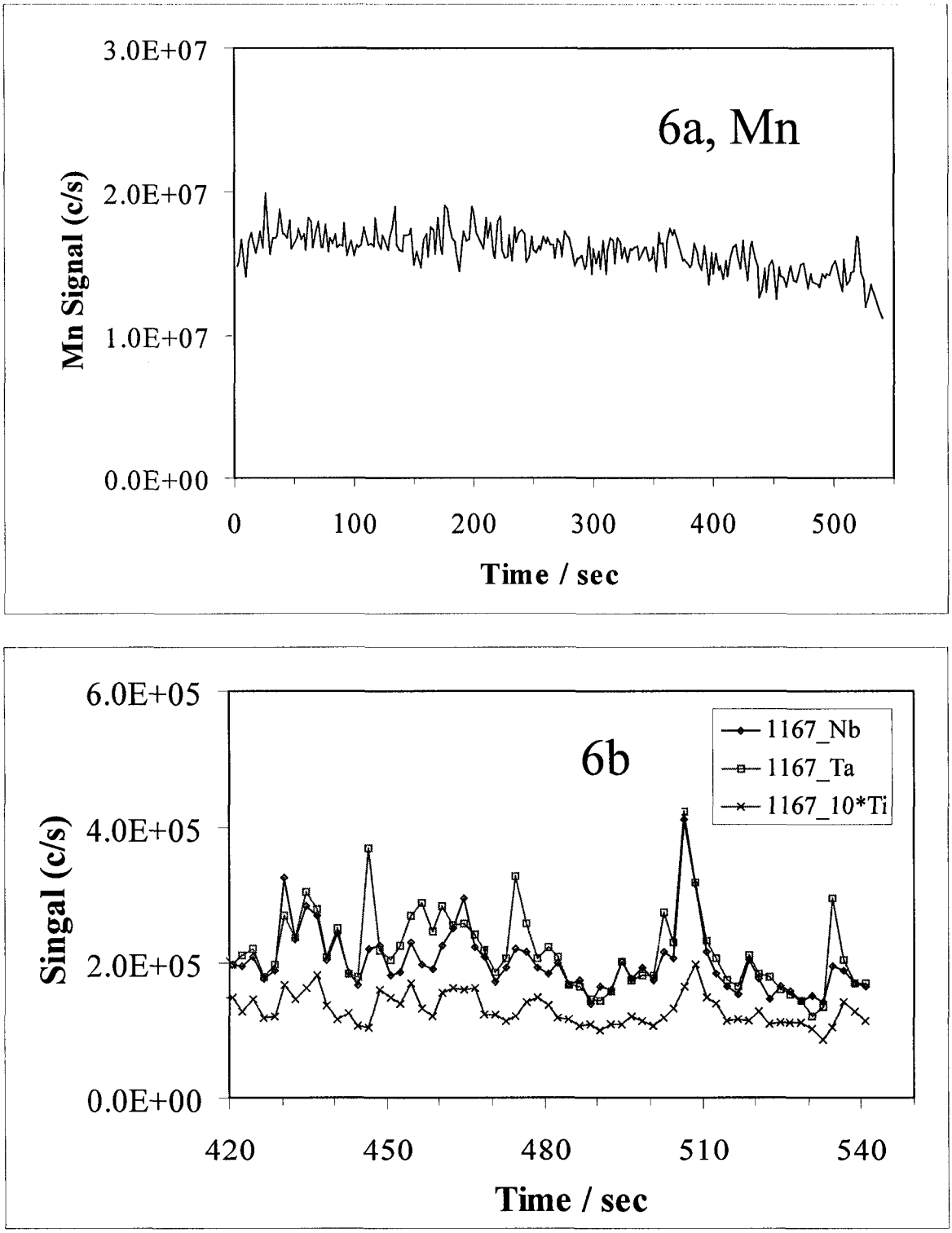

Figure 6a and b. Laser ablation ICP-MS measurements for well-behaved element Mn (6a) and problem elements as Nb, Ta and Ti (6b).

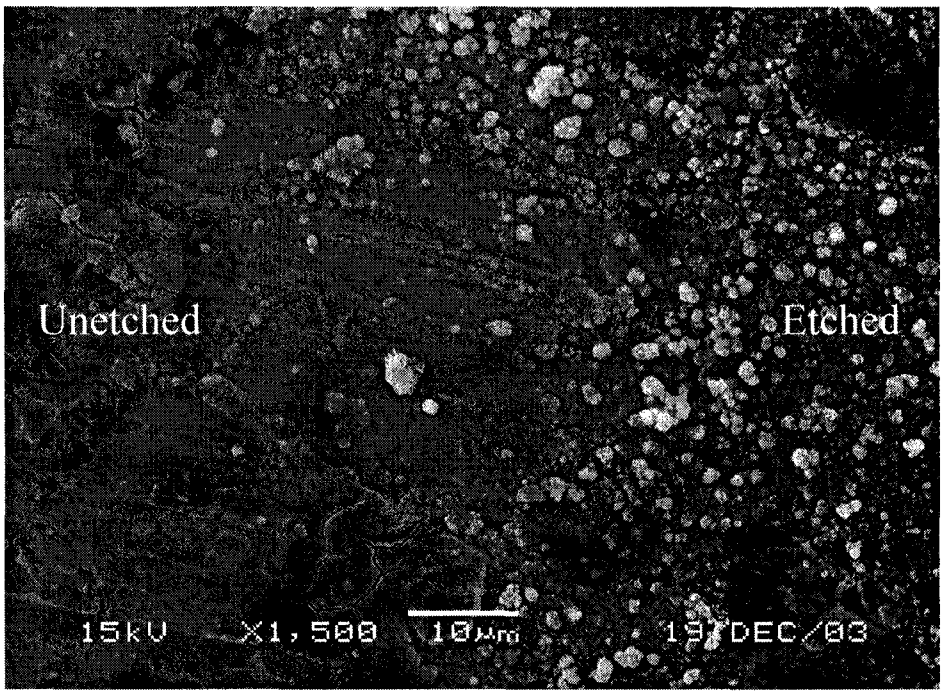

7A

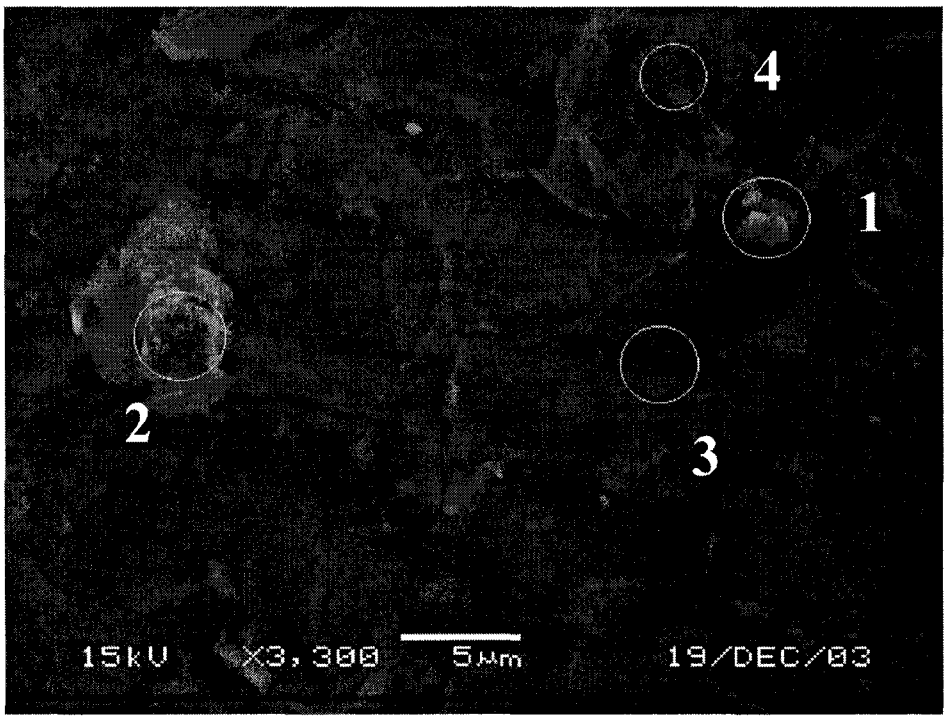

7B

Figure 7A and B. SEM images of etched steel sample. A) The unetched area is shown at the left, with the edge of the etched area on the right. Note the grains remaining in the etched area. B. Magnified image showing four areas analyzed subsequently: small grain (1), large grain (2), flake (3) and iron floor (4). The areas analyzed are roughly equal to the sizes of the circles shown.

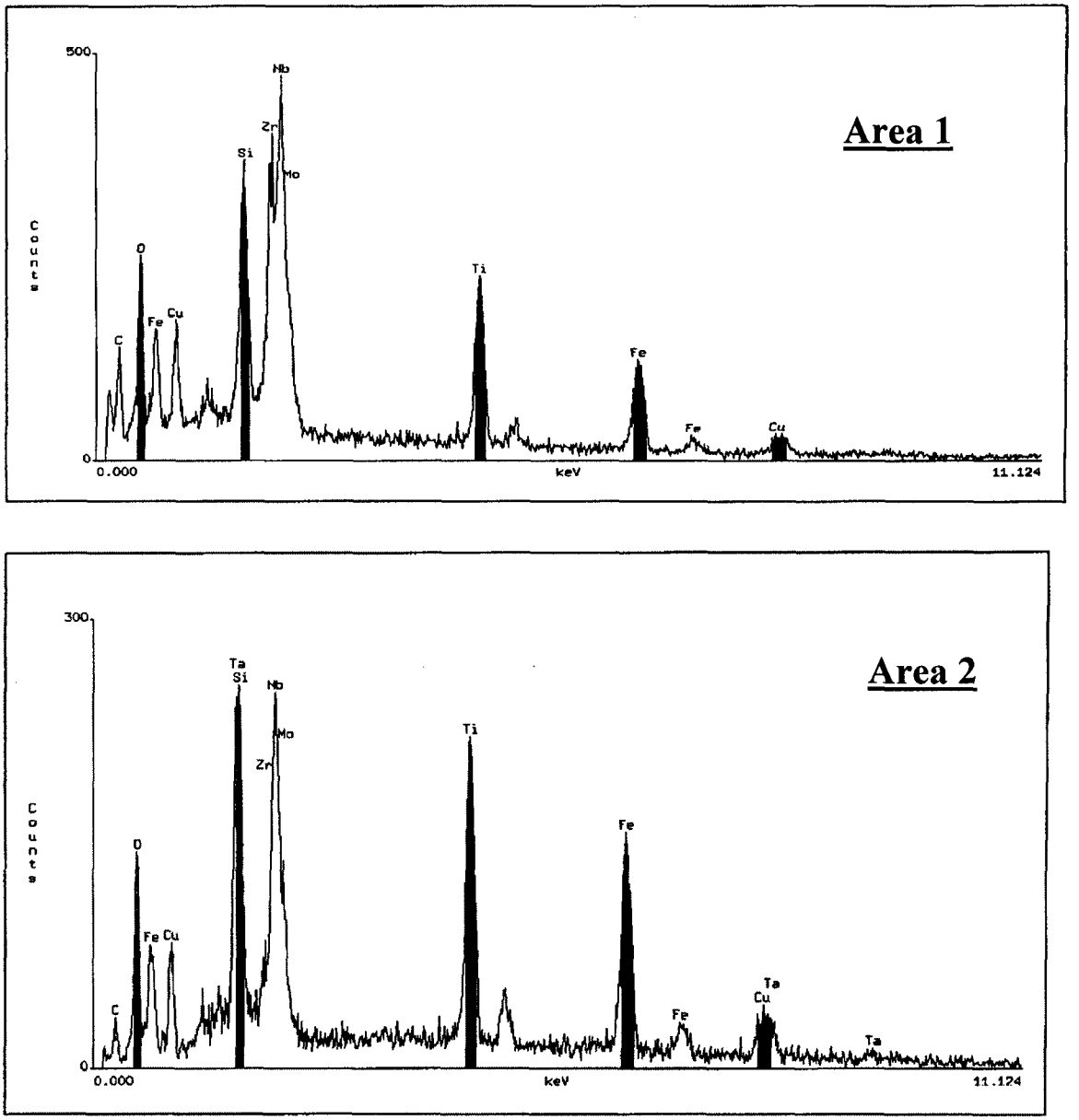

Figure 8. X-ray spectra from localized sections identified by numbers in Figure 7. Lines for certain elements were highlighted by the SEM software.

Fig. 8

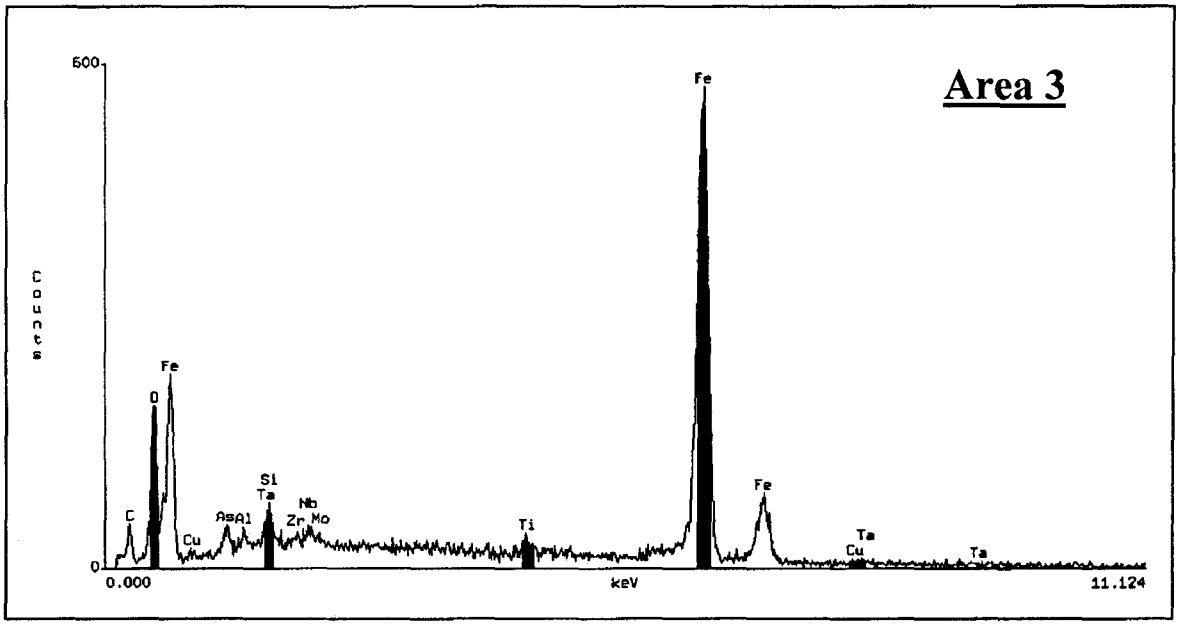
Area 3
600
0
Counts
C
O
Fe
Cu
As
Al
Si
Ta
Nb
Zr
Mo
Ti
Fe
Ta
Cu
Ta
0.000
keV
11.124

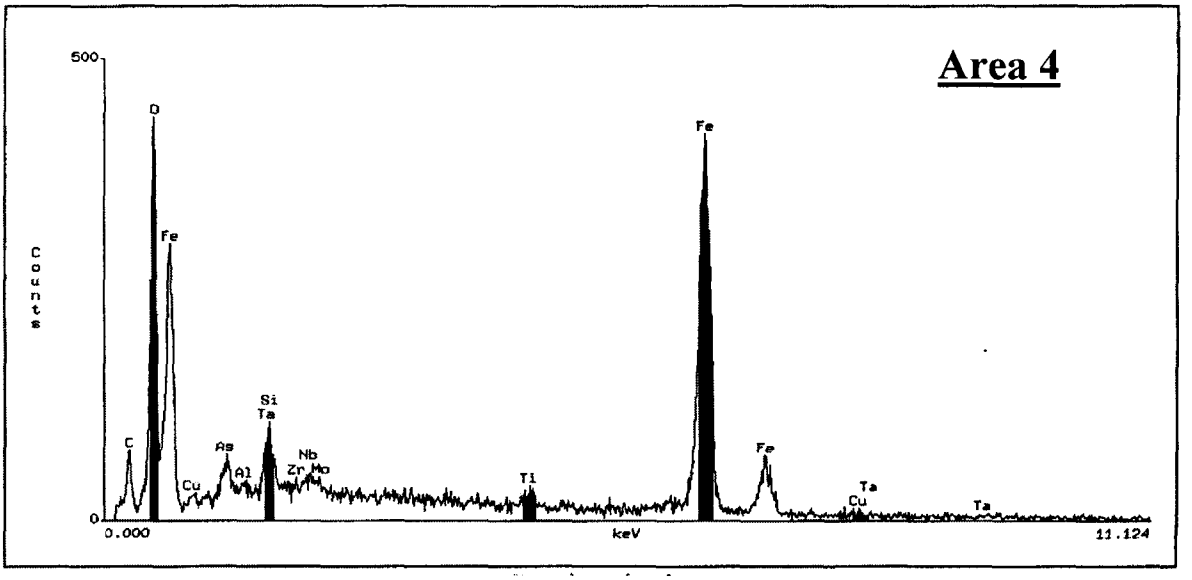
Area 4
500
0
Counts
C
O
Fe
Cu
As
Al
Si
Ta
Nb
Zr
Mo
Ti
Fe
Ta
Cu
Ta
0.000
keV
11.124

CHAPTER 3

The BEHAVIOR OF BACTERIA IN THE ICP

A paper to be submitted to *Analytical Chemistry*

Fumin Li, Daniel W. Armstrong and R. S. Houk

ABSTRACT

The combination of perfusion chromatography (PC) and inductively coupled plasma mass spectrometry (ICP-MS) is found to be a general and fast way to monitor metal incorporation in bacteria during bioremediation. Two questions involving this approach must be addressed: how can it be used to accurately determine the amount of uranium removed by bacteria, and how can the sensitivity be calibrated with an inorganic U standard solution? The behavior of *B. subtilis* in the ICP is investigated by monitoring the time-resolved signals of U, which is incorporated intrinsically in the cells. When U^+ signals from samples containing intact *B. subtilis* are measured directly by ICP-MS, occasional U^+ spikes are observed. The positive U^+ spikes suggest that bacteria behave like large particles in the ICP. The fact that desolvation of the bacteria aerosol does not eliminate the spikes implies that they are not due to solvation or a wet aerosol. The effect of sonication on the U^+ signals is investigated. Sonication of bacteria, i.e. *B. subtilis*, for 5 minutes increases the U^+ response by 30% compared to the untreated sample. Further increase in the sonication time does not further enhance the U^+ signal. The chromatographic results from the PC of a 10 ppb U

standard, partially lysed and fully lysed bacteria samples show that the intracellular U-bound species is released by sonication and is small in size because its retention time is similar to that of the inorganic U standards. Finally, other aspects of introducing intact bacteria into the ICP are of analytical interest. The retention of intact bacteria on the PEEK tubing is also investigated by flow injection analysis (FIA).

INTRODUCTION

Inductively coupled plasma mass spectrometry (ICP-MS) has been widely used for accurate trace and ultra-trace elemental quantification in the semiconductor industry,[1] and for biological[2] and environmental samples.[2-3] The measured signal from the unknown is compared with that of a standard containing a known amount of the analyte element or isotope. Different forms of the analyte are assumed to give the same sensitivity.[4] However, this assumption may not be accurate for trace elements involved with complex biological systems, e.g. cells and tissues. These elements may not behave the same way as the inorganic standards in the ICP. For simplicity, the ionization behavior of the analyte in the ICP hereafter refers to the whole process of vaporization, atomization and ionization (or VAI).

Strategies using trace metals in intact cells from cultures have gained popularity in areas such as proteomics,[5] toxicology[6] and various biological processes[7] to understand the role of minor or trace elements. Both the amounts of these trace elements[10] and the metal speciation,[8-9] i.e. oxidation state, chemical ligand association and complex forms, are important to understand toxicological behavior. The methods used to quantify trace elements

in cells or tissues often involve digestion in the first step, such as acid digestion,[10-12] followed by analytical measurements. The quantification is then carried out by using inorganic metal standards. Kasia et al.[12] investigated the aluminum binding in Al(III)-treated neuroblastoma cells with various hyphenated techniques, including SEC-ICP-MS, CE-ICP-MS and LC/ESI-MS. The cells were lysed and the supernatant was analyzed.

In a previous paper,[13] we coupled PC[14-15] separation with ICP-MS,[16-17] as a fast, general method to monitor the incorporation of heavy metals, namely uranium, during bioremediation by bacteria. Two questions that remain are: how much uranium has been removed by bacteria, and can the U sensitivity be calibrated with an inorganic U standard solution? If the answer is yes in the latter case, one assumption is that the VAI of uranium from a reference aqueous standard is the same as or at least similar to that of uranium, incorporated in the bacteria, whether it is extracellular or intracellular. This may not be the case because bacteria are much larger particles, 0.5 - 4 μm in diameter, compared to the particulates arising from fine aerosols from aqueous solutions, which will be discussed in detail later. In other words, the ionization efficiency or the behavior of bacteria in the ICP affects the U^+ sensitivity, which in turn can cause inaccurate quantification.

There have been several efforts to measure analytical signals from intact bacteria in the ICPs. Kawaguchi et al.[18-20] developed an individual particle analyzer, using ICP atomic emission spectroscopy (AES), to determine the elemental content in individual airborne particles. They measured the pulse height distribution of fast transient signals emitted from the ICP. A related method was used to measure the calcium content in individual biological cells continuously in real time.[21] This method was based on the detection of the emission of a calcium ion line, Ca(II), at 393.4 nm. The cell samples were dissolved in 70% aqueous

ethanol, which did not lyse the cells and preserved the cell structure and components, according to their study. The organic solvent, however, did puncture the cell membranes as can be seen from the Ca emission signal profile from mouse fibroblast cells. The small random spikes in the background were probably partially due to the emission of free calcium, released from holes, penetrated by organic solvent, in the cell membranes. The calcium content in biological cells was then quantified by using an inorganic calcium acetate, assuming that an equal amount of calcium in cells and the inorganic standard generated the same pulse heights.

Despite promise as an analytical method, it could not be completely adapted to our current research for the following reasons. Firstly, the sample in their study was in organic solvent, whereas ours are in saline buffer, vital to keep bacteria intact. The incorporated uranium may otherwise leach out if bacteria are kept in organic solvent. Secondly and more importantly, using an inorganic calcium standard to calibrate the calcium content in biological cells may not be accurate. Furthermore, it is impractical, if not impossible, to find bacterial standards with known amount of trace elements as calibrants. In the current study, we try to investigate the calibration in detail. Sonication is utilized to lyse the bacteria and the lysates are immediately analyzed by ICP-MS to study its effect on U^+ signals from intact cells.

The ionization behavior of analytes in the ICP is of fundamental importance, especially for quantification. ICP-MS has been used to quantify inorganic metals in various biomolecules such as DNA,[22] proteins,[23] peptides,[24] carbohydrates[25] and lipids.[26] Usually the calibration procedure assumes that metals in these molecules and inorganic metal standards undergo comparable ionization in the ICP. Nevertheless, we know of few reports of using

ICP-MS for intact bacteria for the same purpose. Little information is available about the ionization of bacteria within the ICP. There are some high-speed photographic studies of the ionization process for large particles in an ICP. Houk et al.[27] studied the ionization of wet Yttrium droplets and solid particles in the ICP by motion pictures taken at 4000 frames s^{-1}. They found that medium-sized wet droplets passed through the ICP intact or poorly dissociated. A more recent work by Aeschliman et al.[28] examined the validity of a solution calibration procedure for LA-ICP-MS. They clearly showed in video that some large particles produced by laser ablation can fly through the plasma intact.

Olesik[29] reviewed the fate of individual sample droplets in the ICP. Nomizu et al.[30] used ICP-MS, with high-speed digital signal processing, to determine the amount of zinc in individual sub-micron airborne particles. The system was able to resolve signal pulses 20 μs apart, thus has the potential to study the ionization process of each particle in the ICP.

Do bacteria have the analogous fate as these large particles in the plasma? In the present work, we use *B. subtilis*, grown in spiked uranium medium, as a model bacterium to study the behavior of bacteria in the ICP. Results from the previous study[13] show that the U is mostly incorporated intrinsically in *B. subtilis* after careful washing. Therefore, the time-resolved U^+ signals should be able to reflect the ionization of the bacteria in the ICP. In addition, other aspects of introducing intact bacteria into the ICP are of analytical interest. The interaction of the PEEK tubing with intact bacteria is also investigated by flow injection analysis (FIA).

EXPERIMENTAL SECTION

Chemicals and Materials. EDTA was obtained from Fisher Scientific (Fairlawn, NJ). Deionized water (18 MΩ cm^{-1}, 25 °C) was produced by a Nanopure II system (Barnstead, Newton, MA). The bacterial nutrient broth was prepared from DIFCO 234000 concentrate (Becton Dickinson, Sparks, MD). All other chemicals were from Sigma Aldrich (St. Louis, MO). Uranium stock solution (640 ppm) was prepared from a 1000 ppm ICP standard (Plasmachem Associates, Bradley Beach, NJ). Sodium citrate was added at 0.5 g mL^{-1} and the pH was adjusted to 7.0 with 1 M NaOH.

Bacteria Growth and Counting. The culture medium was prepared by dissolving 8 g DIFCO nutrient broth powder in 1 L deionized water. The culture medium was autoclaved at 121 °C and stored at 5 °C. *B. subtilis* was inoculated into the medium in an autoclaved 250-mL Erlenmeyer flask. Uranium was added at a final concentration about 14 ppm. The flask was covered with aluminum foil and placed in a shaker (Model G24, New Brunswick Scientific, Edison, NJ) at 37 °C. The total incubation time was 48 hours with the presence of uranium. Bacterial samples were harvested during the log growth phase[13] and centrifuged at 7000 rpm (Model 228, Fisher Scientific). Cell pellets were washed three times and re-suspended with 0.17% aqueous NaCl prior to ICP-MS analysis. When necessary, bacteria were counted by flow cytometry (Model Epics XL-MCL, 488 nm; Beckman Coulter, Fullerton, CA).

Flow Injection Setup and Sonication Device. The flow injection system consisted of a high-pressure Teflon manual injection valve (9010, Rheodyne, Supelco, Bellefonte, PA) and a 100 μL PEEK injection loop (Alltech, Deerfield, IL). The sonication probe was

operated in continuous mode at 5 W for various periods of time. The bacterial samples were bathed in ice water at 0 °C to dissipate the heat generated during sonication. In some experiments, microbes were separated from molecules by the PC system described previously.[13]

Desolvator. When desolvation was applied, the aerosol was dried by a desolvator, modified from an ultrasonic nebulizer (U-5000AT, CETAC Technologies, Omaha, NE). The transducer was removed and the micro-concentric nebulizer was adapted to the inlet by threading it into the center of a rubber stopper, which sealed the chamber. The bacterial aerosol was first heated (140 °C) and then cooled (3 °C).

ICP-MS and Sample Introduction. The ICP-MS device is a magnetic sector instrument (Element 1, Thermo Finnigan, Bremen, Germany). Generally, $^{238}U^{+}$ is monitored in low resolution ($m/\Delta m \sim 300$), sufficient to resolve it from possible interferences. One benefit of low resolution is high sensitivity because of the large slit widths. The ionization behavior of bacteria is investigated by changing two key parameters of the ICP-MS, i.e. sampling position and acquisition speed. Herein sampling position is defined as the distance between the sampling cone and initial radiation zone (IRZ) for clarity. The sampling position of the plasma is altered by changing the aerosol gas flow rate. Acquisition speed, manipulated by changing acquisition parameters such as samples per peak and magnet settling time, is varied to achieve different time-resolved U^{+} signals to elucidate the behavior of bacteria in the ICP. When measured, $^{24}Mg^{+}$ and $^{44}Ca^{+}$ are monitored in medium resolution ($m/\Delta m \sim 4000$).

The ICP operating conditions and ion optical voltages are optimized to maximize signal for $^{7}Li^{+}$, $^{115}In^{+}$ and $^{238}U^{+}$ during tuning and calibration of the mass range at 1150 W.

The samples are usually introduced and nebulized by a micro-concentric nebulizer (Model 20100, Elemental Scientific, Inc., Omaha, NE). The actual uptake rate is ca. 200 μL/min unless otherwise mentioned. The nebulizer operates by natural uptake without clogging or loss of aspiration throughout the study. For perfusion chromatography and flow injection (FIA) studies, the flow is delivered by the HPLC pump described earlier.

RESULTS AND DISCUSSION

Effect of Lysing Bacteria on U^+ Signal. Sonication is utilized to lyse *B. subtilis*. One *B. subtilis* sample is divided into 5 aliquots, each with the same cell contents. The aliquots are then sonicated for various time periods ranging from 0 to 20 minutes. The samples are nebulized directly without separation by the perfusion column.

Figure 1 shows the normalized signals for $^{24}Mg^+$, $^{44}Ca^+$ and $^{238}U^+$ as sonication time changes. The normalized intensities for these three elements increase substantially as the sample is sonicated for up to 5 minutes. Previous PC studies show that only a small portion of Mg and Ca are from *B. subtilis*, while most of the U is attached to bacteria.[13] The fact that Mg and Ca signals have similar trends as that of the bacteria-incorporated U may be explained by slurry nebulization effect,[31] in which the free Ca and Mg are present in the bacterial slurry aerosol. The similar signal increase for the three elements suggests that the ionization efficiency of these elements is higher from sonicated samples than from intact bacterial sample. The normalized signals reach a plateau after 5 minutes. Further increase in sonication time does not generate more M^+ signals, which implies that 5 minutes of sonication is enough to maximize elemental responses from *B. subtilis* samples from ICP-MS measurements.

A close look at Figure 1 reveals that the normalized U^+ signal for untreated bacteria, 69%, is slightly lower compared to that for Mg^+ and Ca^+, 78% and 75% respectively. The important message is that a different correction coefficient can be obtained for each element and for each microorganism. For instance, a correction factor of roughly 1.43 applied to the sensitivity of U^+, measured directly from intact *B. subtilis*, will give a comparable sensitivity as that obtained from a lysed sample. Interestingly, the sensitivity differences are not very large. Therefore, it is possible to do fairly accurate quantification in intact bacteria using inorganic standards, provided that the correction coefficient is known beforehand.

Effect of Sonication on the Retention of Bacteria on Perfusion Column. The previous study[13] shows most of the U is on intact bacteria. It is reasonable that the ionization efficiency of the uranium from intact bacteria is different from an aqueous inorganic U standard because of the large difference in sizes between the two analytes. In the present study, bacteria are lysed to study the their ionization in the ICP. After lysing cellular components, some of which bind uranium, are expected to be released in free solution. Whether it is with macromolecules, i.e. DNA or proteins, or small molecules, i.e. peptides or lipids, uranium in this case should be small in size and is expected to have similar ionization efficiency as the aqueous inorganic uranium in the ICP.

According to the previous experimental results (Figure 1), sonication for 5 minutes is enough to generate maximum U^+ signal, if not fully lysing *B. subtilis*. Therefore, sonication times of 2 and 10 minutes were chosen for two *B. subtilis* aliquots. The resultant solutions were termed partially and fully lysed bacterial samples, respectively. Figure 2 shows the chromatograms for the 10 ppb U standard solution in 0.17% NaCl and the partially lysed and fully lysed *B. subtilis* samples.

Obviously for the 10 ppb U standard solution, there is just one peak at ~ 480 s, as can be seen from the chromatogram. In comparison, the chromatogram for the partially lysed bacterial sample has two peaks. The first one at ~ 200 s corresponds to the elution time of intact bacteria.[13] The second peak at ~ 480 can be attributed to free uranium in solution, a U complex or small U inorganic ions. This is almost at the same elution time as for the 10 ppb U standard sample. The results suggest that U-incorporated components are released from bacteria by sonication and they are small in size because they have similar retention time to the inorganic U standard. In other words, the perfusion column is not able to resolve them based on their sizes.

Also shown in Figure 2 is the chromatogram of a fully lysed *B. subtilis* sample. Clearly the U^+ peak corresponding to the intact bacteria is almost gone while the relative intensity for the second peak is increased compared to that from the partially lysed bacterial sample. This demonstrates that the U-bound species are indeed small in size since they are totally retained by the perfusion column. As for the small peak at 200 s, there may be some intact *B. subtilis* left in the sample or the bacterial debris that are large in size so they show the same retention pattern in perfusion chromatography as intact bacteria. It is worth noting that there is a tailing peak after 600 s, which is probably caused by the light absorption of U-bound species on the packing materials. The amount of U measured from the partially lysed *B. subtilis* sample agrees quantitatively to that from the fully lysed one.

Based on the above results, it is reasonable to say that these U-bound compounds, released from bacteria by sonication, would have similar ionization efficiency as the inorganic U standard in the ICP. A correction factor can be applied to correct the sensitivity discrepancies due to the ionization differences between U in intact bacteria and the inorganic

uranium standard in the ICP. Therefore, it should be possible to quantify the amount of U removed during bioremediation by using an inorganic U standard instead of a bacterial standard with known amount of U.

Behavior of *B. subtilis* in the ICP. It is interesting that the U^+ signals are observed at all from intact bacteria, as confirmed by UV and polarimetry results.[13] The bacteria in the effluent are intact in the saline mobile phase before entering the nebulizer. These intact bacteria can survive through the sample introduction processes, including chromatography, nebulization and desolvation, prior to the ICP, where they undergo desolvation, vaporization, atomization and ionization.

1. Effect of Acquisition Speed. 1). Dwelling time: 100 ms. The atomization and ionization behavior of *B. subtilis* in the ICP is at least partially reflected by the time-resolved U^+ signals since majority of the U is in bacteria. Figure 3 shows the U^+ signals (in log scale) for three different samples under slow acquisition conditions, which are listed in Table 1. As can be seen from Figure 3, the U^+ signals are less stable with frequent positive spikes for the two bacterial samples, 10^8 and 10^9 cells/mL. The positive spikes are probably due to the fact that one or a few cells survive the ICP, and happen to atomize at the right place before the sampler of the mass spectrometer. Thus, a stream of U^+ is released to generate a positive U^+ spike. In comparison, the U^+ signal from the 10 ppb standard is more stable, which is likely due to the uniform ionization efficiency of the fine aerosol produced from an aqueous U solution.

2). Dwell time: 3 ms. Very rapid measurements are necessary to study the ionization and ion-sampling processes in the ICP. Although the aforementioned results do show, to some extent, the behavior of bacteria in the ICP, the acquisition time of ca. 300 ms per data

point is much longer compared to the typical lifetime of a droplet in the ICP, 2-3 ms. Therefore the sampling time is further pushed to the limit, mainly by reducing the magnet settling time from 100 ms to 1 ms. The operation parameters are listed in Table 2. The time to generate each data point is 4 ms, which is about the fastest achievable sampling from the sector instrument used (Element 1) and comparable to the lifetime of droplets in the ICP.

Figure 4 shows the U^+ signals from the 10 ppb U standard solution and an intact *B. subtilis* sample (~ 10^8 cells/mL). As expected, the U^+ signals for both samples are very noisy because of fast acquisition in which the signals are not averaged. Clearly there are some positive spikes superimposed on the bulk U^+ signal from *B. subtilis* sample, while there are no such spikes in the aqueous U solution. The experiments are repeated many times and similar results are obtained consistently. These results further support the previous hypothesis that the U^+ spikes are due to the passage of intact *B. subtilis* bacteria through the ICP. The aqueous U solution produces a fine uniform aerosol, which does not generate positive signal spikes although some low amplitude negative spikes are observed.

The effects of dry aerosol versus wet droplets are also of interest. A desolvator is utilized to dry the bacterial aerosol. The ICP-MS is re-optimized each time by changing the aerosol gas flow rate to maximize U^+ signal when the desolvation device is turned on and off. Change of nebulizer gas flow rate of only ~ 0.1 L/min is necessary. Note that when the desolvator is off, the aerosols still pass though it at room temperature, without being heated or cooled. Figure 5a and 5b are the U^+ signals from the 10 ppb U standard solution when the desolvator is on and off. The U^+ signals do not show any appreciable positive spikes above the bulk U^+ signals in both situations. The U^+ signals obtained, however, are much noisier with lots of negative spikes when the aerosol is dried.

Figure 6a and 6b are the U^+ signals from the intact *B. subtilis* sample (~ 10^8 cells/mL) when the desolvator is switched on and off. Positive U^+ spikes are observed for both wet and dry bacterial aerosols. These results strongly suggest that the positive U^+ spikes are due to intact bacteria rather than a solvation effect because the desolvator should remove the solvent. As in the case of the standard U solution, the U^+ signal is noisier with the desolvator on than off. The exact cause for this phenomenon is not clear. Perhaps the desolvation process strips the solvent and thus exposes the charged solute to atmosphere, which leads to the deposition of electrically- charged bacteria on the wall of the desolvator. As a result, more negative peaks are shown in the U^+ signal due to the erratic solute losses. Figure 7a and 7b are the expansions of the designated a* and b* areas in Figure 6a. The results indicate that the instrument, operated under the specified conditions, is able to resolve counts that differ by ~ 10 ms although the actual dwell time is believed to be 3 ms.

2. Effect of Aerosol Gas Flow Rate. There is no doubt that the sampling position (as defined earlier) of the ICP will affect the measured signal. The longer the distance along the axis downstream from initial radiation zone (IRZ)[32], the lower the sensitivity for the analyte because the ion plume expands.[4] The optimal sampling position for ICP-MS would be only slightly downstream from the typical sampling position, or about 1-2 mm from the sampling cone. This is to ensure the highest possible ion density in the extracted gas.[4] Remember that this is for a fine aerosol of small molecules/particles produced from aqueous solution, where the residence time of the aerosol in the ICP is sufficient for VAI. In the case of bacteria, the same residence time in the ICP would probably not generate the same degree of ionization, as indicated by the positive spikes in Figure 3. If the observed positive U^+ spikes are really due

to incomplete ionization of intact bacteria in the ICP, the spike effect can be attenuated by changing the sampling position.

Shown in Figure 8 is the relationship of normalized U^+ signals with sonication time using two aerosol gas flow rates, 1.23 L min^{-1} that maximizes U^+ signal from a 10 ppb U standard, and 1.13 L min^{-1}. One thing in common is that the U^+ signals reach a steady state after sonication for 5-10 minutes. The normalized U^+ signal from the unsonicated sample is about 85% of the maximum attainable U^+ signal in the scenario of less aerosol gas flow, whereas the U^+ signal is approximately 70% of maximum at the optimized sample gas flow rate.

These results show that the U ionization efficiency from intact bacteria is ~15% higher at lower aerosol gas flow rate than at optimal one. This can be attributed to the change of sampling position, which moves further from the IRZ at lower nebulizer gas flow rate. Bacteria would thus have more time to completely ionize in the plasma. Nevertheless, this higher ionization efficiency occurs at the expense of U^+ sensitivity (~ 4 times lower at lower aerosol gas flow rate) simply because the lost intensity at non-optimal sampling position exceeds the signal gained due to higher ionization efficiency. Note that different batches of bacteria, grown 2 weeks apart, give similar trend in normalized signal vs. sonication time as far as the ICP is operated at optimal aerosol gas flow rate.

Retention Behavior of Intact Bacteria on the PEEK Tubing. During the project, flow injection analysis (FIA) is utilized to mimic the behavior of bacteria in the self-packed perfusion column. The injection loop is a 100 μL PEEK loop. The flow is maintained at 100 μL/min by deionized water. After many injections of intact *B. subtilis* samples, sodium citrate (10 mM, 100 μL) is injected to wash the loop. The U^+ signal is monitored, as shown

in Figure 9. The U^+ signal increases at ~ 60 s as the incoming sodium citrate reaches the ICP, which contributes partially to the rising U^+ background. It is also possible that some free U and/or U-bound compounds, absorbed at the PEEK surface, are re-dissolved by the sodium citrate.

The signal then levels off and a second broad peak appears with frequent, intense spikes superimposed on it. The U^+ signal rises in two steps, which are attributed to two different effects. The spikes are probably caused by the release of whole bacteria from the PEEK tubing as sodium citrate passes though. The FIA peak is about 110 s wide, which is 50 s longer than the sodium citrate liquid plug. The tailing may result from the slow release of U-associated species from the tubing after the passage of sodium citrate.

More U-doped *B. subtilis* samples are run through the loop, which is kept unused for two days. Sodium citrate at 10 mM is then used to rinse the loop. U^+ signal is acquired for three consecutive sodium citrate washes and the results are shown in Figure 10. It is clear that the double hump peak shape is observed for the first two washes. The U^+ signal is most intense for the first wash and then decreases substantially for the second and third washes, respectively. The fact that the U^+ signal from the first peak decreases with subsequent washes confirms that it is from free U or U-associated molecules absorbed on the surface of the PEEK tubing. In the third wash, the U^+ signal is mostly from sodium citrate background since the U carryover is almost entirely washed out. Overall, the spike effect is most pronounced for the first wash and least marked for the third wash.

CONCLUSIONS

We attempt to study the behavior of bacteria in the inductively coupled plasma, shed some light on its fundamental influence on the elemental quantification, and explore the possibility of using inorganic standards for calibration. The following conclusions can be drawn from this study.

1. The time-resolved U^+ signals from ICP-MS measurements indicate that bacteria behave similarly as the large particles in the ICP. The positive U^+ spikes are not due to a solvation effect.
2. Sonication releases intracellular species that are bound with uranium from the bacteria.
3. The chromatographic results show that the U-bound species have almost the same retention as the free inorganic U standard, implying that they are small in size and would have similar ionization efficiency to U from an aqueous standard in the ICP. Therefore, quantification of U in intact bacteria is possible using an inorganic U standard.
4. PEEK tubing is able to absorb intact bacteria.

REFERENCES:

1. Becker, J. S.; Dietze, H. -J. *Int. J. Mass Spectrom.* **2003**, 228, 127-150.
2. Garcia Alonso, J. I.; Camblor, M. G.; Bayon, M. M.; Marchante-Gayon, J. M.; Sanz-Medel, A. *J. Mass Spectrom.* **1997**, 32, 556-564.
3. Cresser, M. S.; Armstrong, J.; Cook, J.; Dean, J. R.; Watkins, P.; Cave, M. *J. Anal. At. Spectrom.* **1995**, 8, 1R-78R.
4. Jarvis, K. E.; Gray, A. L.; Houk, R. S. **Handbook of Inductively Coupled Plasma Mass Spectrometry** Blackie & Son, Glagow, 1992.
5. Nieves, I.; Dario, E. K.; Mads, G.; Akiko, I.; Akhilesh, P. *Anal. Chem.* **2003**, 75, 6043-6049.
6. Hartung, T.; Balls, M.; Bardouille, C.; Blanck, O.; Coecke, S.; Gstraunthaler, G.; Lewis, D. *Altern. Lab. Anim.* **2002**, 30, 407-414.
7. Riordan, J. F.; Vallee, B. T., Eds. **Metallobiochemistry; Methods in Enzymology**; Academic Press: San Diego, London, 1998; Vol. 158.
8. Gwizdala III, A. B.; Johnson, S. K.; Mollah, S.; Houk, R. S. *J. Anal. At. Spectrom.* **1997**, 12, 503-506.
9. Montes-Bayon, M.; DeNicola, K.; Caruso, J. A. *J. Chromatogr. A,* **2003**, 1000, 457-476.
10. Jackson, B. P.; Hopkins, W. A.; Baionno, J. *Environ. Sci. Technol.* **2003**, 37, 2511-2515.
11. Beliveau, R.; Gelinas, Y.; Ferraris, J.; Schmit, J. P. *Biochemistry and Cell Biology* **1990**, 68, 1272-1280.

12. Poe-Pawlak, K.; Zambenedetti, P.; Szpunar, J.; Lobinski, R.; Zatta, P. *J. Anal. At. Spectrom.* **2003**, 18, advance article.

13. Zhang, B.; Li, F. M.; Houk, R. S.; Armstrong, D. W. *Anal. Chem.* **2003**, 75, 6901-6905.

14. Schneiderheinze, J. M.; Armstrong, D. W.; Schulte, G.; Westenberg, D. J. *FEMS Microbiology Letter* **2000**, *189*, 39-44.

15. Armstrong, D. W.; Schneiderheinze, J. M. *Anal. Chem.* **2000**, *72*, 4474-4476.

16. Houk, R. S. *Acc. Chem. Res.* **1994**, 27, 333-339.

17. Montaser, A. **Inductively Coupled Plasma Mass Spectrometry**, Wiley-VCH, New York, 1998.

18. Kawaguchi, H.; Fukasawa, N.; Mizuike, A. *Spectrochim. Acta Part B* **1986**, 41, 1277-1286.

19. Kawaguchi, H.; Kamakura, K.; Maeda, E.; Mizuike, A. *Bunseki Kagaku* **1987**, 36, 431-435.

20. Nomizu, T.; Nakashima, H.; Hotta, Y.; Tanaka, T.; Kawaguchi, H. *Anal. Sci.* **1992**, 8, 527-531.

21. Nomizu, T.; Kaneco, S.; Tanaka, T.; Ito, D.; Kawaguchi, H.; Vallee, B. L. *Anal. Chem.* **1994**, 66, 3000-3004.

22. Wang, J.; Dreessen, D.; Wiederin, D. R.; Houk, R. S. *J. Am. Chem. Soc.* **1998**, 120, 5793-5799.

23. Wang, J.; Houk, R. S.; Dreessen, D.; Wiederin, D. R. *J. Biol. Inorg. Chem.* **1999**, 4, 546-553.

24. Leopold, I.; Gunther, D. *Fresenius J. Anal. Chem.* **1997**, 359, 364-370.

25. Szpunar, J.; Pellerin, P.; Makarov, A.; Doco, T.; Williams, P.; Lobinski, R. *J. Anal. At. Spectrom.* **1999**, 14, 639-644.

26. Edmonds, J. S.; Shibata, Y.; Francesconi, K. A.; Yoshinaga, J.; Morita, M. *Sci. Total Environ.* **1992**, 122, 321-335.

27. Houk, R. S.; Winge, R. K.; Chen, X. S. *J. Anal. At. Spectrom.* **1997**, 12, 1139-1148.

28. Aeschliman, D. B.; Bajic, S. J.; Baldwin, D. P.; Houk, R. S. *J. Anal. At. Spectrom.* **2003**, 18, 1008-1014.

29. Olesik, J. W. *Appl. Spectrosc.* **1997**, 51, 158A-175A.

30. Nomizu, T.; Hayashi, H.; Hoshino, N.; Tanaka, T.; Kawaguchi, H.; Kitagawa, K.; Kaneco, S. *J. Anal. At. Spectrom.* **2002**, 17, 592-595.

31. Phillip, G.; Michael, E. F.; Les, E. *Spectrochimica Acta* **1993**, 48B, 1563-1577.

32. Koirtyhann, S. R.; Jones, J. S.; Yates, D. A. *Anal. Chem.* **1980**, 52, 1965-1966.

Table 1: Parameters for slow acquisition.

Element monitored: U at 238 (m/z)
Magnet settling time: 300 ms
Sampling time: 10 ms
Samples per peak: 10
Mass window: 100%
Total 400 ms per data point

Table 2: Parameters for fast acquisition.

Element monitored: U at 238 (m/z)
Magnet settling time: 1.0 ms
Sampling time: 1.5 ms
Samples per peak: 20
Mass window: 10%
2 sample position, 3 ms
Total 4 ms per data point

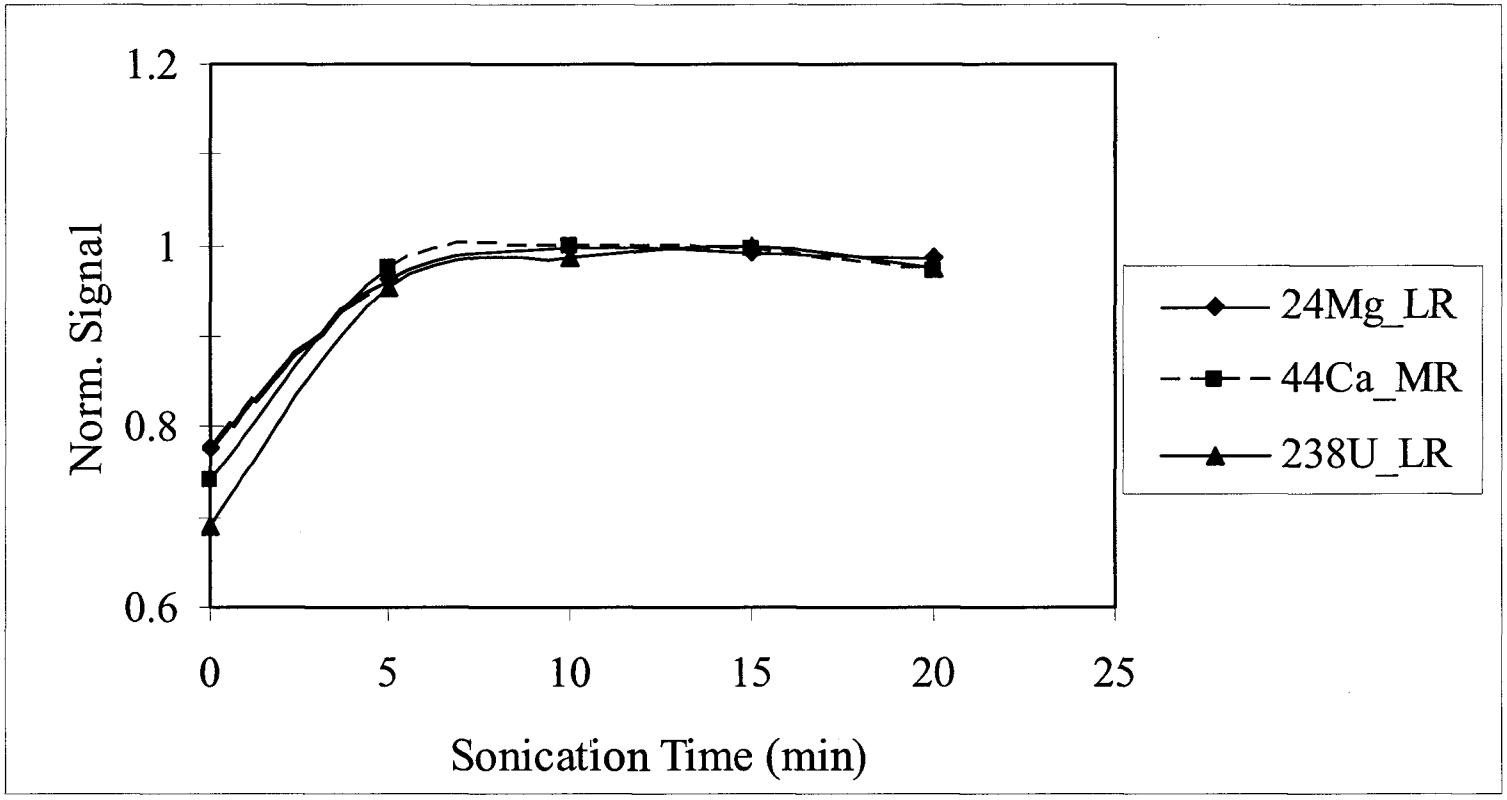

Fig. 1 Relation of the normalized signals of Mg^+, Ca^+ and U^+ with sonication time.

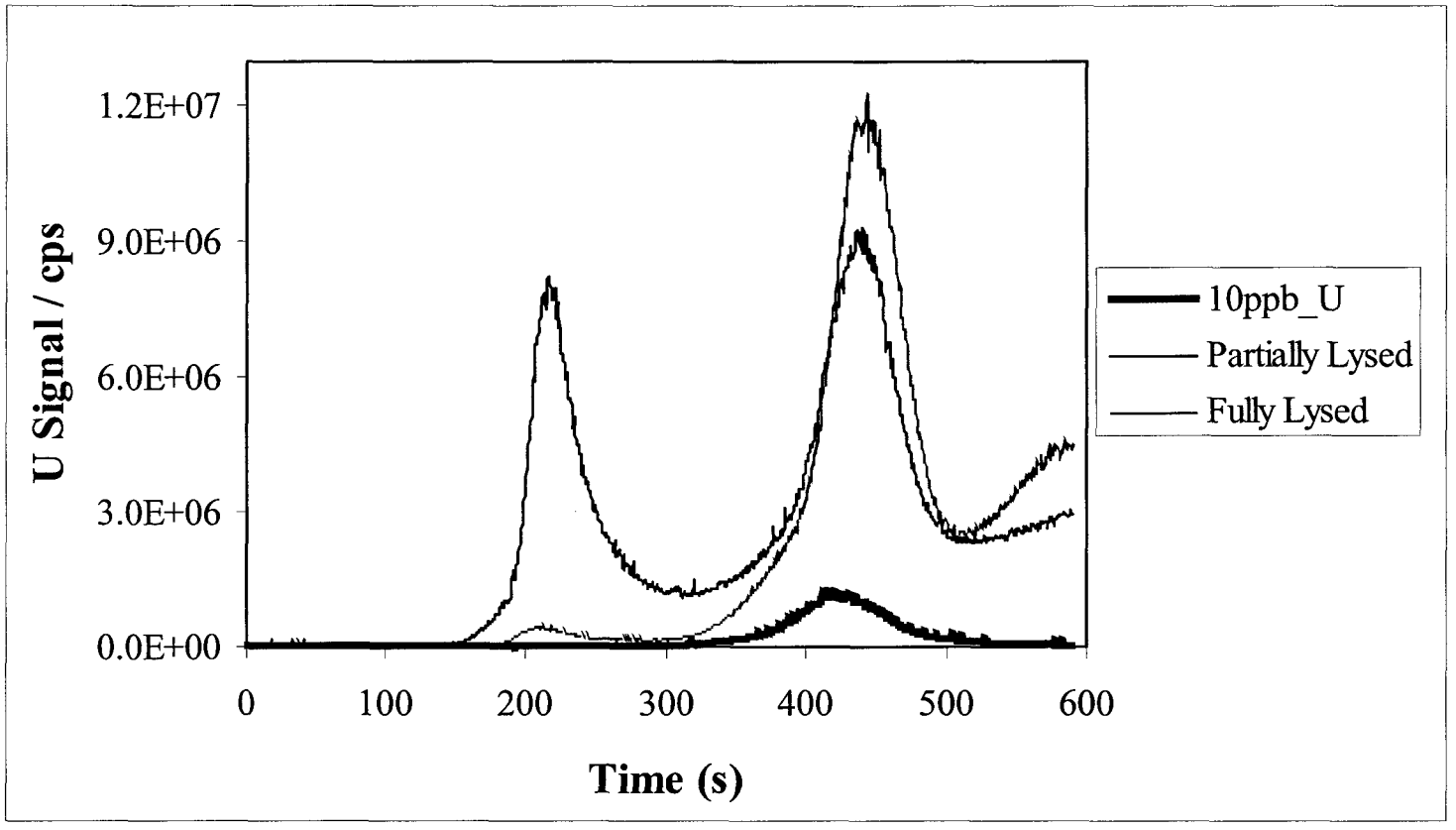

Fig. 2 Chromatograms of 10 ppb U standard, partially and fully lysed bacteria samples.

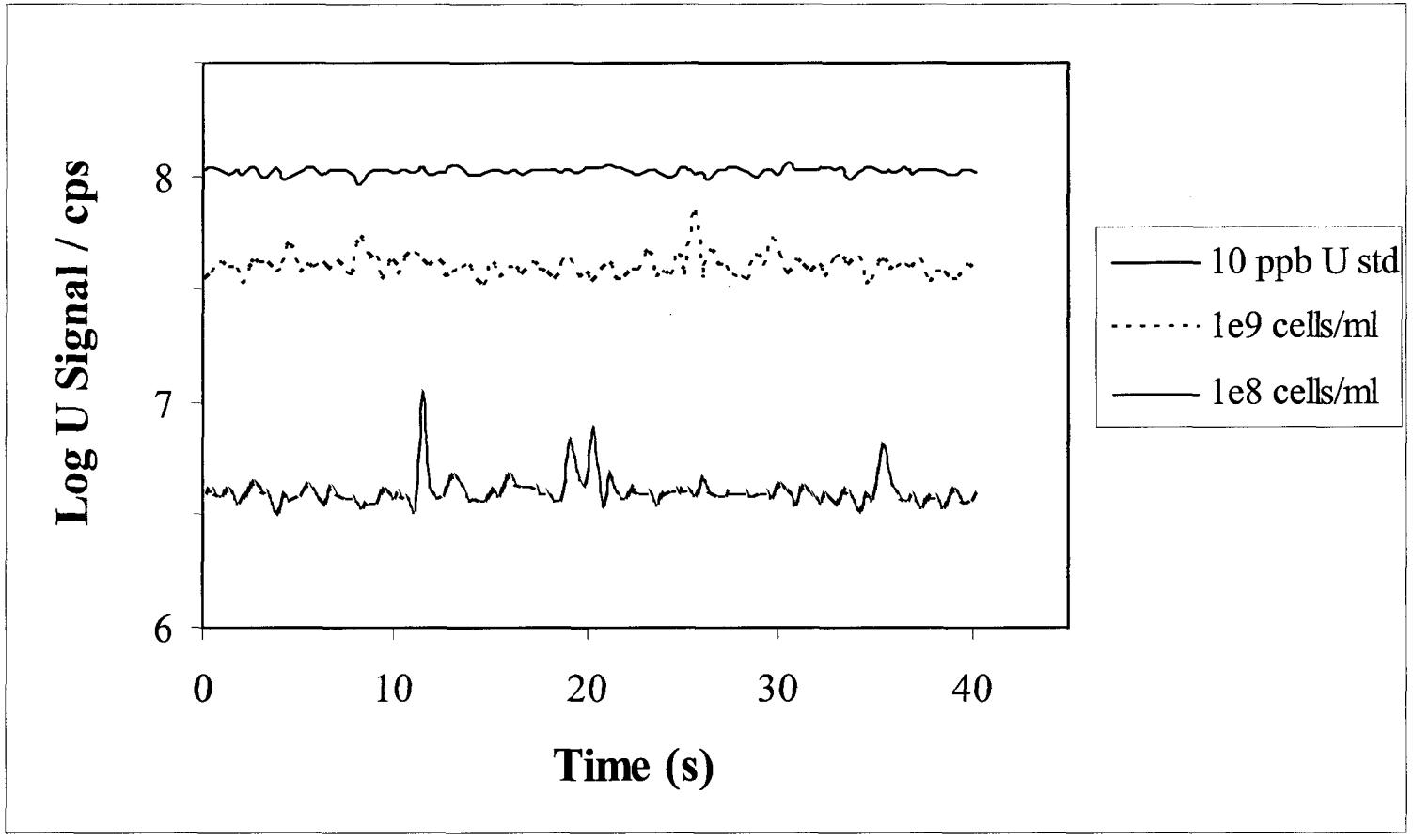

Fig. 3 Effect of slow acquisition on U^+ signal. Acquisition conditions are listed in Table 1.

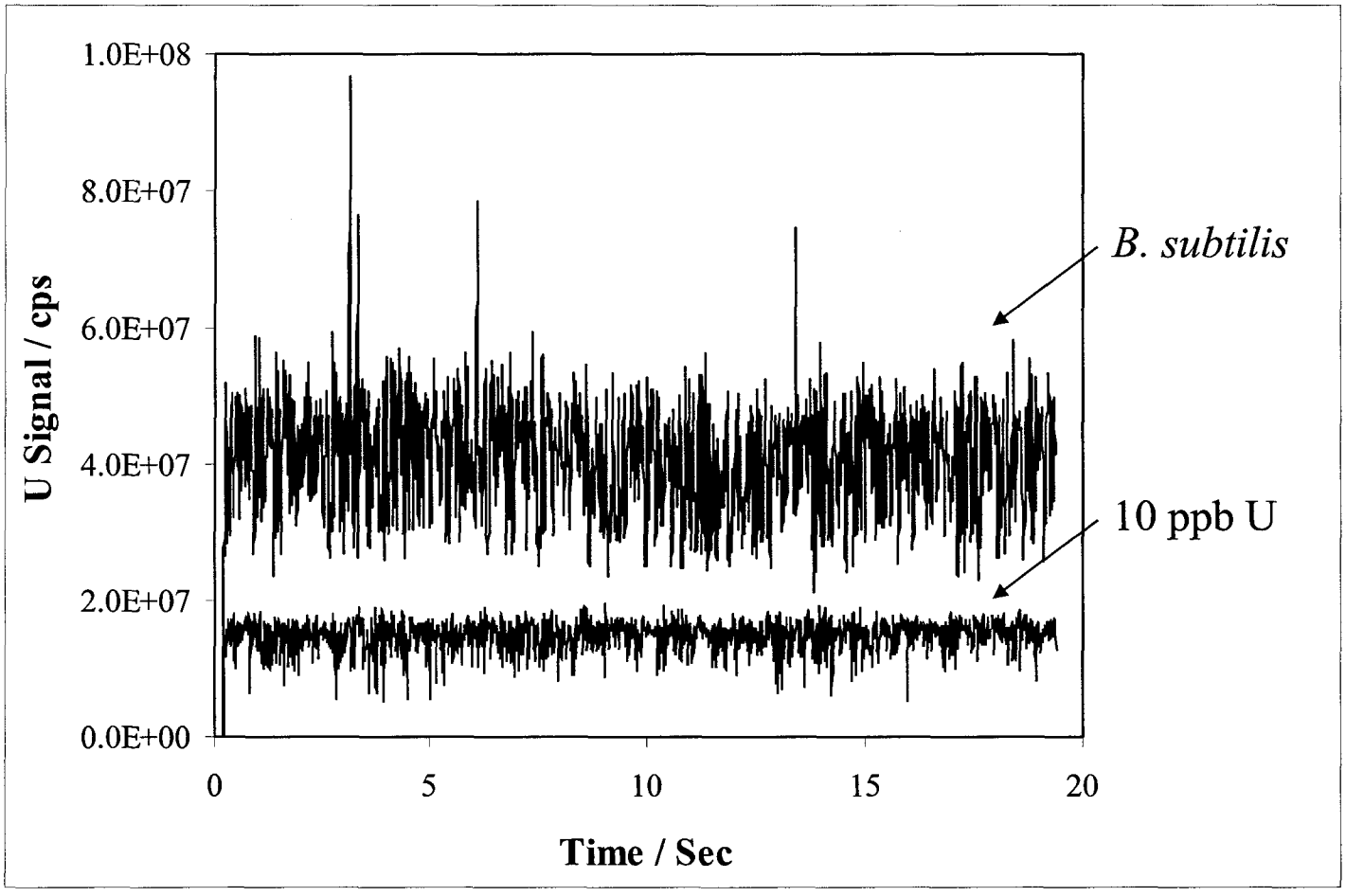

Fig. 4 Effect of fast acquisition on U^+ signal. Acquisition conditions are listed in Table 2.

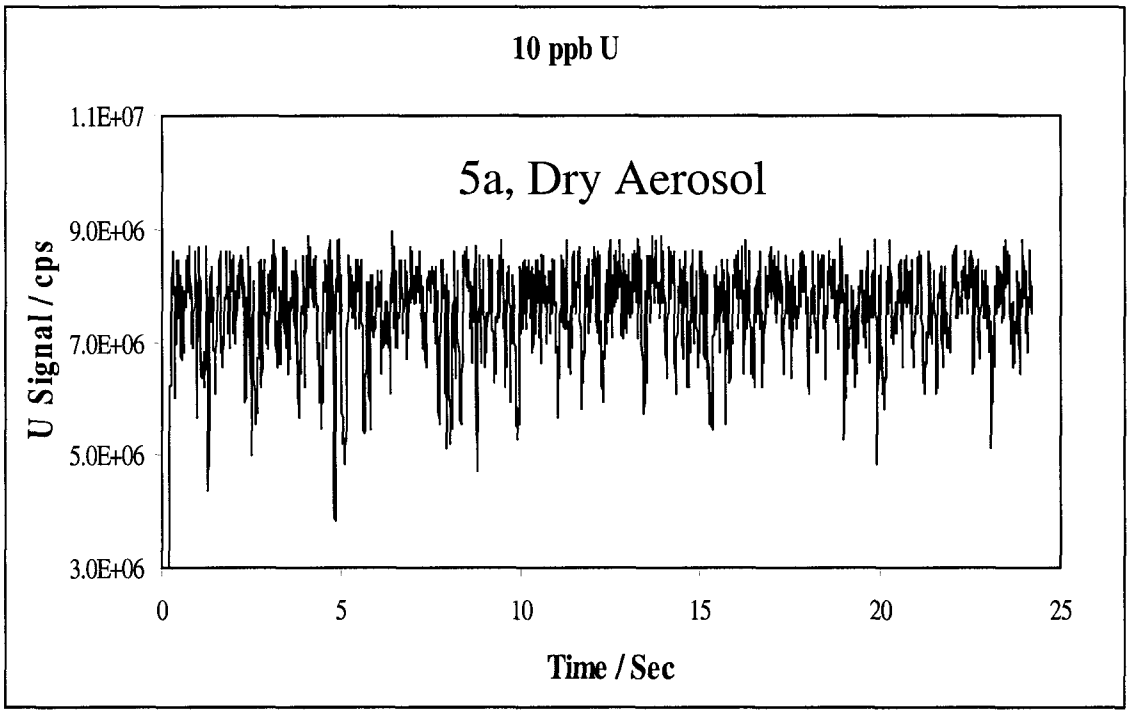

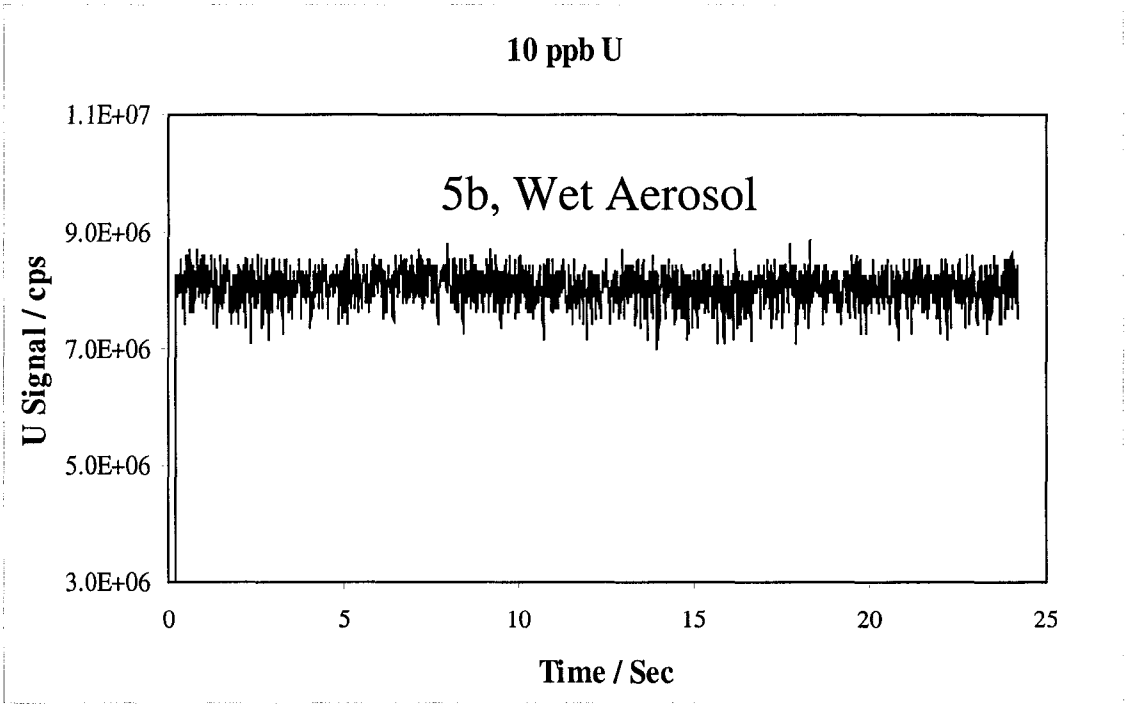

Figure 5a and b. U^+ signals for the 10 ppb U standard solution under dry and wet aerosol conditions.

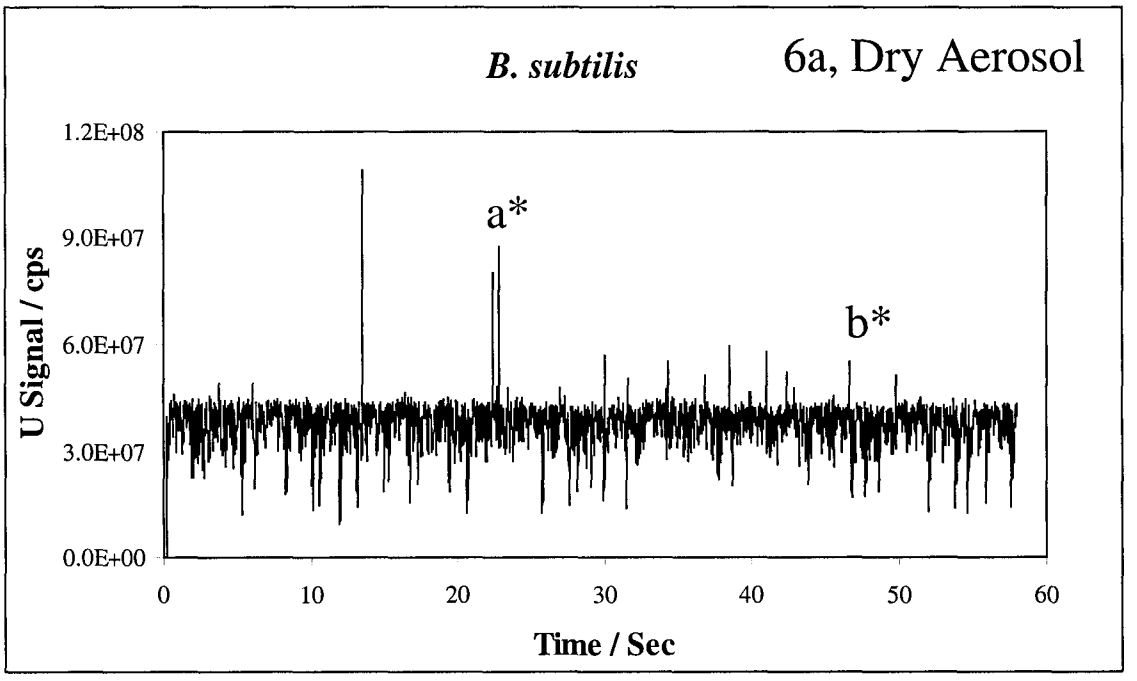

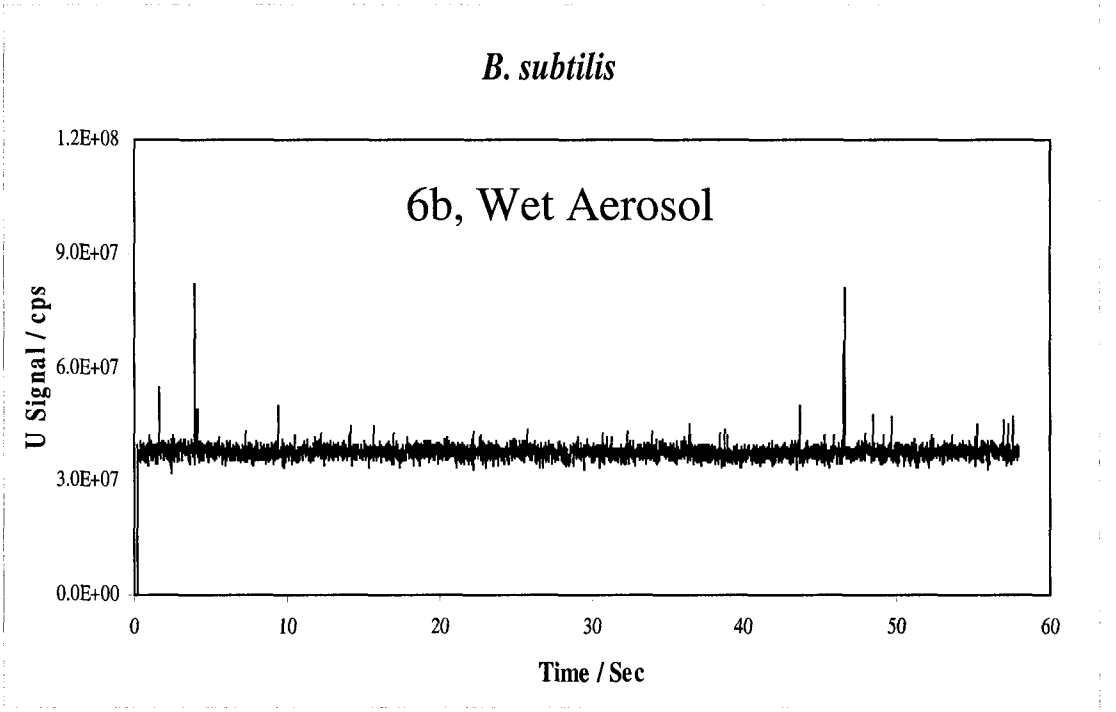

Figure 6a and b. U^+ signals for the *B. subtilis* sample (~ 10^8 cells/mL) cultured with 14 ppm U spike in the medium under dry and wet aerosol conditions.

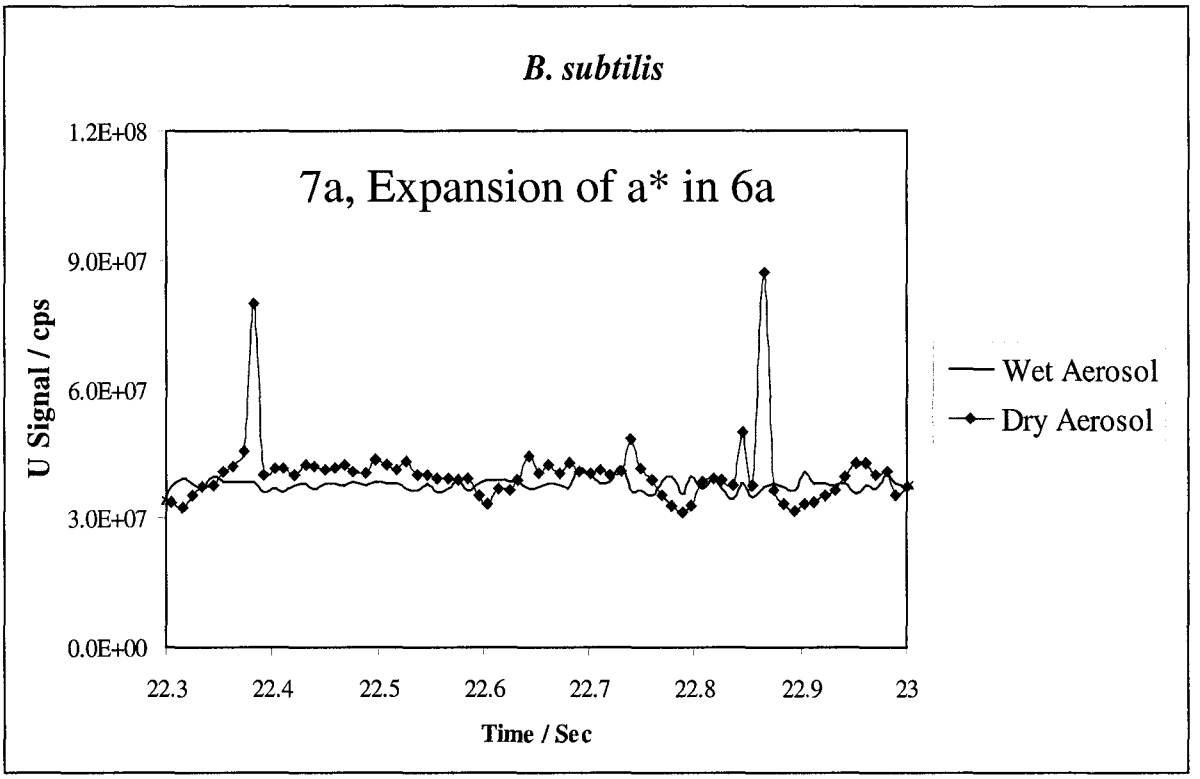
B. subtilis
7a, Expansion of a* in 6a
1.2E+08
9.0E+07
6.0E+07
3.0E+07
0.0E+00
U Signal / cps
22.3
22.4
22.5
22.6
22.7
22.8
22.9
23
Time / Sec
Wet Aerosol
Dry Aerosol

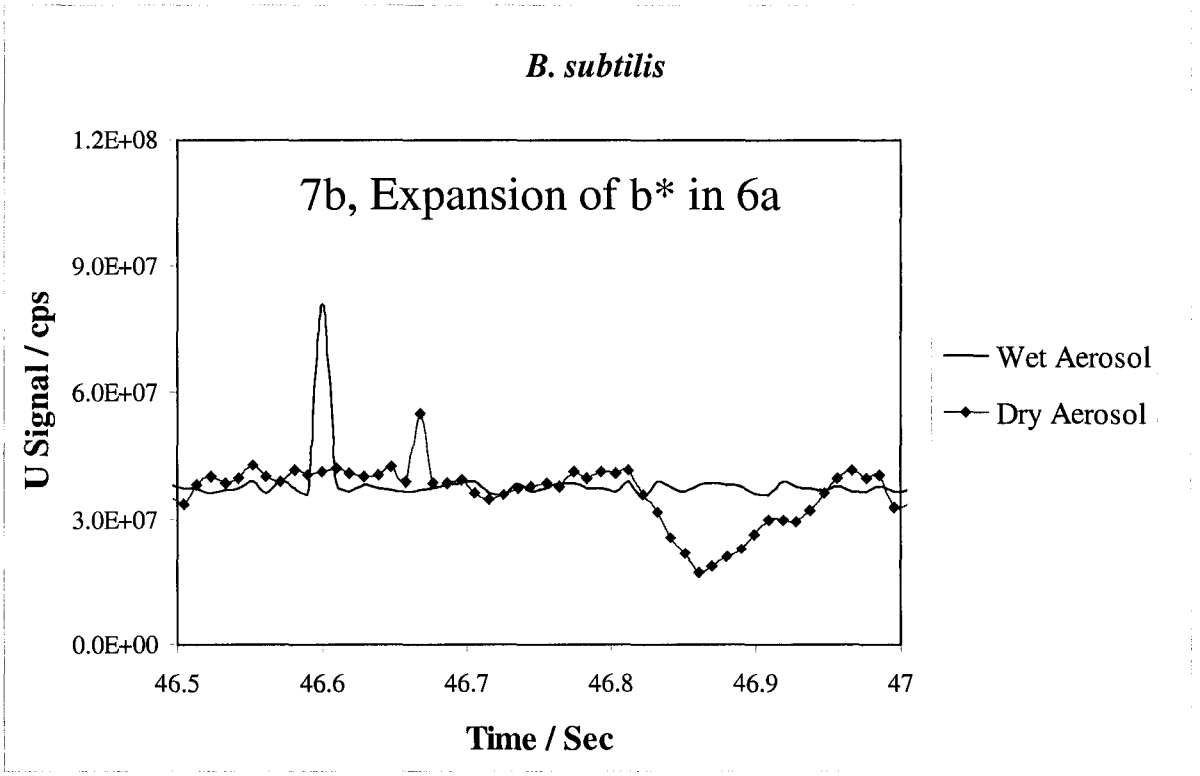
B. subtilis
7b, Expansion of b* in 6a
1.2E+08
9.0E+07
6.0E+07
3.0E+07
0.0E+00
U Signal / cps
46.5
46.6
46.7
46.8
46.9
47
Time / Sec
Wet Aerosol
Dry Aerosol

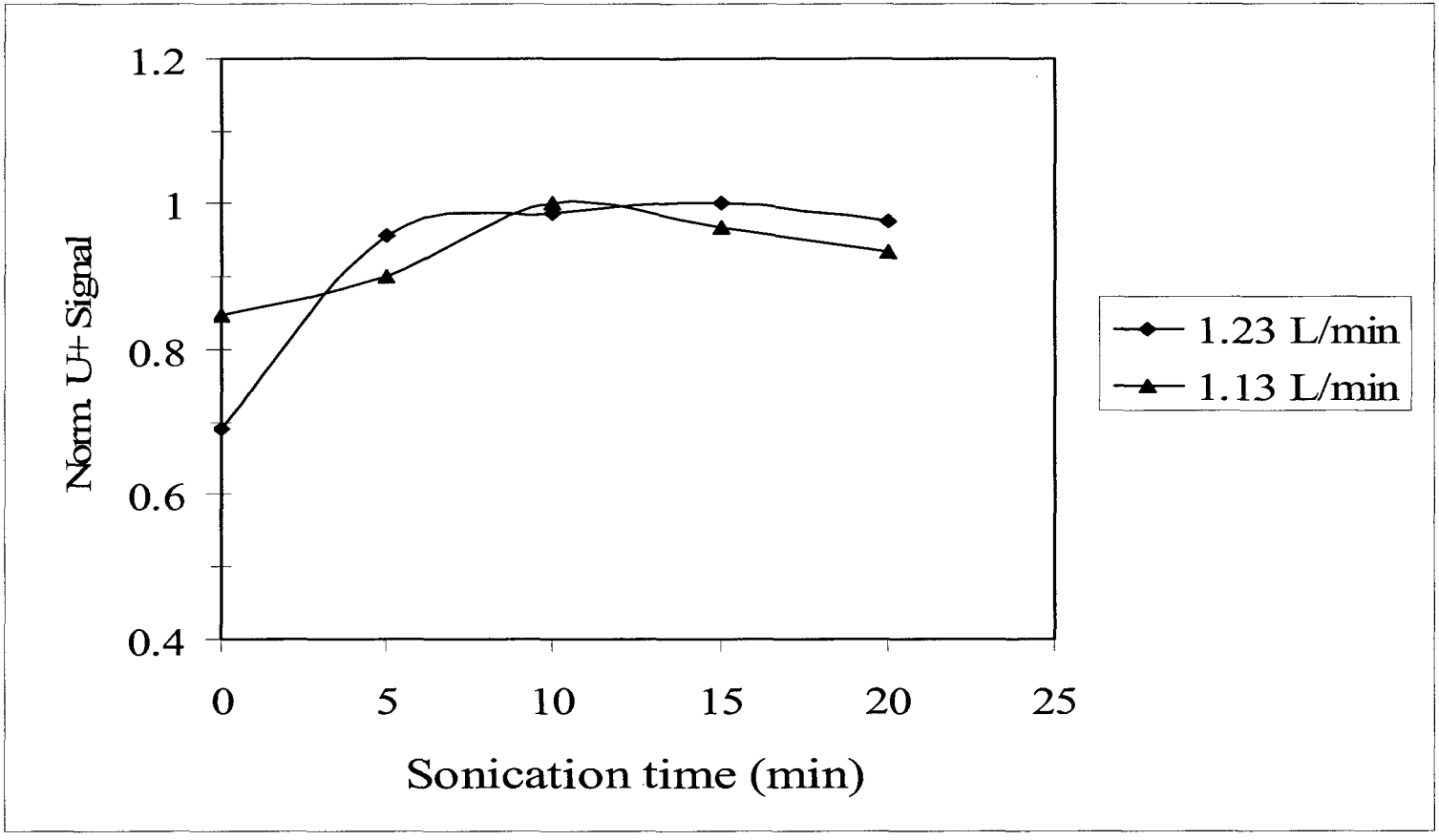

Fig. 8 Relation of the normalized U^+ signal with sonication time under two aerosol gas flow rates.

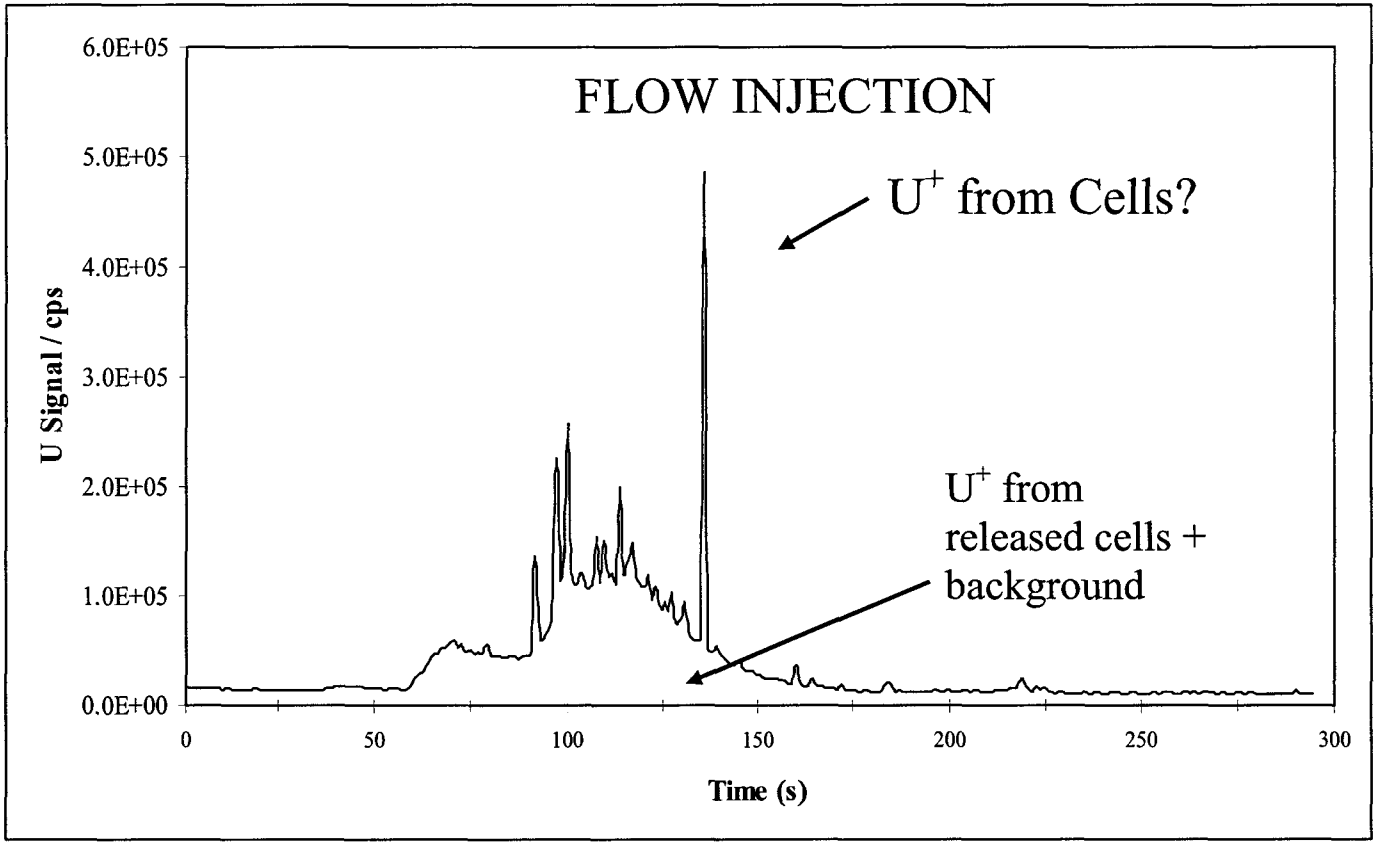

Fig. 9 Effect of PEEK injector tubing, which was washed by 10 mM sodium citrate.

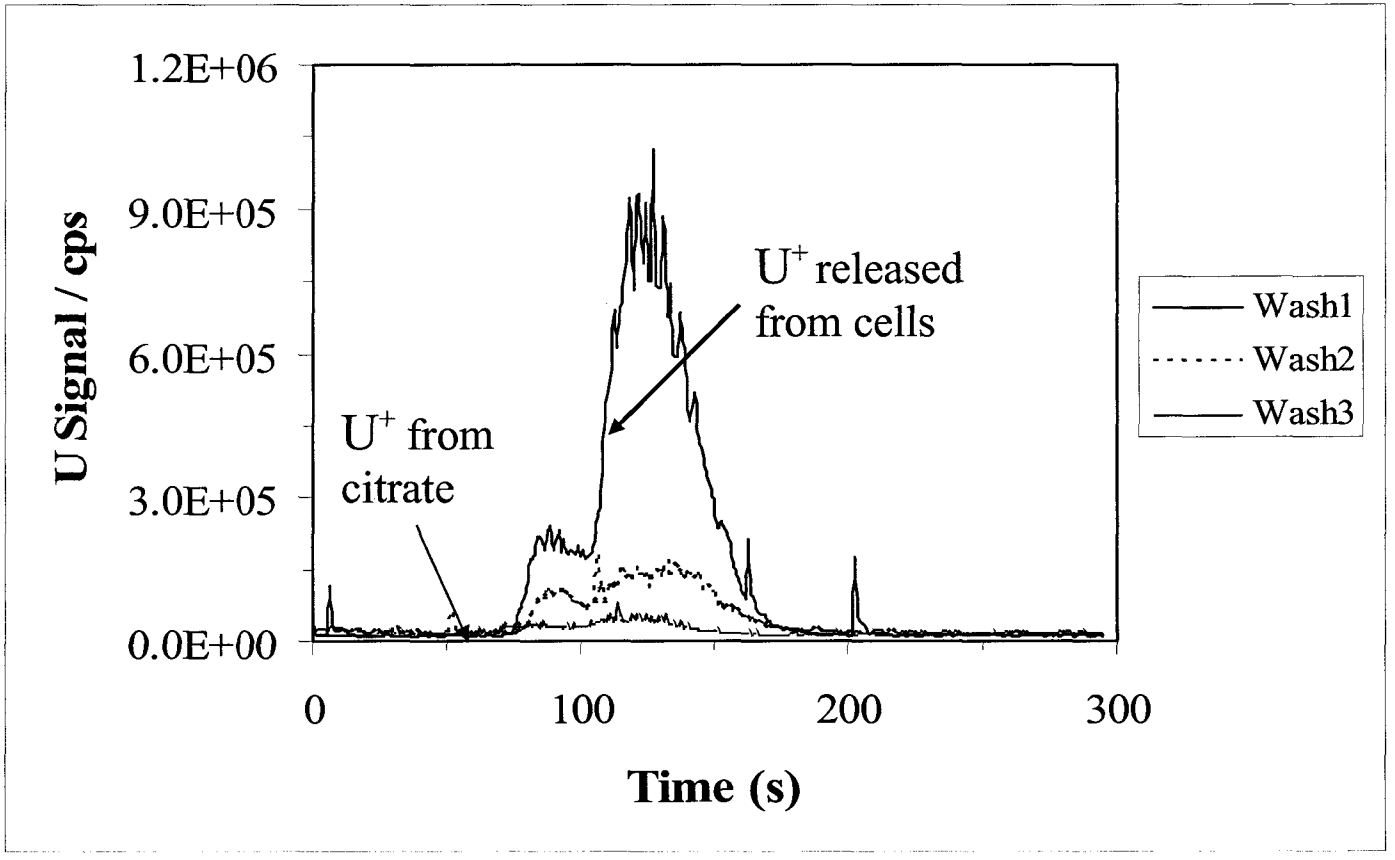

Fig. 10 Effect of PEEK injector tubing on bacteria. The loop was washed with 10 mM sodium citrate three times consecutively after interaction for two days with bacteria.

CHAPTER 4

TANDEM MASS SPECTROMETRY OF METAL NITRATE NEGATIVE IONS PRODUCED BY ELECTROSPRAY IONIZATION

A paper published in *Journal of the American Society for Mass Spectrometry*

Fumin Li, Matthew A. Byers and R. S. Houk

ABSTRACT

$M(NO_3)_x^-$ ions are generated by electrospray ionization (ESI) of metal solutions in nitric acid in negative ion mode. Collision-induced reactions of these ions are monitored in a tandem mass spectrometer (MS) of quadrupole–octopole-quadrupole (QoQ) geometry. For Group 1 and 2 elements, the $M(NO_3)_x^-$ ions dissociate into NO_3^- and neutral metal nitrate molecules. These elements also form some $M_x(NO_3)_{x+1}^-$ clusters, especially Li^+. Metal nitrate ions from transition elements and Group 13 elements fragment into oxo products and also undergo internal electron transfer to leave the M atom in a lower oxidation state. To calibrate the collision energy, the dissociation energy of $O\text{-}NO_2^-$ is found to be 5.55 eV, about 0.76 eV lower than a value derived from thermochemistry. The product ions from $Fe(NO_3)_4^-$ ions have low formation thresholds of only 0.5 to 2 eV.

INTRODUCTION

After the pioneering studies of Yamashita and Fenn,[1] ESI-MS has revolutionized the analysis of biological molecules.[2-5] This method also provides valuable information about inorganic and organometallic compounds[6-8] and the interactions and binding of metal ions to biological molecules.[9-11] The use of high mass resolution allows identification of the metal atom[12] and even its oxidation state[13] using intact metal-protein ions.

Most studies of small inorganic ions have been done in positive ion mode.[14-18] Many metal-solvent clusters, e.g. $M^{x+}(H_2O)_n$, n=1 to 6, are typically formed under "soft" ion extraction conditions.[7,17,18] Highly charged metal ions tend to react with solvent molecules to yield hydroxy or methoxy ions when energetic collision conditions are used to remove solvent during ion extraction. Preserving the original form of the metal ion in positive mode generally requires element-specific optimization of ion extraction conditions and leads to a variety of ion-solvent clusters.

Previous work from our group[19] showed that an excess of nitric acid can be used to produce $M(NO_3)_x^-$ ions in negative ion mode. A single set of ion extraction conditions yields these ions for many elements. This early work was done with only one stage of MS. The present work reports collision-induced dissociation (CID) reactions of these $M(NO_3)_x^-$ ions in a triple "quadrupole" MS, actually a QoQ instrument. The properties of these ions are relevant in a number of areas. Nitrate is an important agricultural material and can be a pollutant. Nitrate and nitric acid cluster ions are also the main negative charge carriers in certain regions of the Earth's atmosphere.[20] The related neutral compounds NO_2 and NO_3 and their acids HNO_2 and HNO_3 are also important atmospheric species.[21] Metal nitrate compounds are used as explosives; Zhao and Yinon[22] recently describe ESI mass spectra and

CID properties of complexes and clusters of alkali metals and ammonium with various anions, including nitrate.

EXPERIMENTAL

Samples and Sample Preparation

Concentrated nitric acid is purchased from J. T. Baker and used without further purification. Aliquots of the concentrated acid are mixed with HPLC grade methanol and deionized water (18 MΩ, Barnstead Nanopure) to form a solvent of 0.05% nitric acid in 25% water:75% methanol. Aliquots of aqueous, acidic metal stock solutions (1000 ppm, Spex Certipure) are diluted with solvent to the desired concentrations.

ESI-MS

A triple quadrupole MS (TSQ 7000, Thermo Finnigan, San Jose, CA) equipped with an on-axis electrospray source is used. The m/z range is 10 to 2500. Solutions are infused continuously with a syringe pump (5 μL/min, Model 22, Harvard Apparatus, Southnatic MA). Nitrogen (60 psi) and high-purity Ar are used as nebulizing gas and collision gas, respectively. The ESI capillary voltage is - 2.5 kV, and the heated capillary is kept at 250 °C, - 5 V. The ring electrode, skimmer and first octopole are at - 4.7, 0 and + 3 V, respectively. The pressure in the gas line into the octopole collision cell is usually 0.13 Pa but is reduced to 0.026 Pa for threshold measurements. The collision energies (i.e., potential offsets between grounded skimmer and collision cell) are 10 to 30 eV (lab frame) for normal tandem MS and 3 to 43 eV for single reaction mode (SRM) experiments. The resolution of the first mass analyzer was reduced deliberately to obtain better signals in tandem MS experiments.

The octopole collision cell is tilted slightly relative to the line of sight from the source through the first mass analyzer.

RESULTS AND DISCUSSION

Comparison of Ion Extraction Methods

In the previous work, a PE Sciex API1 instrument was used; ions were extracted through a single, thin metal orifice (250 μm diam.) directly through a supersonic jet and into RF only rods at a background pressure of ~ 1 mPa. During ion extraction, the ions underwent collisions only with the N_2 in the curtain gas and supersonic jet. Few collisions with the metal walls are expected with this extraction device.

The Finnigan TSQ 7000 used in the present work has a heated capillary interface. Here the ions are entrained in gas flow through a long, thin stainless steel tube (114 mm long x 400 μm inner diam.). The ions then pass through a supersonic expansion and skimmer into an octopole ion guide, which transports the ions into a third chamber housing the MS.

In general, it is much more difficult to observe metal chloride ions MCl_x^- using the heated capillary interface. $M(NO_3)_x^-$ ions often dominate even if the sample contains no HNO_3 and percent levels of HCl. Recent measurements on a API 3000 triple quadrupole instrument at PE Sciex corroborate these observations.[23] In atmospheric aerosols, nitric acid sticks readily to surfaces and can cause degassing and loss of HCl, with replacement by HNO_3.[21] Perhaps analogous processes occur during droplet production, desolvation or ion extraction in ESI, especially when the ions pass through a long, narrow tube in a heated capillary extraction device.

MS and CID of Nitrate Complexes of Group 1 and 2 Metals

A mass spectrum for a Li sample is shown in Figure 1. Nitrate monomer (NO_3^-, m/z = 62) and protonated dimer ($H(NO_3)_2^-$, m/z = 125) are the main background ions. Alkali metals are singly charged in solution and thus yield $M(NO_3)_2^-$ ions.

A typical CID product ion spectrum is shown for $Li(NO_3)_2^-$ in Figure 2. Nitrate is the only product ion observed from CID of any Group 1 $M(NO_3)_2^-$ species . Presumably, the remaining products are neutral MNO_3 molecules; their presence is assumed but not confirmed directly. The only CID reaction for these ions can be written as follows:

$$M(NO_3)_2^- \rightarrow NO_3^- + MNO_3 \qquad (1)$$

As shown for Li in Figure 1, a variety of cluster ions with several metal atoms are also observed. These cluster ions have the general formula $M_x(NO_3)_{x+1}^-$ and are especially abundant for Li, less so for Na and other, heavier M atoms (data not shown). These clusters are also much more abundant from the heated capillary interface than from the curtain gas interface used previously.[19] In general, the intensity distributions of the Li isotope peaks in the cluster ions correspond to the expected patterns, as shown by the measured and calculated spectra for $Li_8(NO_3)_9^-$ in Figure 3.

A product ion spectrum from CID of the cluster $Li_2(NO_3)_3^-$ is shown in Figure 4. The only ionic product is the next lower species $Li(NO_3)_2^-$; nitrate is not formed. CID of the larger lithium nitrate clusters yields various $Li_x(NO_3)_{x+1}^-$ products, in decreasing abundance as more $LiNO_3$ molecules are lost (Figure 5). Again, no free NO_3^- is formed from metal nitrate clusters with more than one metal atom.

The Group 2 metals give primarily $M(NO_3)_3^-$ ions, with some $M_2(NO_3)_5^-$ clusters (Figure 6), as expected for metal ions in the 2+ oxidation state. On CID the $M(NO_3)_3^-$ ions give only NO_3^-, and the $M_2(NO_3)_5^-$ clusters give only $M(NO_3)_3^-$(Figure 7).

$$M(NO_3)_3^- \rightarrow NO_3^- + M(NO_3)_2 \qquad (2)$$

$$M_2(NO_3)_5^- \rightarrow M(NO_3)_3^- + M(NO_3)_2 \qquad (3)$$

These ions thus behave like those from the Group 1 metals. No $M^I(NO_3)_2^-$ ions, are formed, i.e., the M^{2+} ion is not reduced during CID reactions of $M^{II}(NO_3)_3^-$ for the Group 2 elements.

MS and CID of Nitrate Complexes of Transition Metals and Group 13 Metals

In the previous paper, 3+ metal ions in solution gave mainly $M(NO_3)_4^-$ ions. Those elements with a stable 2+ oxidation state in solution were also seen as $M(NO_3)_3^-$ ions.[19] With the present system, more in-source fragmentation is observed, as shown in the spectrum for Fe^{3+} in Figure 8. While $Fe(NO_3)_4^-$ is the most abundant ion from the Fe^{3+} sample , there is a substantial amount of the oxo product $FeO(NO_3)_3^-$ and also $Fe(NO_3)_3^-$ A small amount of the cluster $Fe_2O(NO_3)_5^-$ is observed. The assignment of this ion is confirmed by the expanded view of the spectrum in Figure 9. The signal ratio for (m/z 436 / m/z 438) is 0.12, in approximate agreement with the value of 0.126 expected for a species with Fe_2 stoichiometry.

The various ions observed and their CID reactions are summarized in Table 1. A typical product ion spectrum is shown for $Y(NO_3)_4^-$ in Figure 10. The product ions are similar to the fragments observed just from CID in the ESI source. For example, the CID spectrum of $Fe(NO_3)_4^-$ looks much like the source spectrum in Figure 8, without the cluster $Fe_2O(NO_3)_5^-$, of course.

In general, the CID products observed correspond to the following reactions, which can occur either in the source and/or during CID in the collision cell. Again, the neutral molecules written in italics are identified by implication; they are not observed directly.

1. Elimination of NO_2 with Formation of Oxo-Nitrate Complex

$$M(NO_3)_4^- \rightarrow MO(NO_3)_3^- + NO_2 \quad (4)$$

$$\rightarrow MO_2(NO_3)_2^- + 2NO_2 \quad (5)$$

$$\rightarrow MO_3(NO_3)^- + 3NO_2 \quad (6)$$

These reactions are favored for early transition metals but occur to some extent for Cu^{2+} and Zn^{2+} as well. Initially, we felt the metal atom was oxidized to higher oxidation states during these reactions. For example, the Fe atom in $FeO(NO_3)_3^-$ could be considered to be in the +4 state, if O is present as the conventional O^{2-}. However, the ionization energy of Fe^{3+} is almost 55 eV[24], too high to be accessible with the collision energies used here. Thus, we consider that the metal atom stays in the same oxidation state in the oxo-nitrate complex, with the O atom present as O^-.

2. Reduction of Metal Atom with Oxidation of Nitrate to NO_3

$$Cu^{II}(NO_3)_3^- \rightarrow Cu^{I}(NO_3)_2^- + NO_3 \quad (7)$$

$$Fe^{III}(NO_3)_4^- \rightarrow Fe^{II}(NO_3)_3^- + NO_3 \quad (8)$$

The metal atom is reduced, while a nitrate ion is oxidized to NO_3. The NO_3 product molecule may also dissociate. Ions containing Fe^{2+} from solutions of Fe^{3+} were originally attributed to electrochemical reduction in solution at the ESI needle.[19] The fact that they can also be observed as CID products shows that such ions can be formed in the gas phase via this internal redox process. For the metals In^{3+} and Ga^{3+}, this internal redox process can occur to yield M^{2+}, detected as $M^{II}(NO_3)_3^-$, even though the 2+ oxidation state is not common

in solution for these elements. In contrast, $Y^{III}(NO_3)_4^-$ yields $Y^{I}(NO_3)_2^-$ but not $Y^{II}(NO_3)_3^-$ (Figure 10).

3. Elimination of Nitrate, Generation of Neutral Metal Nitrate Complex

$$Fe(NO_3)_4^- \rightarrow NO_3^- + Fe(NO_3)_3 \qquad (9)$$

Complexes with one transition metal or Group 13 metal atom yield NO_3^- as a minor CID product, in contrast to the Group 1 and 2 metals, where NO_3^- is the only product ion .

Threshold Kinetic Energy Measurements for $NO_3^- \rightarrow NO_2^- + O$

Armentrout[25-26] describes a number of validation criteria for determining the kinetic energy threshold for CID reactions.[27-29] These validation experiments are particularly important here because the present work is done with a commercial triple quadrupole MS built for analysis, not for accurate thermochemical measurements.[30-34]

One point is to evaluate the kinetic energy spread of the ion beam. Application of a stopping potential to the quadrupole rods indicates the ion energy spread is ~ 0.7 eV FWHM in the lab frame. A second point is to use a low collision gas pressure to minimize complications due to multiple collisions. For threshold measurements the inlet pressure is reduced from 0.13 to 0.026 Pa. At 0.026 Pa the mean free path in the collision cell is estimated to be approximately 24 cm, slightly longer than the ocotopole (18 cm). Thus, there still may be some contribution from multiple collisions. Reducing the pressure attenuates the product ions to only a few percent of the parent ion signal, but measurable signals remain.

A third criterion is to calibrate the collision energy using a known process. We measure CID of NO_3^-, m/z = 62, a species produced in the same fashion as the $M(NO_3)_x^-$ complexes of direct interest.

$NO_3^- \rightarrow NO_2^- + O$ (10)

$D_0(O\text{-}NO_2^-) = D_0(O\text{-}NO_2) + EA(NO_2) - EA(NO_3)$

$= 4.648 + (-2.273) - (-3.937) = 6.312$ eV[35-36]

NO_2^- is the only measurable product.

One plot in Figure 11 shows the measured cross section for Reaction (10) as a function of collision energy in the center-of-mass frame of reference. These data are also converted to cross sections by the method described by Armentrout, [26] Eqn. 7 with σ_0 =18, n=1.1, E_0 = 5.55. The measured threshold for appearance of NO_2^- is 5.55 eV, lower than the calculated value by 0.76 eV. If anything, the apparatus underestimates the actual collision energy.

Threshold Measurements for Daughter Ions from $Fe(NO_3)_4^-$

Data obtained in single reaction mode for three CID products from $Fe(NO_3)_4^-$ are shown in Figure 12. The thresholds for production of $FeO(NO_3)_3^-$ and $Fe(NO_3)_3^-$ are very low, only 0.5 and 0.8 eV, respectively. Those for $FeO_2(NO_3)_2^-$ and $FeO(NO_3)_2^-$ are slightly higher, 1.5 and 1.8 eV (data for the latter value are not shown). These values should be treated as approximations only, as the 0.76 eV offset found from dissociation of NO_3^- and other sources of error in the threshold measurements may be substantial. The main point is that low collision energy is sufficient to initiate these CID processes.

The threshold for elimination of NO_3^- from $Fe(NO_3)_4^-$ is presented in Figure 13. Nitrate ion is a minor product, so there is more scatter in the plot than in those of previous figures. Nevertheless, the threshold for nitrate elimination (Reaction 9) can be assigned to be approximately 2.0 eV. If the offset found for $NO_3^- \rightarrow NO_2^- + O$ is added, the actual

threshold is 2.76 eV, a reasonable value for a bond energy between a metal ion and an anionic ligand of moderate complexing strength.

Thermochemical Considerations

Consider the following thermodynamic cycle for conversion of $Fe(NO_3)_4^-$ to $Fe(NO_3)_3^-$:

$Fe(NO_3)_4^-$	$\rightarrow Fe(NO_3)_3 + NO_3^-$	$D_0(^-O_3N-Fe(NO_3)_3) \sim 2.76$ eV	
$Fe(NO_3)_3$	$\rightarrow Fe^{3+} + 3NO_3^-$	$\Sigma D_0 (Fe^{3+}\text{-}NO_3^-) =$	?
$Fe^{3+} + e^-$	$\rightarrow Fe^{2+}$	$-IE(Fe^{2+})$ =	-30.651 eV
NO_3^-	$\rightarrow NO_3 + e^-$	$-EA(NO_3)$ =	3.937 eV
$\underline{Fe^{2+} + 3NO_3^- \rightarrow Fe(NO_3)_3^-}$		$-\underline{\Sigma D_0(Fe^{2+} - NO_3^-) = ?}$	
$Fe(NO_3)_4^-$	$\rightarrow Fe(NO_3)_3^- + NO_3$		

Most of the Fe - NO_3^- dissociation energies are not known, but the difference between the D_0 sums for the Fe^{3+} and Fe^{2+} nitrates can hardly be more than a few eV. Thus, the very large negative value for the third ionization energy of Fe should make this reaction highly exothermic. It is interesting that the ion $Fe(NO_3)_4^-$ survives the collisions in the extraction process at all; it is, in fact, the most abundant ion from Fe^{3+} solutions under the conditions used.

CONCLUSIONS

The observations reported herein can be summarized as follows:

1. Complexation with nitrate can stabilize some highly reactive species with high internal energies.

2. Some metal nitrate ions undergo internal redox processes during CID, such as conversion of M^{3+} to M^{2+}, even for elements like In^{3+} and Ga^{3+} that do not normally have lower oxidation states in solution. Presumably, such reductions are accompanied by oxidation of NO_3^- to NO_3.

3. Oxo ions are prominent from CID of triply charged metal nitrate complexes, as expected for "hard" metal cations.

4. Cluster ions with more than one metal atom are most evident for small metals with low charges

5. The type of ion extraction device affects the species observed. Nitrate ions are apparently enhanced by the heated capillary interface. The ESI conditions may also play a role.

6. The CID reactions of $Fe(NO_3)_4^-$ ions have low kinetic energy onsets of ~ +0.5 to 2 eV and are expected to be exothermic.

ACKNOWLEDGMENTS

Ames Laboratory is operated by Iowa State University for the U. S. Department of Energy, Contract No. W-7405-Eng-82. This work was supported by the Chemical and Biological Sciences Program, Office of Basic Energy Sciences, Division of Chemical Sciences. The authors thank L. Huang and Bayer Co. for donating the triple quadrupole MS, Bruce

Thomson and Perkin Elmer Sciex for providing access to a triple quadrupole instrument with a curtain gas interface, and James Espenson and Gabor Lente for valuable discussions.

REFERENCES:

1. Yamashita, M.; Fenn, J. B. Electrospray Ion Source. Another Variation on the Free-Jet Theme. *J. Phys. Chem.* **1984,** *88*, 4451-4459.
2. Kebarle, P.; Tang, L. From Ions in Solution to Ions in the Gas Phase - the Mechanism of Electrospray Mass Spectrometry. *Anal. Chem.* **1993,** *65*, 972A-986A.
3. Chait, B. T.; Kent, S. B. H. Weighing Naked Proteins: Practical, High-Accuracy Mass Measurement of Peptides and Proteins. *Science* **1992,** *257*, 1885-1894.
4. Cole, R. B. *Electrospray Ionization Mass Spectrometry*, John Wiley & Sons: New York, **1997,** 527-570.
5. Burlingame, A. L.; Boyd, R. K.; Gaskell, S. J. Mass Spectrometry. *Anal. Chem.* **1996,** *68*, 599-652.
6. Colton, R.; D' Agostino, A.; Traeger, J. C. Electrospray Mass Spectrometry Applied to Inorganic and Organometallic Chemistry. *Mass Spectrom. Rev.* **1995,** *14*, 79-106.
7. Stewart, I. I. Electrospray Mass Spectrometry: a Tool for Elemental Speciation. *Spectrochimica Acta Part B* **1999,** *54*, 1649-1695.
8. Henderson, W.; Nicholson, B. K.; McCaffrey, L.J. Applications of Electrospray Mass Spectrometry in Organometallic Chemistry. *Polyhedron* **1998,** 17, 4291–4313.

9. Feng, R; Castelhano, A.L.; Billedeau, R.; Yuan, Z. Y. Study of Noncovalent Enzyme-Inhibitor Complexes. Stoichiometry of Matrilysin by Electrospray Ionization Mass Spectrometry. *J. Am. Soc. Mass Spectrom.* **1995,** *6*, 1105-1111.

10. Bayer, E.; Bauer, T.; Schmeer, K.; Bleicher, K.; Maier, M.; Gaus, H. J. Analysis of Double-Stranded Oligonucleotides by Electrospray Mass Spectrometry. *Anal. Chem.* **1994,** *66*, 3858-3863.

11. Yu, X. L.; Wojciechowski, M.; Fenselau, C. Assessment of Metals in Reconstituted Metallothioneins by Electrospray Mass Spectrometry. *Anal. Chem.* **1994,** *66*, 1355-1359.

12. McLafferty, F. W.; Guan, Z.; Haupts, U.; Wood, T. D.; Kelleher, N. L. Gaseous Conformers of Cytochrome c. *J. Am. Chem. Soc.* **1998,** *120*, 4732-4730.

13. He, F.; Hendrickson, C.L.; Marshall, A.G. Unequivocal Determination of Metal Atom Oxidation State in Naked Heme Proteins: Fe(III)myoglobin, Fe(III)cytochrome c, Fe(III)cytochrome b5, and Fe(III)cytochrome b5 L47R. *J. Am. Soc. Mass Spectrom.* **2000**, *11*, 120-126.

14. Sharp, B. L.; Sulaiman, A. B.; Taylor, K. A.; Green, B. N. Observations on the Use of Ion Spray Mass Spectrometry for Elemental Speciation in Aqueous Solutions Without Recourse to Chromatography. *J. Anal. Atomic Spectrom.* **1997,** *12*, 603-609.

15. Cheng, Z. L.; Siu, K. W. M.; Guevremont, R.; Berman, S. S. Electrospray Mass Spectrometry: a Study on Some Aqueous Solutions of Metal Salts. *J. Am. Soc. Mass Spectrom.* **1992,** *3*, 281-288.

16. Cheng, Z. L.; Siu, K. W. M.; Guevremont, R.; Berman, S. S. Solvent-Derived Metal Oxides in Electrospray Mass Spectrometry of Metal Salt Solutions. *Org. Mass Spectrom.* **1992,** *27*, 1370-1376.

17. Agnes, G. R.; Horlick, G. Electrospray Mass Spectrometry as a Technique for Elemental Analysis: Preliminary Results. *Appl. Spectrosc.* **1992,** *46*, 401-406.

18. Blades, A. T.; Jayaweera, P.; Ikonomu, M. G.; Kebarle, P. First Studies of the Gas Phase Ion Chemistry of M^{3+} Metal Ligand Complexes. *Int. J. Mass Spectrom. Ion Processes* **1990,** *101*, 325-336.

19. Mollah, S.; Pris, A. D.; Johnson, S. K.; Gwizdala III, A. B.; Houk, R. S. Identification of Metal Cations by Electrospray Mass Spectrometry in the Negative Ion Mode. *Anal. Chem.* **2000,** *72*, 985- 991.

20. Viggiano, A. A. In Situ Mass Spectrometry and Ion Chemistry in the Stratosphere and Troposphere. *Mass Spectrom. Reviews* **1993**, *12*, 115-137; Viggiano, A. A.; Hunton, D. E. Airborne Mass Spectrometers: Four Decades of Atmospheric and Space Research at the Air Force Research Laboratory. *J. Mass Spectrom.* **1999**, *34*, 1107-1129.

21. Finlayson-Pitts, B. J.; Pitts, J. N, Jr. Chemistry of the Upper and Lower Atmosphere. Theory, Experiment and Applications. Academic, San Diego, 2000. Chap. 7E and p. 285.

22. Zhao, X.; Yinon, J. Forensic Identification of Explosive Oxidants by Electrospray Ionization Mass Spectrometry. *Rapid Commun. Mass Spectrom.* 2002, 16, 1137-1146.

23. Houk, R. S.; Thomson, B. A. Unpublished results, 2002.

24. Huheey, J. E. *Inorganic Chemistry: Principles of Structure and Reactivity.* Harper, New York, 1972, p. 46.

25. Armentrout, P. B. Thermochemical Measurement by Guided Ion Beam Mass Spectrometry. Adams, N. G.; Babcock, L. M., Eds. *In Advances in Gas Phase Ion Chemistry, Vol. 1.* JAL: Greenwich, **1992,** pp. 83-119.

26. Armentrout, P. B. Mass Spectrometry – Not Just a Structural Tool: The Use of Guided Ion beam Tandem Mass Spectrometry to Determine Thermochemistry. *J. Am. Soc. Mass Spectrom.* **2002**, *13*, 419-434.

27. Muntean, F.; Armentrout, P. B. Guided Ion Beam Study of Collision-Induced Dissociation Dynamics: Integral and Differential Cross Sections. *J. Chem. Phys.* **2001,** *115*, 1213-1228.

28. Armentrout, P. B. The Kinetic Energy Dependence of Ion-Molecule Reactions: Guided Ion Beams and Threshold Measurements. *Int. J. Mass Spectrom.* **2000,** *200*, 219-241.

29. Rodgers, M. T.; Ervin, K. M.; Armentrout, P. B. Statistical Modeling of Collision-Induced Dissociation Threshold. *J. Chem. Phys.* **1997,** *106*, 4499-4508.

30. Rodgers, M. T.; Armentrout, P. B. Collision-Induced Dissociation Measurements on $Li^+(H_2O)_n$, n=1-6: The First Direct Measurement of the Li^+-OH_2 Bond Energy. *J. Phys. Chem. A* **1997,** *101*, 1238-1249.

31. Andersen, A.; Muntean, F.; Walter, D.; Rue, C.; Armentrout, P. B. *J. Phys. Chem. A* **2000,** 104, 692-705.

32. Ariston, N.; Armentrout, P. B. Collision-Induced Dissociation of Vanadium Monoxide Ion. *J. Phys. Chem.* **1986,** *90*, 5135-5140.

33. Armentrout, P. B.; Hales, D. A.; Lian, L. Duncan, M. A., Ed. *In* Advances in Metal and Semiconductor Clusters, Vol. II. JAI: Greenwich, **1994,** pp. 1-39.

34. Rodgers, M. T.; Armentrout, P. B. Noncovalent Metal-Ligand Bond Energies as Studied by Threshold Collision-Induced Dissociation. *Mass Spectrometry Reviews* **2000,** *19*, 215-247.

35. Ervin, K. M.; Ho, J.; Lineberger, W. C. Ultraviolet Photoelectron Spectrum of NO_2^- *J. Phys. Chem.* 1988, *92*, 5405-5412.

36. Weaver, A.; Arnold, D. W.; Bradforth, S. E.; Neumark, D. M. Examination of the $^2A_2'$ and $^2E''$ States of NO_3 by Ultraviolet Photoelectron Spectroscopy of NO_3^-. *J. Chem. Phys.* **1991,** *94*, 1740-1751.

Table 1: MSMS of alkali and alkaline earth metal complexes with nitrate.

Metal complex / parent	**Product(s) / Reactions**
$Li(NO_3)_2^-$	$Li(NO_3)_2^- \rightarrow LiNO_3 + NO_3^-$
$Li_2(NO_3)_3^-$	$Li_2(NO_3)_3^- \rightarrow LiNO_3 + Li(NO_3)_2^-$
$Na(NO_3)_2^-$	$Na(NO_3)_2^- \rightarrow NaNO_3 + NO_3^-$
$Na_2(NO_3)_3^-$	$Na_2(NO_3)_3^- \rightarrow NaNO_3 + Na(NO_3)_2^-$
$K(NO_3)_2^-$	$K(NO_3)_2^- \rightarrow KNO_3 + NO_3^-$
$K_2(NO_3)_3^-$	$K_2(NO_3)_3^- \rightarrow KNO_3 + K(NO_3)_2^-$
$Rb(NO_3)_2^-$	$Rb(NO_3)_2^- \rightarrow RbNO_3 + NO_3^-$
$Cs(NO_3)_2^-$	$Cs(NO_3)_2^- \rightarrow CsNO_3 + NO_3^-$
$Cs_2(NO_3)_3^-$	$Cs_2(NO_3)_3^- \rightarrow CsNO_3 + Cs(NO_3)_2^-$
$Be(NO_3)_3^-$	$Be(NO_3)_3^- \rightarrow Be(NO_3)_2 + NO_3^-$
$Mg(NO_3)_3^-$	$Ng(NO_3)_3^- \rightarrow Mg(NO_3)_2 + NO_3^-$
$Ca(NO_3)_3^-$	$Ca(NO_3)_3^- \rightarrow Ca(NO_3)_2 + NO_3^-$
$Ca_2(NO_3)_5^-$	$Ca_2(NO_3)_5^- \rightarrow Ca(NO_3)_2 + Ca(NO_3)_3^-$
$Sr(NO_3)_3^-$	$Sr(NO_3)_3^- \rightarrow Sr(NO_3)_2 + NO_3^-$
$Ba(NO_3)_3^-$	$Ba(NO_3)_3^- \rightarrow Ba(NO_3)_2 + NO_3^-$

Table 2: MSMS of transition metal and 3A metal complexes with nitrate.

Metal complex / parent	Product(s) / Reactions
$Sc(NO_3)_4^-$	$Sc(NO_3)_4^- \rightarrow ScO(NO_3)_3^- + NO_2$
	$Sc(NO_3)_3^- \rightarrow ScO_2(NO_3)_2^- + 2NO_2$
	$Sc(NO_3)_3^- \rightarrow Sc(NO_3)_3 + NO_3^-$
$Cr(NO_3)_4^-$	$Cr(NO_3)_4^- \rightarrow CrO(NO_3)_3^- + NO_2$
	$Cr(NO_3)_3^- \rightarrow CrO_2(NO_3)_2^- + 2NO_2$
	$Cr(NO_3)_3^- \rightarrow CrO_3(NO_3)_2^- + 3NO_2$
$Mn(NO_3)_3^-$	$Mn(NO_3)_3^- \rightarrow MnO(NO_3)_2^- + NO_2$
	$Mn(NO_3)_3^- \rightarrow MnO_2(NO_3)^- + 2NO_2$
	$Mn(NO_3)_3^- \rightarrow Mn(NO_3)_2 + NO_3^-$
$Fe(NO_3)_4^-$	$Fe(NO_3)_4^- \rightarrow FeO(NO_3)_3^- + NO_2$
	$Fe(NO_3)_4^- \rightarrow FeO_2(NO_3)_2^- + 2NO_2$
	$Fe(NO_3)_4^- \rightarrow FeO_3(NO_3)^- + 3NO_2$
	$^{III}Fe(NO_3)_4^- \rightarrow {}^{II}Fe(NO_3)_3^- + NO_3^-$
$FeO(NO_3)_3^-$	$FeO(NO_3)_3^- \rightarrow FeO_2(NO_3)_2^- + NO_2$
	$FeO(NO_3)_3^- \rightarrow FeO_3(NO_3)^- + NO_2$
$Fe(NO_3)_3^-$	$Fe(NO_3)_3^- \rightarrow FeO(NO_3)_2^- + NO_2$
	$Fe(NO_3)_3^- \rightarrow FeO_2(NO_3)^- + NO_2$
$Co(NO_3)_3^-$	$Co(NO_3)_3^- \rightarrow CoO(NO_3)_2^- + NO_2$
	$Co(NO_3)_3^- \rightarrow CoO_2(NO_3)^- + 2NO_2$
	$Co(NO_3)_3^- \rightarrow Co(NO_3)_2 + NO_3^-$
$Ni(NO_3)_3^-$	$Ni(NO_3)_3^- \rightarrow NiO(NO_3)_2^- + NO_2$
	$Co(NO_3)_3^- \rightarrow Co(NO_3)_2 + NO_3^-$

$^{II}Cu(NO_3)_3^-$	$^{II}Cu(NO_3)_3^- \rightarrow {}^{I}Cu(NO_3)_2^- + NO_3$
	$^{II}Cu(NO_3)_3^- \rightarrow {}^{II}Cu(NO_3)_2^- + \mathit{NO_3^-}$
$^{I}Cu(NO_3)_2^-$	$^{I}Cu(NO_3)_2^- \rightarrow {}^{\mathit{I}}\mathit{CuO(NO_3)}^- + NO_3$
	$^{I}Cu(NO_3)_2^- \rightarrow {}^{\mathit{I}}\mathit{Cu(NO_3)} + \mathit{NO_3^-}$
$Zn(NO_3)_3^-$	$Zn(NO_3)_3^- \rightarrow Zn\mathit{O(NO_3)_2^-} + NO_2$
	$Zn(NO_3)_3^- \rightarrow Zn(NO_3)_2 + \mathit{NO_3^-}$
$Al(NO_3)_4^-$	$Al(NO_3)_4^- \rightarrow \mathit{AlO(NO_3)_3^-} + NO_2$
	$Al(NO_3)_4^- \rightarrow \mathit{AlO_2(NO_3)_2^-} + 2NO_2$
	$Al(NO_3)_4^- \rightarrow \mathit{Al(NO_3)_3} + \mathit{NO_3^-}$
$Ga(NO_3)_4^-$	$Ga(NO_3)_4^- \rightarrow \mathit{GaO(NO_3)_3^-} + NO_2$
	$^{III}Ga(NO_3)_4^- \rightarrow {}^{II}\mathit{Ga(NO_3)_3^-} + NO_3$
	$Ga(NO_3)_4^- \rightarrow Ga(NO_3)_3 + \mathit{NO_3^-}$
$In(NO_3)_4^-$	$In(NO_3)_4^- \rightarrow \mathit{InO(NO_3)_3^-} + NO_2$
	$^{III}In(NO_3)_4^- \rightarrow {}^{II}\mathit{In(NO_3)_3^-} + NO_3$
	$Al(NO_3)_4^- \rightarrow \mathit{Al(NO_3)_3} + \mathit{NO_3^-}$

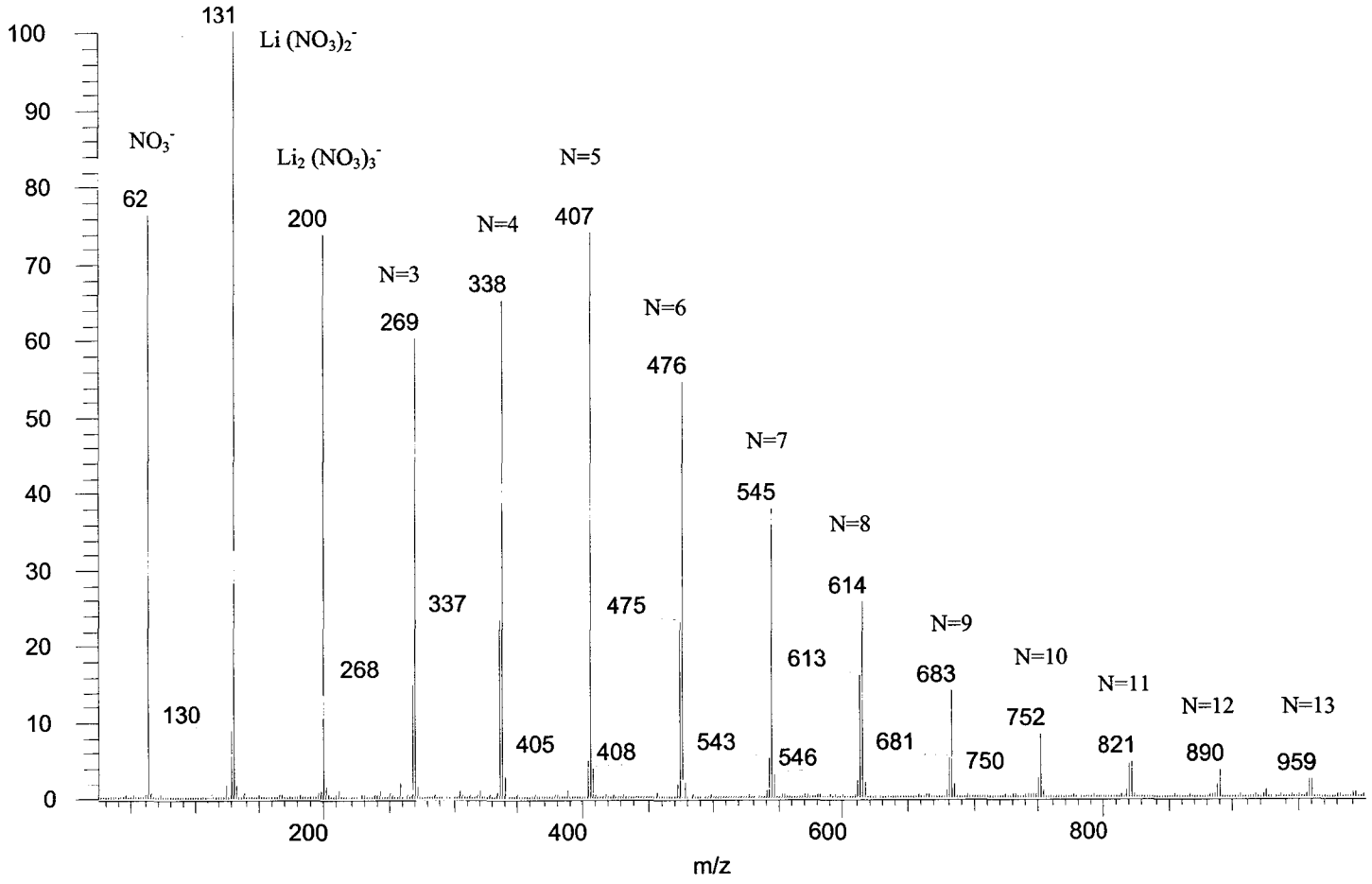

Fig. 1. Mass spectrum of 0.1 mM Li in 25/75 water/methanol solvent with 0.05% HNO_3. Cluster ions $Li_n(NO_3)_{n+1}^-$ (n=1-13) are observed.

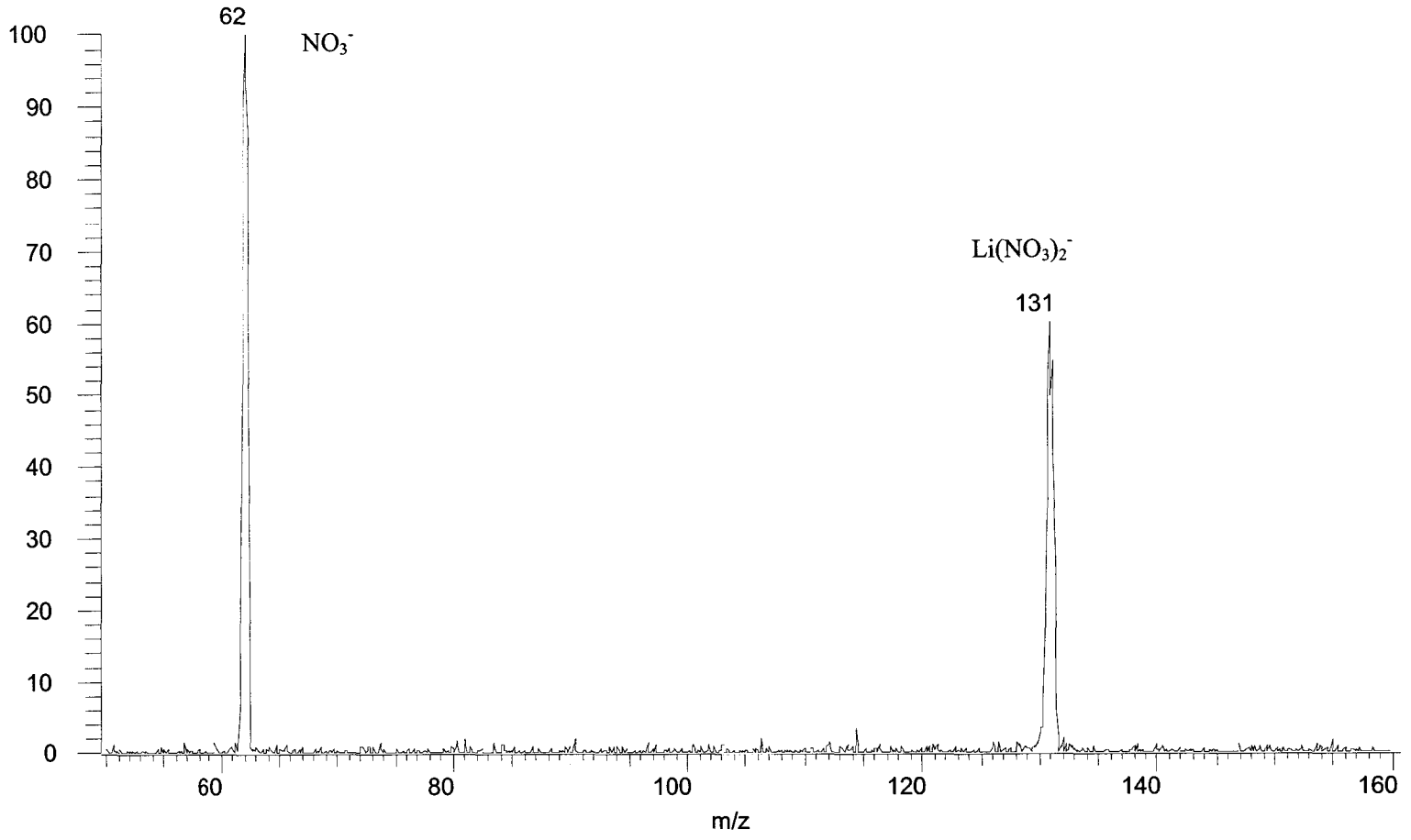

Fig. 2. CID product spectrum of $Li(NO_3)_2^-$ (m/z 131), which fragments into $LiNO_3$ and NO_3^-. The collision energy and collision gas pressure were 15 eV lab and 0.13 Pa.

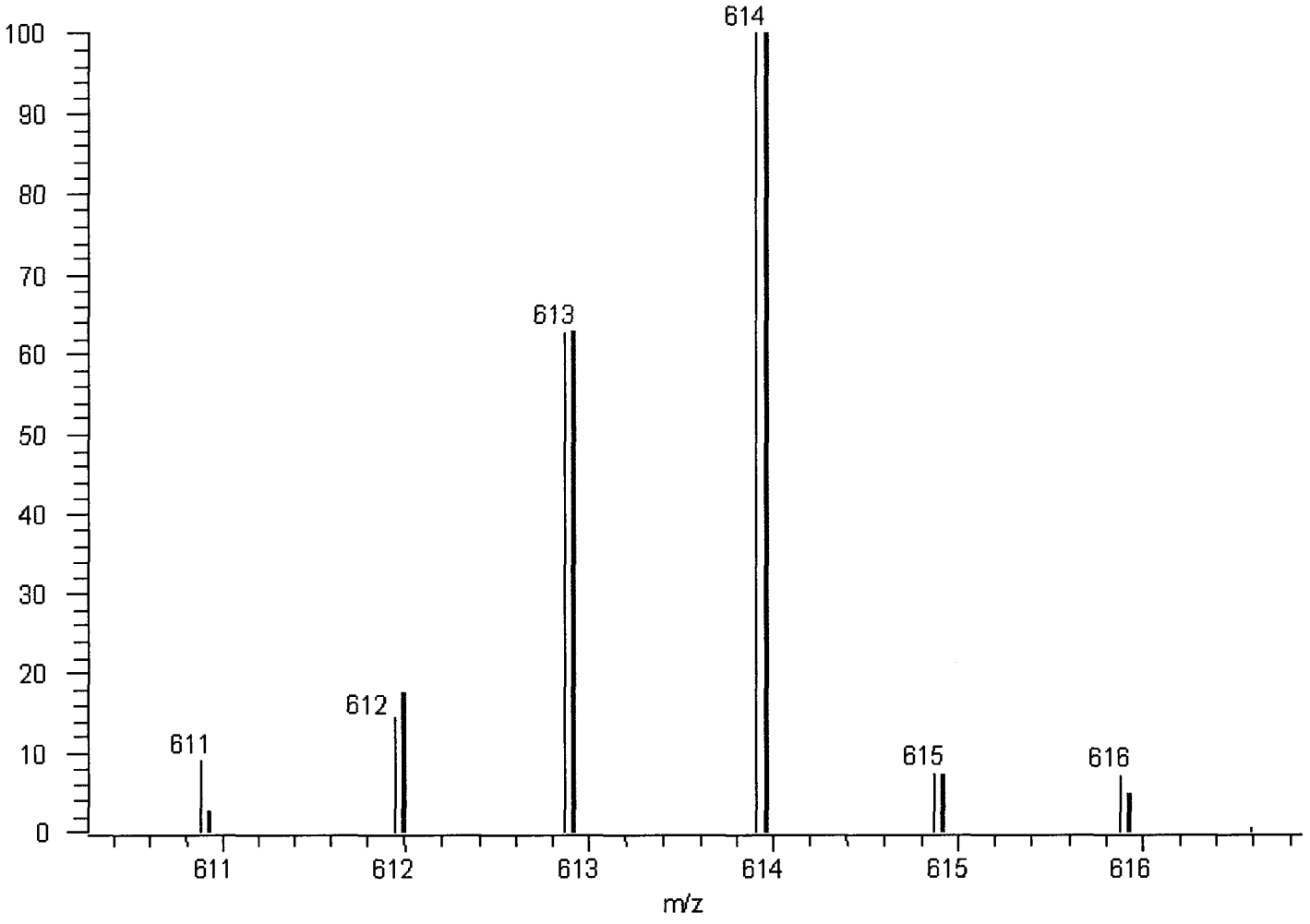

Fig. 3. Expanded scan of isotope peaks of $Li_8(NO_3)_9^-$. Thin black lines are the measured intensities, gray bars are the calculated isotope distributions.

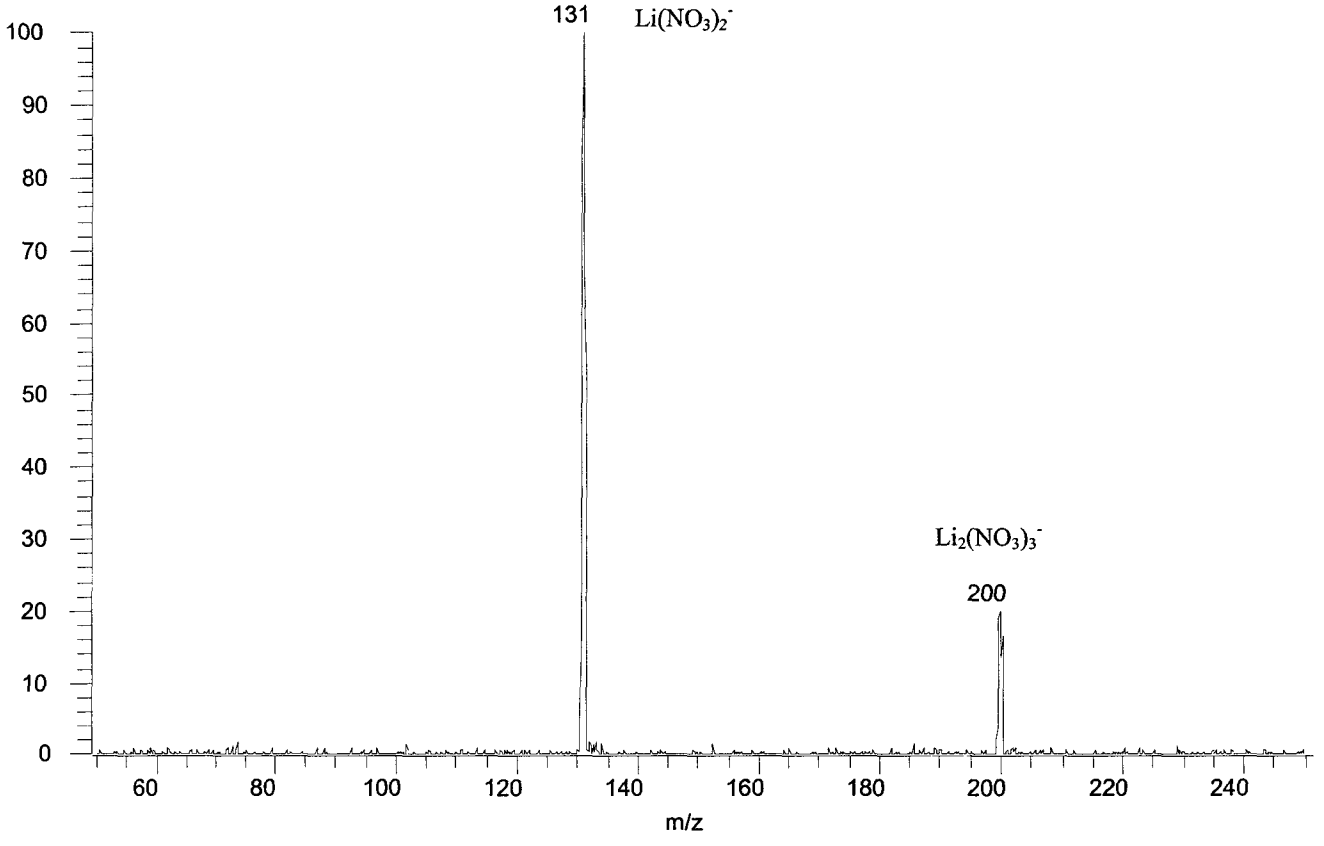

Fig. 4. CID product spectrum of $Li_2(NO_3)_3^-$ (m/z 200), which fragments into $Li(NO_3)_2^-$ and $LiNO_3$. Note that $Li_2(NO_3)_3^-$ does not make NO_3^- directly. The collision energy and collision gas pressure were 10 eV lab and 0.13 Pa.

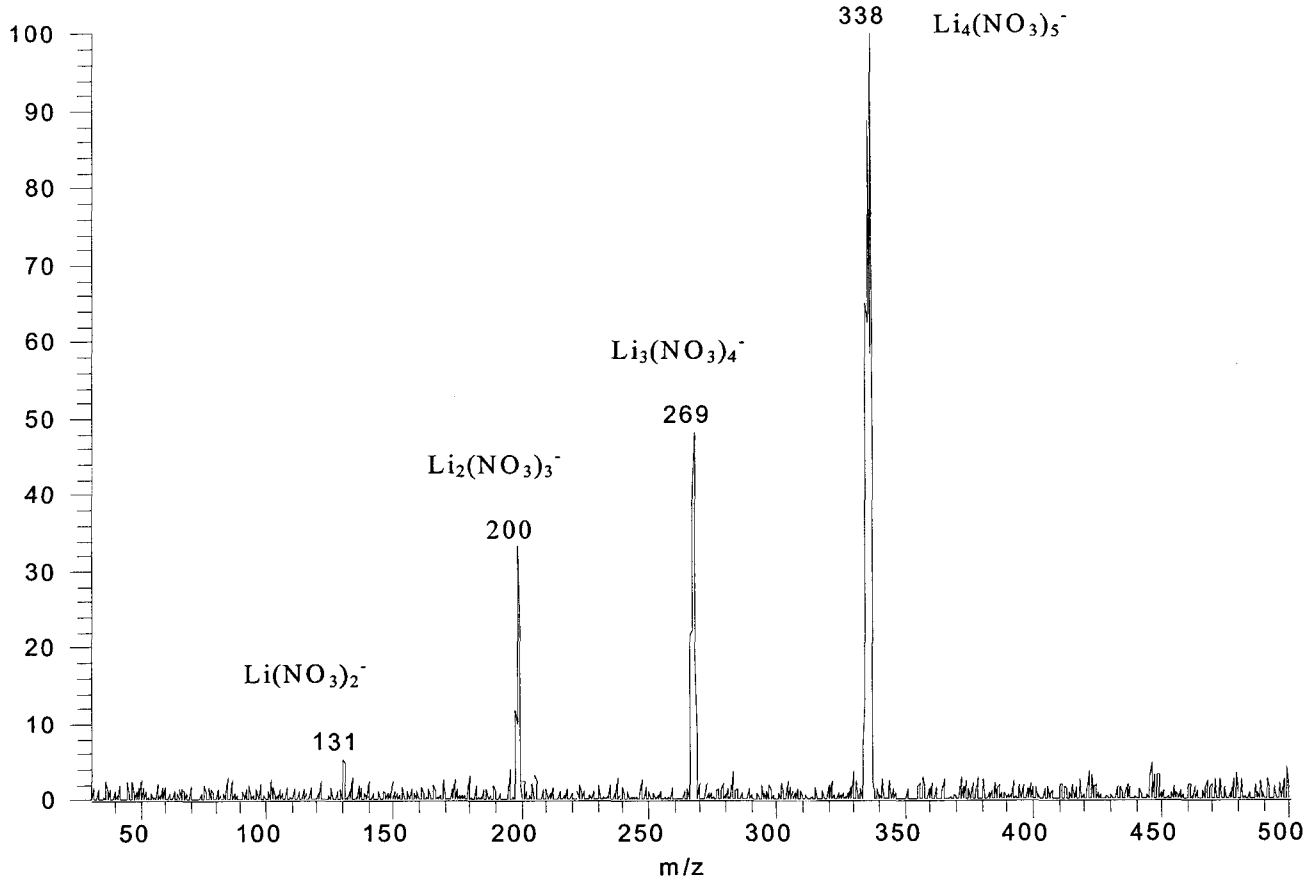

Fig. 5. CID product spectrum of $Li_4(NO_3)_5^-$ (m/z=338), which fragments into various Li nitrate clusters, but not NO_3^-. The collision energy and collision pressure were 22 eV lab and 0.10 Pa, respectively.

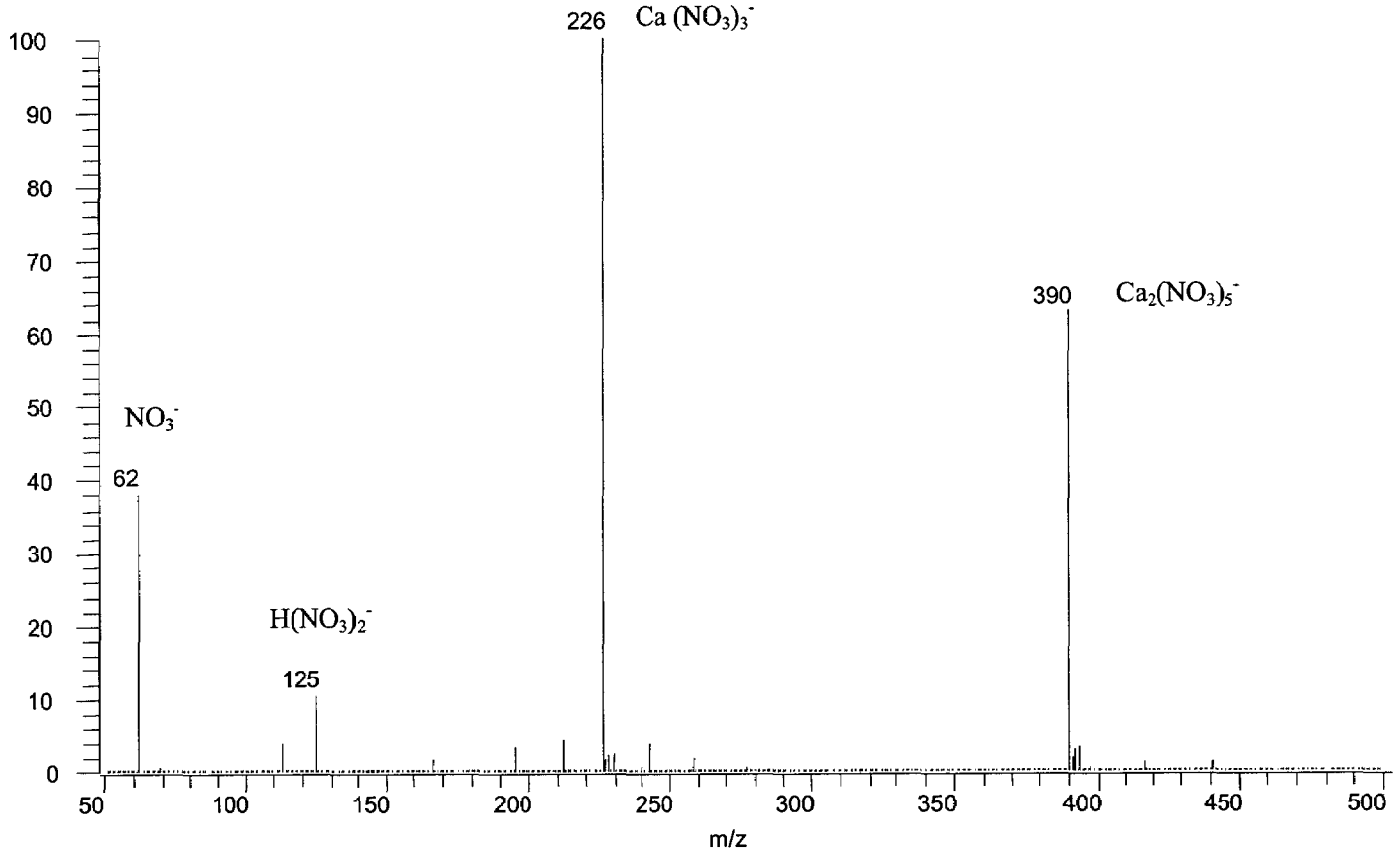

Fig. 6. Mass spectrum of 0.1 mM Ca in 25/75 water/methanol solvent with 0.05% HNO_3. $Ca(NO_3)_3^-$ (m/z=226) and $Ca_2(NO_3)_5^-$ (m/z=390) were observed.

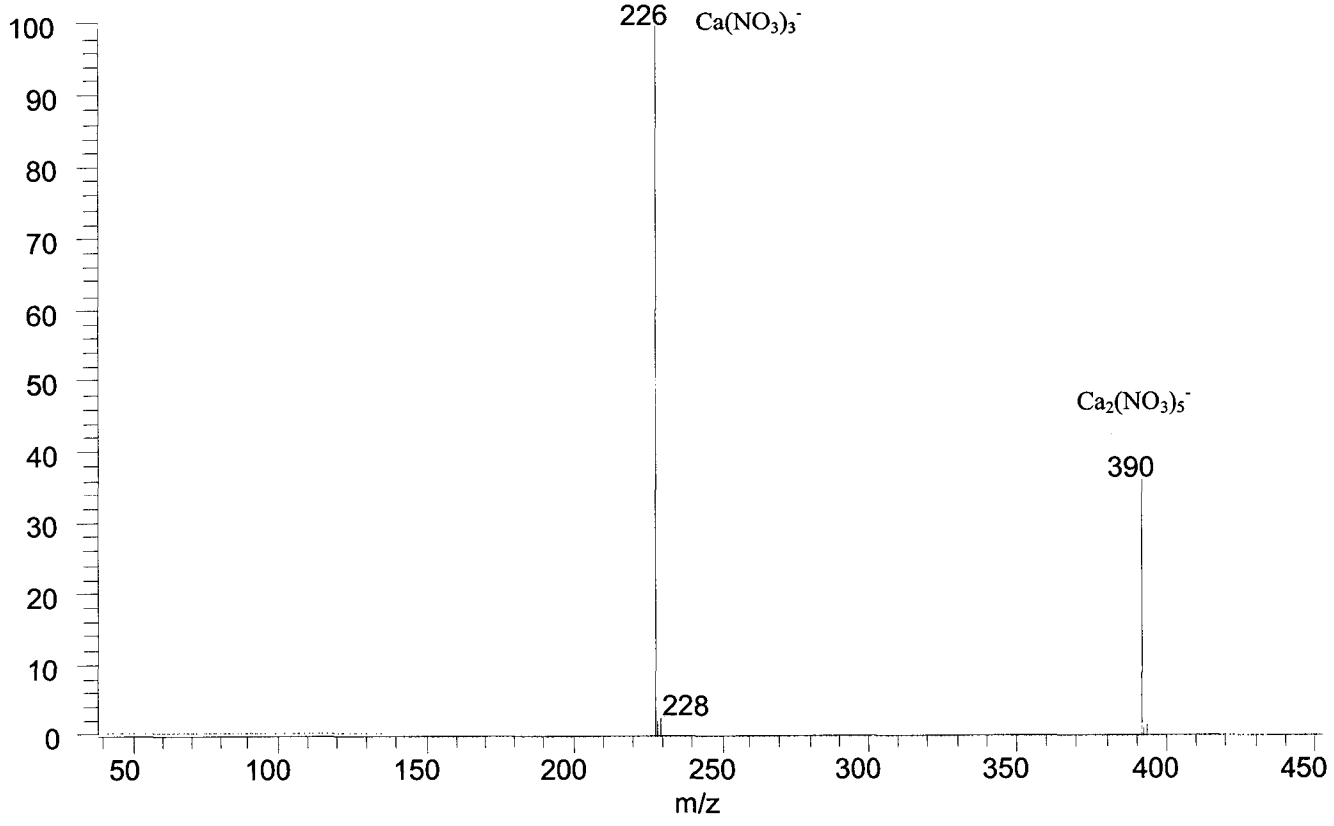

Fig. 7. CID product spectrum of $Ca_2(NO_3)_5^-$ (m/z=390), which fragments into $Ca(NO_3)_2$ and $Ca(NO_3)_3^-$. Collision energy and pressure are 20 eV lab and 0.13 Pa.

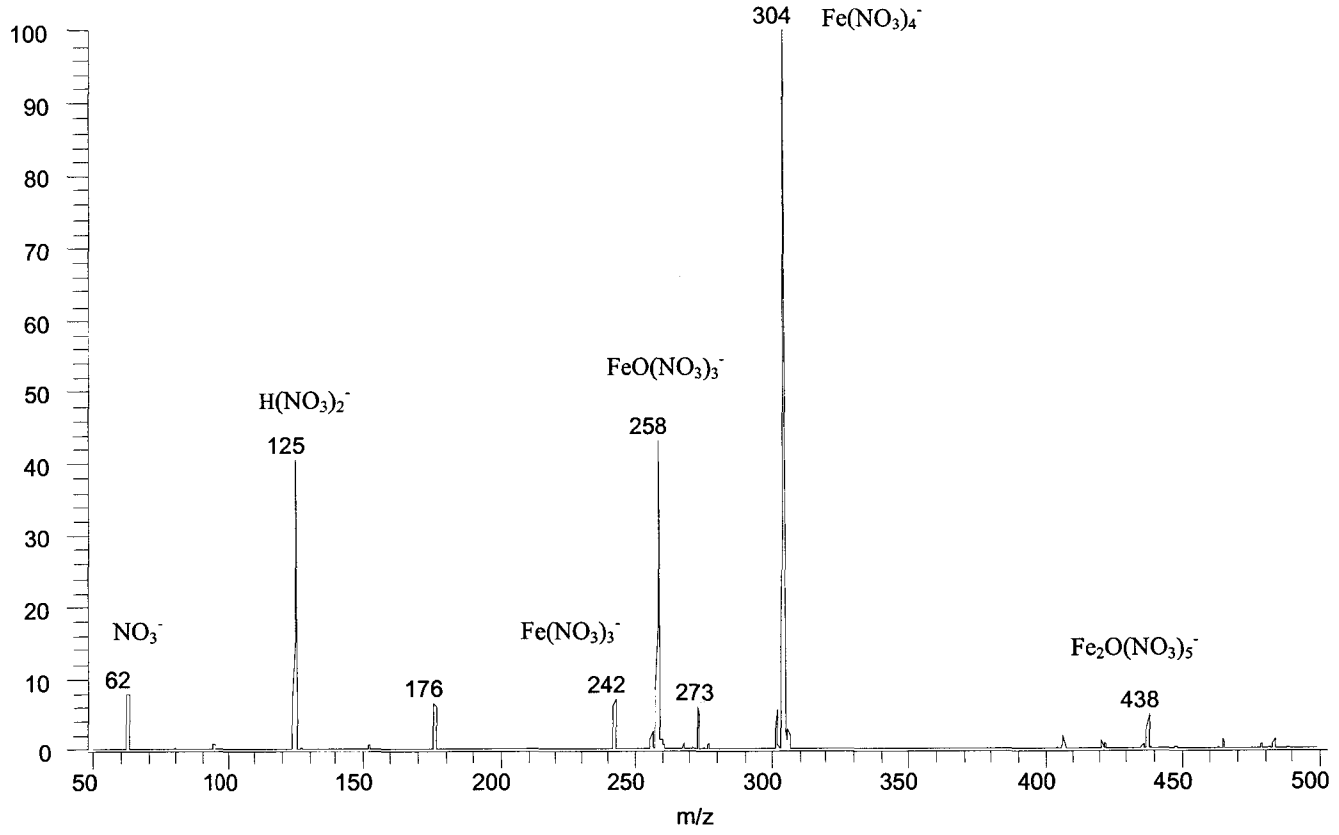

Fig. 8. Mass spectrum of 50 ppm Fe in 25/75 water/methanol solvent with 0.05% HNO_3. The major ions are $Fe(NO_3)_4^-$ (m/z 304), $FeO(NO_3)_3^-$ (m/z 258) due to in-source fragmentation, and some $Fe^{II}(NO_3)_3^-$ (m/z 242) from reduction of $Fe^{III}(NO_3)_4^-$. See next figure for enlargement of region around m/z = 438.

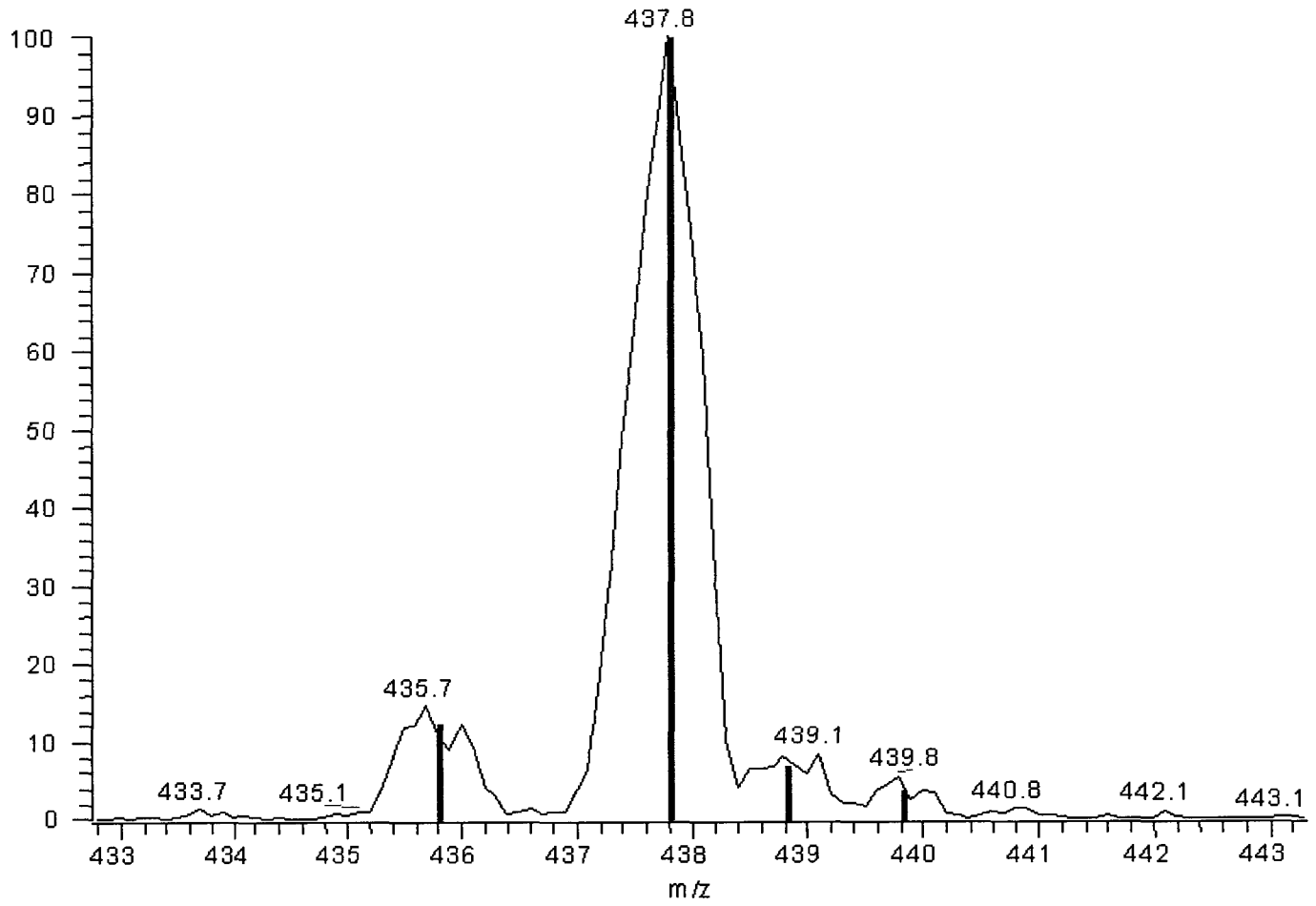

Fig 9. Expanded scan of region containing $Fe_2O(NO_3)_5^-$ ions. The gray bars show the calculated isotope distribution for the four most abundant ions at m/z 435.81 (12.64%), 437.81 (100%), 438.81 (7.01%) and 439.81 (3.98%).

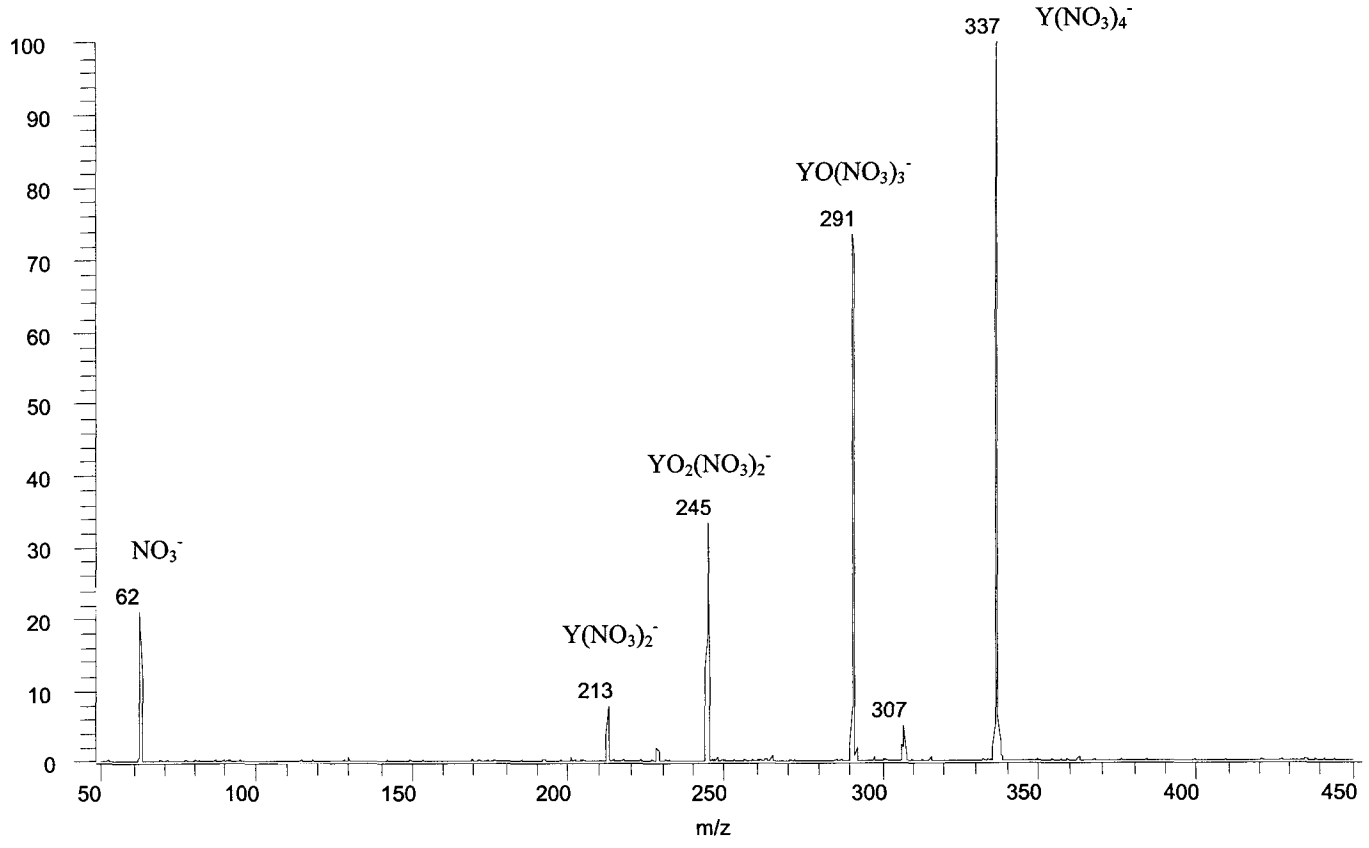

Fig. 10. CID product spectrum of $Y(NO_3)_4^-$ (m/z=337), which fragments into $YO(NO_3)_3^-$, $YO_2(NO_3)_2^-$, $Y(NO_3)_2^-$ and NO_3^-. The collision energy and pressure are 20 eV lab and 0.13 Pa.

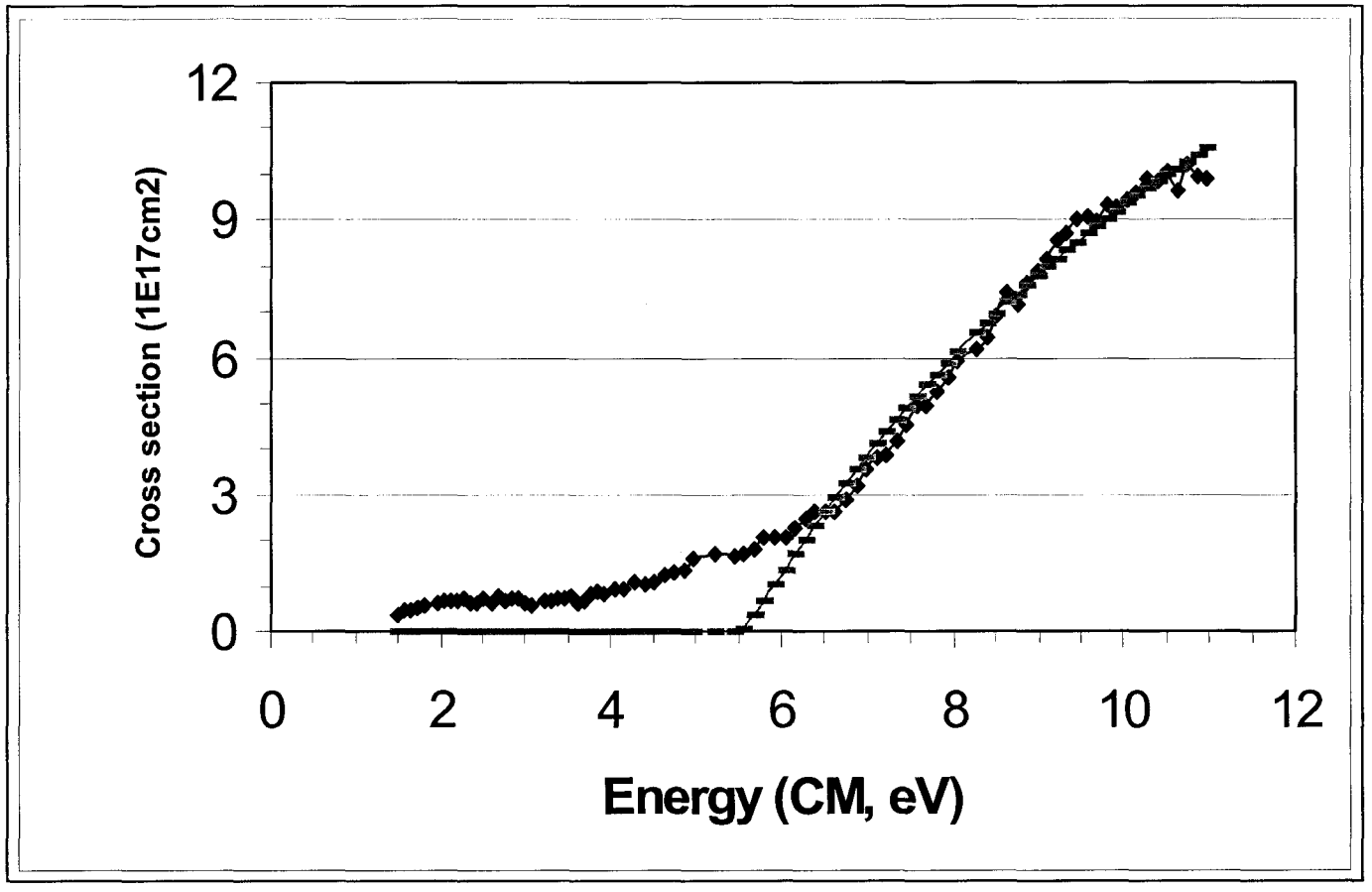

Fig. 11. Cross section for NO_3^- ® NO_2^- + O vs. collision energy in center of mass frame of reference. The diamonds are the direct experimental results, while the dashes are the converted experimental results using the procedure in ref. 26. NO_2^- has an appearance threshold of 5.55 eV.

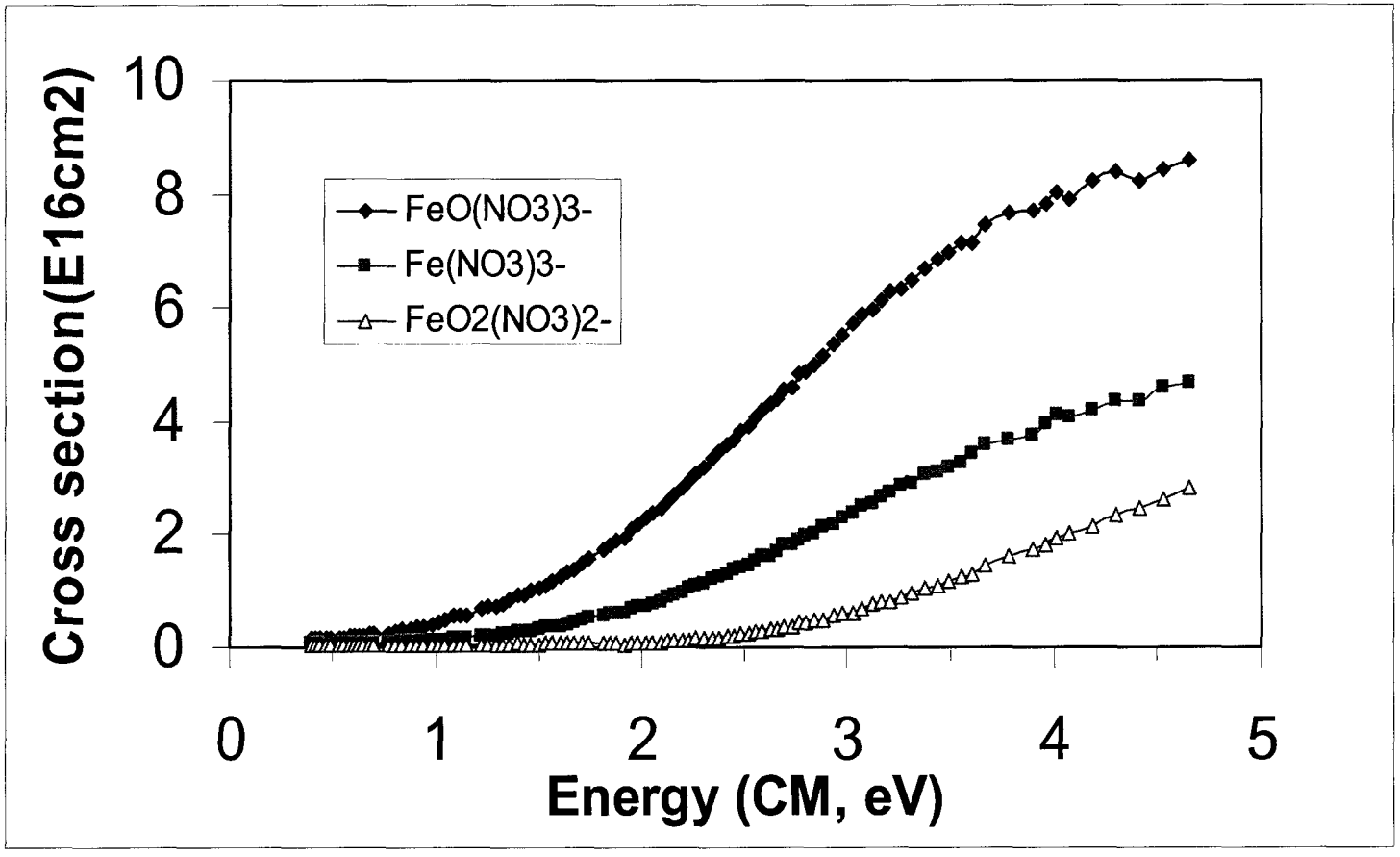

Fig. 12. Measured cross sections for production of $FeO(NO_3)_3^-$, $Fe(NO_3)_3^-$ and $FeO_2(NO_3)_2^-$ from $Fe(NO_3)_4^-$. The thresholds are only 0.5, 0.8 and 1.5 eV respectively.

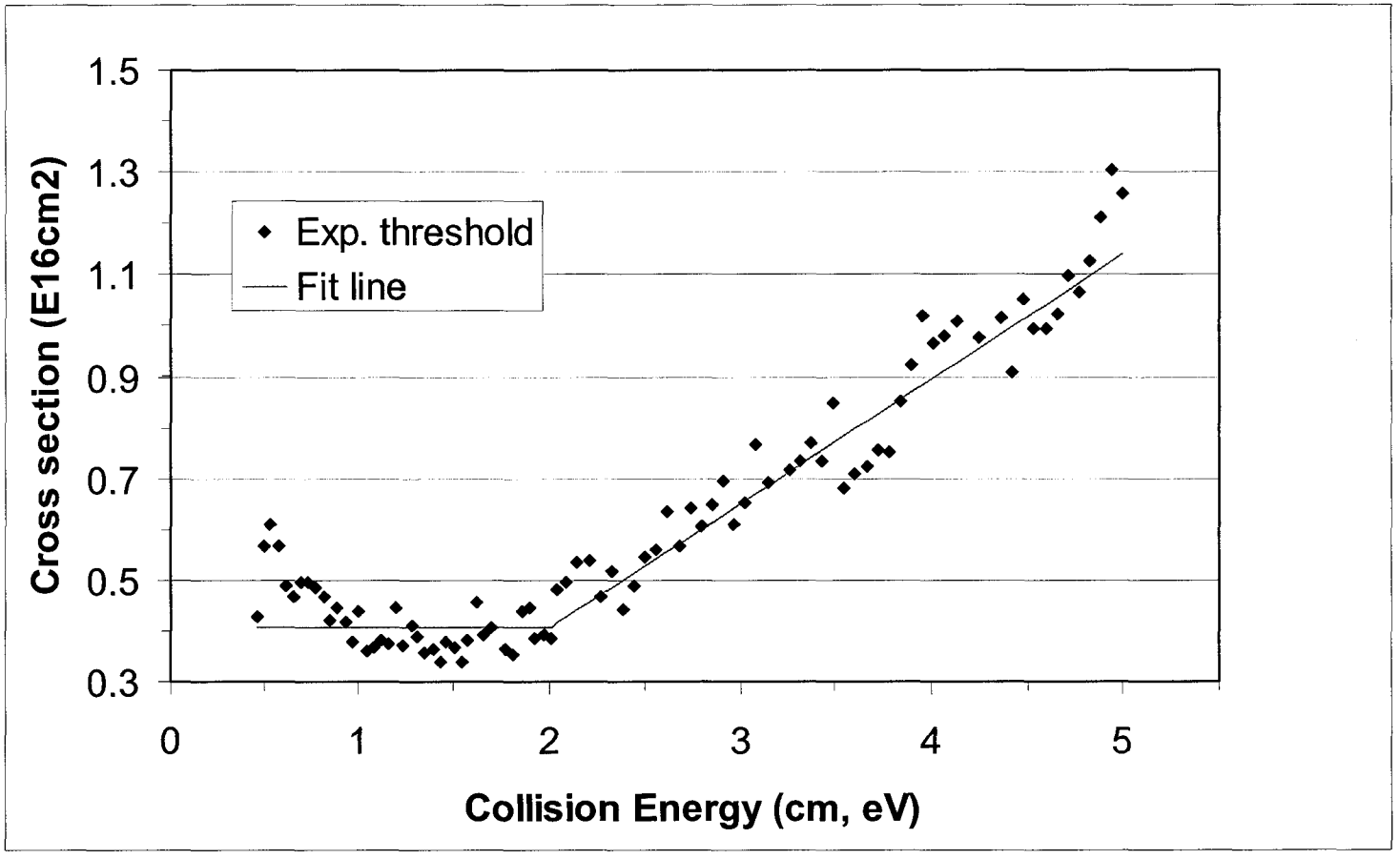

Fig. 13. Measured cross sections for production of nitrate: $Fe(NO_3)_4^- \rightarrow NO_3^- + Fe(NO_3)_3$. The threshold is 2.0 eV.

CHAPTER 5

CONCLUSIONS AND SUGGESTIONS FOR FUTURE WORK

The focus of this dissertation work is to expand the novel applications of inductively coupled plasma mass spectrometry (ICP-MS) and electrospray mass spectrometry (ESI-MS) to inorganic and biological fields. In Chapter 2, a new method was developed to characterize the surface of steel by confined acid dissolution. It was found that in a complex matrix as steel the contents of elements, i.e. Mn and Al, that are closely related to the bulk element, i.e. Fe, can be determined pretty accurately. Conversely, other refractory elements like Ti and Ta have poor recovery, which is probably due to the difference in the acid dissolving kinetic rates. The methodology can be readily adapted to metals or alloys containing simple matrix to determine trace element contents. Interestingly, this partial dissolution procedure also provides information about the speciation of the elements in the solid, which may have other practical applications.

Future work on the project can investigate the optimal acid mixture for sample with either complex or simple matrix, and to reduce the amount of material removed by the dissolution. It would be valuable to study whether heating the solid sample or some of the new microwave extraction procedures, like those used for "soft" extraction of intact compounds from solids,[1] would make the dissolution rate more uniform yet still slow enough for depth resolution for the problem elements found in this study.

We successfully coupled perfusion chromatography and ICP-MS to monitor the incorporation of heavy metal, namely uranium, during bioremediation. It was demonstrated

that *B. subtilis* and *S. putrefacient* were able to uptake U, spiked in the growing medium. Most of the u was incorporated intrinsically to the bacteria although bacteria can bind U extrinsically. Please refer to APPENDIX for the abstract and *analytical chemistry*[2] for the full article. In Chapter 3, we attempted to study the behavior of bacteria in the inductively coupled plasma, shed some light on its fundamental influence on the elemental quantification, and explore the possibility of using inorganic standards as the calibrant. The time-resolved U^+ signal from ICP-MS measurements indicated that bacteria behave similarly as the large particles in the ICP.[3] The positive U^+ spike was not due to the salvation effect. Sonication released intracellular species that are bound with uranium from the bacteria. The chromatographic results showed that the u-bound species had almost the same retention as the free inorganic U, implying that they are small in size and would have similar ionization efficiency as aqueous u standard. Therefore, quantification of U in intact bacteria is possible using inorganic u standard. This method can be readily applied in the biological and medical research where accurate quantification of trace elements, such as Zn and Mg, in human, is vital. It was found that PEEK tubing was able to absorb intact bacteria.

Future research can be on two parts. The first one is to apply the method to monitor the bioremediation of other environmentally important elements such as plutonium. It would be interesting to know what mechanism is truly responsible for the transportation of U from the outside medium into the intracellular environment. This later part may need to use 2-D gel electrophoresis, followed by structural determination by ESI-MS.

Finally, in Chapter 4, electrospray mass spectrometry was proved to be a valuable technique for inorganic metal study. Complexation with nitrate can stabilize some highly reactive species with high internal energies. Some metal nitrate ions undergo internal redox

processes during CID, such as conversion of M^{3+} to M^{2+}, even for elements like In^{3+} and Ga^{3+} that do not normally have lower oxidation states in solution. Presumably, such reductions are accompanied by oxidation of NO_3^- to NO_3. The study demonstrated that commercial grade triple quadrupole device can be used to estimate the bond dissociation energy. The CID reactions of $Fe(NO_3)_4^-$ ions have low kinetic energy onsets of ~ + 0.5 to 2 eV and are expected to be exothermic. Future work will continue to investigate how well the anion ligands, such as nitriate and chloride, can stabilize reactive organic compounds.

REFERENCES:

1. R. Bock, *A Handbook of Decomposition Methods in Analytical Chemistry*, Wiley, 1979, p. 197 and 199.
2. Zhang, B.; Li, F. M.; Houk, R. S.; Armstrong, D. W. *Anal. Chem.* **2003**, 75, 6901-6905.
3. Aeschliman, D. B.; Bajic, S. J.; Baldwin, D. P.; Houk, R. S. *J. Anal. At. Spectrom.* **2003**, 18, 1008-1014.

ACKNOWLEDGEMENTS

Given the second chance, I would choose chemistry as my major. I am myself amazed how much I have learnt about chemistry, especially inorganic and biological mass spectrometry, merits of being a strong and determined person, and capabilities to tackle difficulties independently as a graduate student here at Iowa State University. It would be impossible to acknowledge everyone who contributed to my academic success in such a limited space. I, however, would still try my best to say a little bit about them.

First of all, I would like to thank my major professor, Dr. R. S. Houk. My enthusiasm toward research is inspired from his perceptiveness, wholehearted dedication to science and wisdom in front of challenges. My passion to teaching is motivated from his patience to students, his care to the subject matter and his wealthy knowledge not only on chemistry also on history and sports. He is a great teacher! My living in Ames as an international student is eased because of his kind support and great friendship. I am proud to be a student of such a respected scholar, the inventor of modern ICP-MS, and to meet his high research standard.

I greatly appreciate the help and friendship of the previous Houk research group, Narong Praphairasksit (who taught me how to use the first Houk-made ICP-MS instrument), Towhi Hansan, Kent and Yougjin Hou. A special thank goes to Dave Aeschilman for his great patience teaching me how to use and troubleshoot Element 1. I owe many thanks to current members as well: Jill Furguson, Josh Messerly, Pat Sullivan, Cory Gross, Nathan Saetveit, and Nicholas Lentz. Additionally, I would like to express thanks to Matthew A.

Byers, an outstanding undergraduate student, who participated in the "study the CID behavior of metal nitrate complexes" project.

I am grateful for the collaboration with Dr. Armstrong for the bacteria projects, which turned out to be very successful. His instructive discussion and advice helped me gain insight into the separation sciences. He is a first-class scientist. I thank Bo Zhang, from whom I obtained some practical skills on liquid chromatography, column packing and bacteria culturing.

Sincere thanks are extended to Dr. Porter, Dr. Yeung, Dr. Johnson, Dr. Lin and Dr. Trahanovsky offering excellent courses and the exceptional research atmosphere at the chemistry department. I am grateful to Joe Burnett, my 211 TA instructor, for his benevolence to international students and much help throughout my study. I would also like to express my appreciation to Armstrong and Yeung group members for their friendship and assistance. You know what I am doing in their labs although they do not have mass spectrometers!

I greatly appreciate Dr. Lee Huang at Bayer Pharmaceuticals for his donation of TSQ 7000, which opened the door of biological mass spectrometry to me. I thank Steve Vessey for his useful discussion on TSQ 700. Meanwhile, I thank Dr. Tabatabi, Joe and Chou from the protein facility and many others at BBMB, who taught me molecular biology and useful skills on a wide range of biomolecules, i.e. protein, lipid, carbohydrate and nucleic acid as well as cell.

Thanks to Dick Webber, a technical support professional at Thermo. He instructed me how to troubleshoot most of the common problems about TSQ 7000 via the phone, free of charge even though the instrument is not under service contract.

I would also like to thank my undergraduate advisor, Dr. Pengyuan Yang, who led me into the mass spectrometry world, Rubin Huang and Xiunian Li at Xiamen University who encouraged me to come to the States to continue my Ph.D. study.

I am eternally indebted to my parents, Hongji Li and Xiucong Xin, my sisters and brothers. Without their unconditional love, support and understanding, I wouldn't be able to go this far! Lastly, I greatly thank my wife, Jie Ding, who puts up with my shortcomings, encourages me all the time and gives me complete freedom, and my son, Brad Li, for the joy he brings to our family!

APPENDIX

PORE EXCLUSION CHROMATOGRAPHY – INDUCTIVELY COUPLED PLASMA – MASS SPECTROMETRY FOR MONITORING ELEMENTS IN BACTERIA: A STUDY ON MICROBIAL REMOVAL OF URANIUM FROM AQUESOUS SOLUTION

A paper published in *Analytical Chemistry* (**2003**, 75, 6901-6905)

Bo Zhang, Fumin Li, R. S. Houk and Daniel W. Armstrong

ABSTRACT The interstitial spaces between spherical particles in a packed column can act as a sieve that passes microorganisms below a certain size. If the bed is a perfusion-type material (containing a binary distribution of large and small pores), colloidal-size microorganisms are subject only to pore exclusion, while all molecules are subject to size exclusion among the various pores. Thus, microorganisms elute first, followed by macromolecules, and then small molecules. Coupling this separation method to an ICP magnetic sector mass spectrometer provides a sensitive, direct means to study the microbial uptake of heavy metals (i.e., uranium) from their surrounding environments. Multiple metal ions can be monitored in the microorganism and in the surrounding solution. In this way, definitive information can be provided for the remediation of radioactive waste sites. The effect of uranium on microbial growth is also discussed.